# INFLUENCE OF HIGHER TIME HARMONICS ON THE ELECTRICAL AND MECHANICAL PERFORMANCE OF AN INVERTER-FED SQUIRREL CAGE INDUCTION MOTOR.



by

Jochen Erich ROEBER

September 1991

Dissertation submitted to the Department of Electrical Engineering, University of Cape Town, in partial fulfillment of the requirements for a degree of M.Sc. in Electrical Engineering.

# ACKNOWLEDGEMENTS.

*SERDECZNIE DZIEKUJE MOJEMU PROMOTOROWI PROF. JACKOWI GIERASOWI ZA PODZIELENIE SIE SWOIM DOŚWIADCZENIEM I ZA POMOC W PRZYGOTOWANIU MOJEJ PRACY DYPLOMOWEJ.*

My sincere thanks to my supervisor, Prof. Jack Gieras, for sharing his expertise and for his guidance throughout my thesis.

To Rössing Uranium, my appreciation for their financial and other support throughout my University career. Also for deferring my bursary obligations to enable me to complete my M.Sc. May the economic circumstances be more favourable in the future to enable the company to support the education of many more Namibians in the time to come. My personal thanks to Johan Stander, Lionel Louw, Margit Mansfield and Herbert Hanke.

My gratitude also to Philip Titus, Paul Daniels, Peter Lewis, Dave Kenyon and Steve Schrire for their help.

The Foundation of Research and Development (FRD) is thanked for their financial assistance.

Einen Dank auch meinen Eltern für Ihre Unterstützung.

Regine, Deine Freundschaft weiß ich sehr zu schätzen.

# ABSTRACT.

**Abstract:**

Due to the ruggedness, reliability and low maintenance required, small inverter-fed induction motors (1.5 kW to 25 kW) have earned a reputation and are utilized more and more frequently in industry for variable speed applications. The applied voltage and current waveforms are generally quite non-sinusoidal and polluted with **higher time harmonic components.** The higher time harmonics affect the electrical and mechanical performance significantly, and adverse effects are investigated. Literature on the effect of higher time harmonics is reviewed. Recommendations referring to various aspects under non-sinusoidal excitation are made when installing inverter-fed induction motors.

Different inverter supplies (6-Pulse Square Wave voltage source inverter (VSI), PWM VSI and sinusoidal excitation) are used with a small 3-Phase, 3-kW squirrel cage induction motor, configured under synchronous characteristic $V_r/50$ and subsynchronous characteristic $V_r/87$. The respective voltage and current frequency spectrums of the excitation source are analyzed and the harmonic content determined. Performance tests are executed under identical operating conditions respectively and results are compared with respect to pure sinusoidal (fundamental) excitation.

To determine the electrical performance the **efficiency, power factor, temperature** rise of the stator and **induced shaft voltages** were analyzed. The mechanical performance under inverter operation was analyzed by measuring the **torque, torque pulsations, critical speeds** and **resonance frequencies of frame vibrations** and **torque oscillations** as well as **vibrations in x-, y-, and z-direction** of the inverter-fed induction machine. Consequences of time harmonics on the induction motor and system are discussed. Conclusions on the effect of time harmonics and performance of different inverter types compared to sinusoidal excitation are drawn and are theoretically summarized and justified.

**Auszug:**

Umrichter gespeiste Induktionsmaschinen mit niedriger Leistung (1.5 kW bis 25 kW) werden zunehmend in industriellen Anwendungen mit drezahlveränderlichen Antrieben eingesetzt, da sie fast wartungsfrei und sehr robust sind. Die zugefügten Spannungen und Ströme von Umrichtern sind nicht sinusförmig und beinhalten eine Reihe von **zeitlich bedingten Oberschwingungen.** Die neben der Grundschwingung (Ordnungszahl n = 1) auftretenden Oberschwingungen beeinflussen das elektrische und mechanische Verhalten der Asynchronmaschine nachteilhaft. Umfangreiche Literatur zu diesem Thema ist vorhanden und einige Veröffentlichungen werden kurz besprochen. Vorschläge zur Installierung von Umrichter gespeisten Asynchronmachinen in Bezug auf vergrößerte Beanspruchung durch die nicht sinusförmige Speisung des Induktionsmotors werden vorgeschlagen.

Verschiedene Spannungs gespeiste Umrichter (6-Puls Block Spannungsumrichter, PWM (Puls Breiten Modulation) und sinusförmige Speisung) unter Normalkennlinie $V_r/50$ und $V_r/87$ werden benutzt um einen 3-Phasen, 3-kW Käfigläufer zu untersuchen. Das Frequenzspektrum der Spannungs- und Stromoberschwingungen wird jeweils bestimmt. Das Verhalten des Induktionsmotors und die Leistung wurden unter identischen Betriebszuständen gemessen. Die Resultate werden mit Ergebnissen verglichen, die unter sinusförmiger Grundschwingung bestimmt wurden.

Um das elektrische Verhalten zu untersuchen, wurden der **Wirkungsgrad, Netzleistungsfaktor, Temperaturanstieg** des Ständers und die induzierten **Wellenspannungen** gemessen. Das mechanische Verhalten des Käfigläufers unter Umrichterspeisung wurde analysiert durch die Bemessung des **Drehmoments, Pendelmoments, Resonanzfrequenzen des Pendelmoments** und der **Vibrationen im Betriebsbereich,** und **Ständervibrationen in x-, y- und z- Richtung.** Die Auswirkungen der Oberschwingungen auf den Induktionsmotor werden besprochen. Schlußfolgerungen über die Auswirkung der Oberschwingungen in verschiedenen Umrichtern im Vergleich zur Grundschwingung werden theoretisch ausgelegt und zusammengefaßt.

# TABLE OF CONTENTS.

# LIST OF FIGURES AND TABLES.

## FIGURES.

# TABLES.

# LIST OF PRINCIPAL SYMBOLS.

All symbols are explained as required and used in the text. A brief list is given below.

---

| Symbol | Meaning |
|---|---|
| A,B | Constants |
| B | Magnetic shaft density |
| $f_1$ | Fundamental stator frequency |
| $f_n$ | Frequency ofinduced harmonic |
| $f_r$ | frequency of the excitation force |
| $f_{sup}$ | Supply frequency |
| $f_{rip}$ | Ripple frequency |
| g | Any integer, g = 0, ±1, ±2, ... |
| G | Conductance |
| H | Inertia of the motor-load system |
| I | $\|I\|e^{j\sigma}$ the current phasor |
| I* | Conjugate current phasor |
| $I_1$ | Fundamental stator current |
| $I_d$ | Current flowing in the dc circuit |
| $I_{du}$ | Alternating current in the dc circuit |
| K | Initial VSI boost |
| k | Any integer, k = ±1, ±2, ±3, ... |
| $k_E$ | Eddy constant |
| $k_H$ | Hysteresis constant |
| $k_T$ | Constant |
| $k_{VSD}$ | Factor to include extra heating of a VSI |
| l | Length of shaft flux path |
| m | number of phases |
| n | Harmonic $n^{th}$ component |
| n | Subscript denoting higher time harmonic order |
| $N_1$ | Number og stator slots |
| $N_2$ | Number of rotor slots |
| $N_s$ | Speed ofsynchronous field of the fundamental |
| N | Actual the rotor speed |
| p | number of pole pairs |
| P | Active power |
| Pf. | Power factor |
| $P_{oH}$ | Output power under inverter supply |
| $P_o$ | Output power sinusoidal supply |

| Symbol | Meaning |
|---|---|
| $P_r$ | Amplitude of the force wave |
| $P_{str1}$ | Stray Losses due to the fundamental frequency |
| $P_{Fe1}$ | Iron loss due to the fundamental frequency |
| Q | Reactive power |
| $R_1$ | Stator winding resistance |
| $R_m$ | Series resistance corresponding to core losses |
| $R_2'$ | Rotor winding resistance referred to stator side |
| $R_s$ | Radius of the shaft |
| $R_{1n}$ | Harmonic winding stator resistance |
| $R_{2n}'$ | Harmonic secondary winding resistance referred to stator referred to stators |
| s | Slip |
| $s_n$ | Slip of the rotor for higher time harmonics |
| S | Apparent power |
| t | Time |
| T | Absolute temperature |
| T | Torque |
| $T_0$ | Dc torque magnitude |
| $T_1$ | Oscilating torque magnitude |
| $T_{rip}$ | Amplitude of the torque ripple |
| $T_{SIN}$ | Steady state temperature under sinusoidal exc. |
| $T_{1\_DE}$ | Temperature at the drive end |
| $T_{3\_NDE}$ | Temperature at the non drive end |
| $T_{Grad}$ | Temperature gradient between $T_{1\_DE}$ and $T_{3\_NDE}$ |
| $T_{ds}$ | Average temperature increase compared to sinusoidal excitation |
| $T_{dSP}$ | Temperature increase under Square Wave excitation compared to PWM excitation |
| u | Order of the harmonic in the dc circuit, with u = 2, 4, 6 ..., ∞ |
| V | $\|V\|e^{j\phi}$ the voltage phasor |
| $V_b$ | Voltage across bearing |
| $V_1$ | Fundamental stator voltage |
| $V_{CV}$ | Core volume |
| $V_r/50$ | VSI characteristic with 50 Hz max. excitation frequency characteristic |
| $V_r/87$ | VSI characteristic with 100 Hz max.excitation frequency characteristic |
| $w_T$ | Oscillating frequency of the torque |
| $w_0$ | Dc speed amplitude |
| $w_1$ | Oscillating speed amplitude |
| $w_w$ | Oscillating frequency of the speed |

| Symbol | Meaning |
|---|---|
| $w_{rip}$ | Ripple speed |
| $x$ | Relative stator airgap circumference position |
| $X_1$ | Stator winding leakage reactance |
| $X_{1n}$ | Harmonic winding stator leakage reactance |
| $X_{2n}'$ | Harmonic secondary winding leakage reactance |
| $X_2'$ | Rotor winding leakage reactance referred to stator side |
| $X_m$ | Mutual reactance |
| $\mu$ | (for stator force waves) |
| $\epsilon$ | (rotor force waves) |
| $\Gamma$ | Vibration severity |
| $\tau_{r0}$ | Rotor time constant $(L_m+L_2')/R_2'$ |
| $\Phi$ | Flux density |
| $\Phi_S$ | Shaft flux |
| $\delta_e$ | Skin depth |
| $\cap$ | Efficiency |
| $\theta$ | Power factor, $\cos(\theta)$, $\phi - \sigma$ the phase shift |
| $\nu$ | Space harmonic |

***Abbreviations.***

| Symbol | Meaning |
|---|---|
| DF | Voltage distortion factor as defined by the IEEE |
| DUT | Device under test |
| e.m.f. | Electromagnetic force |
| exc. | Excitation |
| FFT | Fast Fourier Transform |
| m.m.f. | Magnetomotive force |
| PWM | Pulse Width Modulated VSI |
| SQWave | Square Wave 6-Pulse VSI |
| synch. | Synchronous |
| subsync. | Subsynchronous |
| r.m.s. | Root mean square |
| r.p.m. | Revolutions per minute |
| VSI | Voltage Sourec Inverter |
| VSD | Variable Speed Drive |
| w.r.t. | With respect to, compared to |

# CHAPTER 1. INTRODUCTION.

## 1.1 Topic.

The research topic is a commonly used standard small power variable speed drive (VSD) with a 3-phase 3-kW cage induction motor. The induction motor is fed from voltage-source static inverters with variable-frequency variable-voltage amplitude output. With the present technology it is difficult to achieve a distortion-free sinusoidal output. Higher time harmonics in the inverter output voltage influence the electrical and mechanical characteristics of an induction motor. Existing design variants of cage induction motors when fed with non-sinusoidal voltage produce usually smaller torque and higher vibrations than on a sinusoidal voltage.

For example, derating curves and dangerous resonant frequencies for standard motors supplied by static inverters have tremendous practical importance. These problems should be carefully investigated especially in relation to small VSDs which are the most popular drives.

VSDs are used to an ever increasing extend in industry for all various applications. The main requirement are for process engineering and also for energetic reasons. The effect of higher time harmonics on the electrical and mechanical performance of induction motors must be understood and well established for integration of VSDs into operating plants. Necessary precautions to remedy or avoid any adverse effects can then be taken.

VSDs are considered as a whole systems, which include electrical as well as mechanical performance characteristics. Each system consists of a supply unit, the variable frequency inverter, control unit, asynchronous machine, shafting and couplings and the load.

Different types of inverters rated between 0.5 kW and 2000 kW are used at present. Each inverter has its own specific characteristic and deviates from sinusoidal supply. These cause a variety of different (changed) stresses on the motor. The performance (especially with

reference to the load being driven) may be affected adversely.

The research topic can be divided into (i) electrical and (ii) mechanical phenomena associated with inverter operation. Clearly the excitation with higher time harmonics creates higher space harmonics which then influence mechanical operating characteristics.

## 1.2 Purpose.

In the IEC Standards [1.1], on the application of cage induction motors when fed from inverters, steady state operation applications are discussed. Indirect type (intermediate DC bus) frequency inverters are considered. The standard attempts to quantify the selection of power components and their induced characteristics on the drive - motor system. The standards [1.1] recommend to check the frequency spectrum, harmonic losses, torque derating, oscillating torques, noise, over-voltages and shaft voltages during inverter operation of a typical motor.

Mathematical models on torque pulsations, loss models for inverter-fed asynchronous motors are available in literature. Noise and vibration phenomena are also described. On the other hand only very limited information was found on induced shaft voltages due to higher time harmonics, and no measurement data on torque pulsations was published.

Additional stresses in various forms and dimensions due to variable frequency, non-sinusoidal and variable voltage and currents influence induction motor operation.

**The purpose of this thesis is to investigate the electrical and mechanical performance of small inverter-fed induction motors, i.e.**

- **Losses and efficiency.**
- **Temperature rise.**
- **Shaft voltages.**
- **Torque pulsations.**
- **Vibrations.**

Variable quantities as:

(i) variable frequency;
(ii) variable voltage and currents;
(iii) Non-sinusoidal voltage and currents;

influence the operation and performance of induction motors in various forms.

**The electrical consequences of non-sinusoidal excitation of induction motors are [1.1 - 1.5]:**

(i). higher time harmonic losses and increased temperature stresses in motors;

(ii). reduced efficiency, power factor and rated machine power;

(iii). increased induced shaft voltage and bearing currents;

(iv). stresses on the insulating materials due to voltage and current spikes as well as increased temperature;

(v). increased noise levels with distinct frequency components due to adjustable frequencies and harmonic voltages and currents.

**The mechanical consequences of non-sinusoidal excitation of inverter-fed induction motors are [1.1 - 1.5]:**

(i). oscillating torques and forces due to harmonic voltages and currents;

(ii). operating range influenced by critical speeds, resonance, increased vibrations;

(iii). reduced inter lubrication periods and reduced bearing life-time;

(iv). reduced ventilation effect at low speeds;

(v). noise due to torque pulsations and increased vibrations due to variable frequency, voltage and current harmonics.

Secondary effects of high frequency harmonics, especially in high power applications are the interference in control systems, communication networks and general power system pollution [1.6].

## 1.3 Approach.

The effects of higher time harmonics on the performance of induction machines are theoretically well understood phenomena. Assorted literature has been published on most of their aspects, eg. [1.2 - 1.5]. However, the largest literature component lies in modelling effects and phenomena under non-sinusoidal excitation, but only limited reliable actual measurements on performance and other phenomena have been published eg. [1.2].

**In this thesis the consequences of higher time harmonics are measured on a physical model.** It is limited to a single standard inverter-fed squirrel cage induction motor, as particular attention should be given to non-special motors. All measurements can be analyzed on a relative basis as data was captured under the same operating conditions but at different frequencies and separate excitations:

(i). Square Wave (6-Pulse) ;
(ii). Puls Width Modulated (PWM) ;
(iii). Sinusoidal ;

excitation with known frequency content. Sinusoidal excitation (fundamental frequency component only) is used as reference. The effect of known higher harmonic content can then be deduced and analyzed.

# CHAPTER 2. PHYSICAL MODEL AND LABORATORY DATA ACQUISITION SYSTEM.

## 2.1 General Requirements.

For an experimental investigation on a physical model all concrete measurement parameters must be acquired to the highest possible accuracy. All measurement parameters must be transformed into a measurable voltage or current signal. Considerable design effort is required to eliminate all sources of noise and interference which could be severe in an environment with radio frequency interference due to current spikes. To obtain a high level of confidence in the measurements taken the calibration procedure must be accurate, repeatable and compared to a reliable calibration source. The interface between the data acquisition system (PC-based) and the actual voltage signals must be done carefully. Ground loop elimination, input buffers and protection circuits must be incorporated. Analog measuring devices with suitable specifications (accuracy, voltage offset, bandwidth, drift etc.) must be selected and used in the signal transducer design.

To determine the efficiency precisely it is important to measure the power supplied to the motor under non-sinusoidal excitation and the mechanical output power accurately. Power measurement under inverter conditions was investigated and is discussed in some detail below due to its relevance, especially with respect to determining the efficiency. Alternative methods to determine the efficiency, measurement considerations and their signal conditioning are discussed in this chapter.

## 2.2 Description.

The physical model concept is presented in the Fig. 2.1. The induction motor is the Device Under Test (DUT) with all sensor positions indicated. Design data of the induction motor manufactured by GEC (Johannesburg, RSA) are given in Table 2.1.

**Table 2.1** Design data of tested 3-Phase Cage Induction Motor.

| | |
|---|---|
| Rated power: | 3000 W |
| Rated frequency: | 50 Hz |
| Rated voltage: | 380 r.m.s. V |
| Connection: | Delta |
| Rated speed: | 1430 r.p.m. |
| Rated current (Sine): | 6.9 A |
| No. of turns per coil: | 58 |
| Stator winding type: | Single layer concentric |
| No. of stator layers: | 1 |
| Diameter of stator conductor: | 0.8 mm |
| No. of parallel paths: | 1 |
| Stator coil pitch: | 1-12, 2-11, 3-10 |
| No. of stator slots: | 36 |
| No. of rotor slots: | 28 |
| Outer/inner diameter, stator core: | 165.1 mm; 104.8 mm |
| Outer/inner diameter, rotor core: | 104.8 mm; 38,1 mm |
| BH curve and core loss: | 8 W/kg at 1.5T, 50 Hz |
| Rotor cage material, resistivity: | Al. (LMo), |
| Resistivity of stator winding: | $0.146*10^{-5}$ Ω at 75°C, per 2.54 cm |



A load in form of a separately excited dc generator is connected via a torque transducer (slip ring type - HBM). The load is varied by changing the field excitation and the armature terminals are connected via resistor bank. The advantage of this configuration is that for the no load and locked rotor test the dc generator can be reconfigured as variable speed dc motor.

To avoid exceeding the inverter current limit, and the rated motor current, the load and torque was only measured at low values of slip i.e. up to maximum two times rated conditions.

Also for vibration and torque pulsations without exciting the induction machine, the system inherent mechanical behaviour can be approximated. An external trigger was designed for (i) synchronizing and (ii) to obtain the shaft position over time. A second torque transducer was

used as a reference. A flexible coupling (Fenner-type) was used between the HBM torque transducer and load to eliminate vibrations and torque ripples originating from the dc generator. Furthermore this would improve the shaft voltage observation as the coupling isolates the shaft from the actual load.

(a)

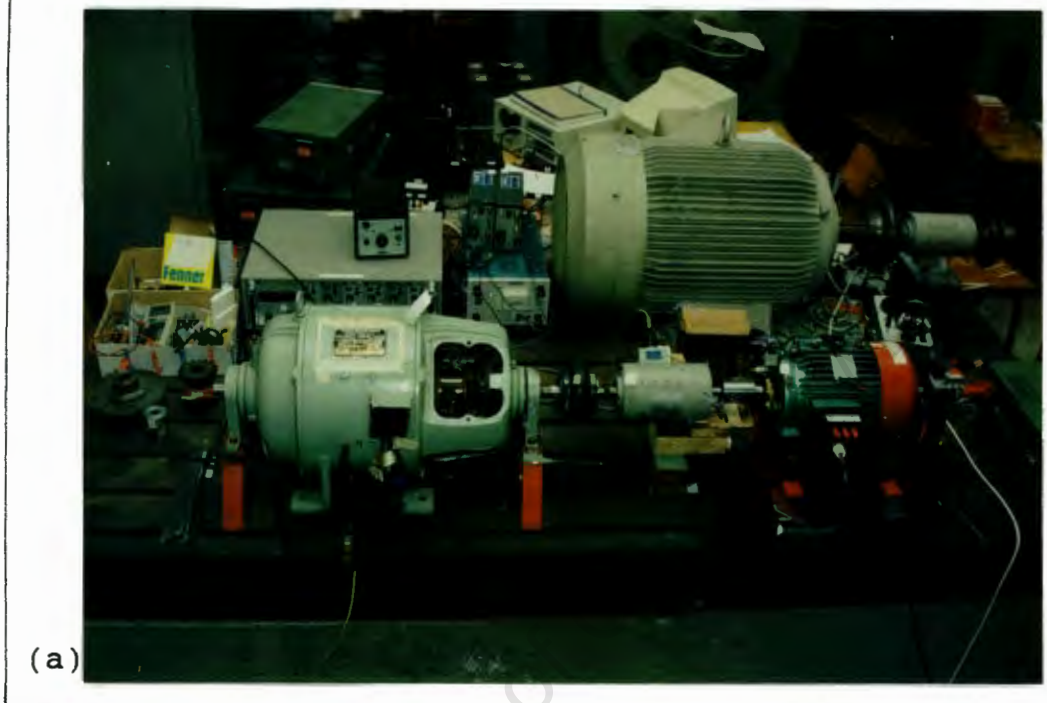


(b).

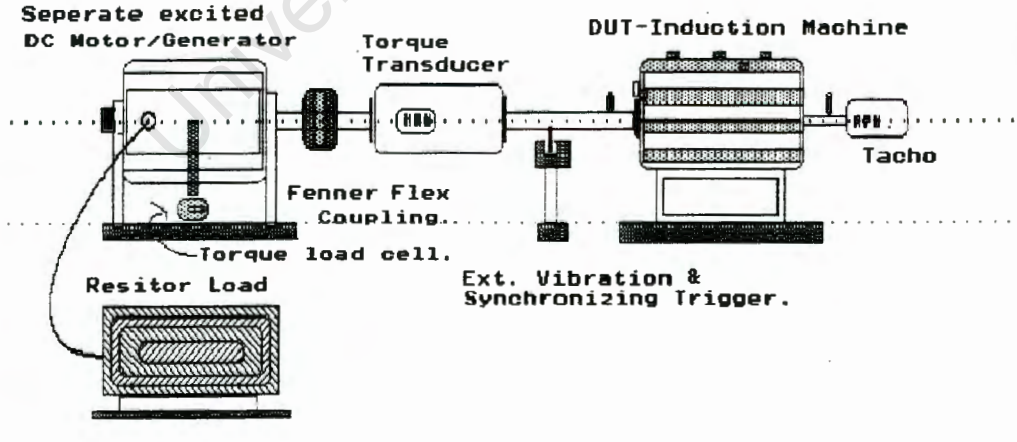


**Fig. 2.1** Test-bench setup: (a) General view, (b) Configuration.

In Fig. 2.2 a flow chart outlines the inter-connection of equipment and the general procedure for measurements.

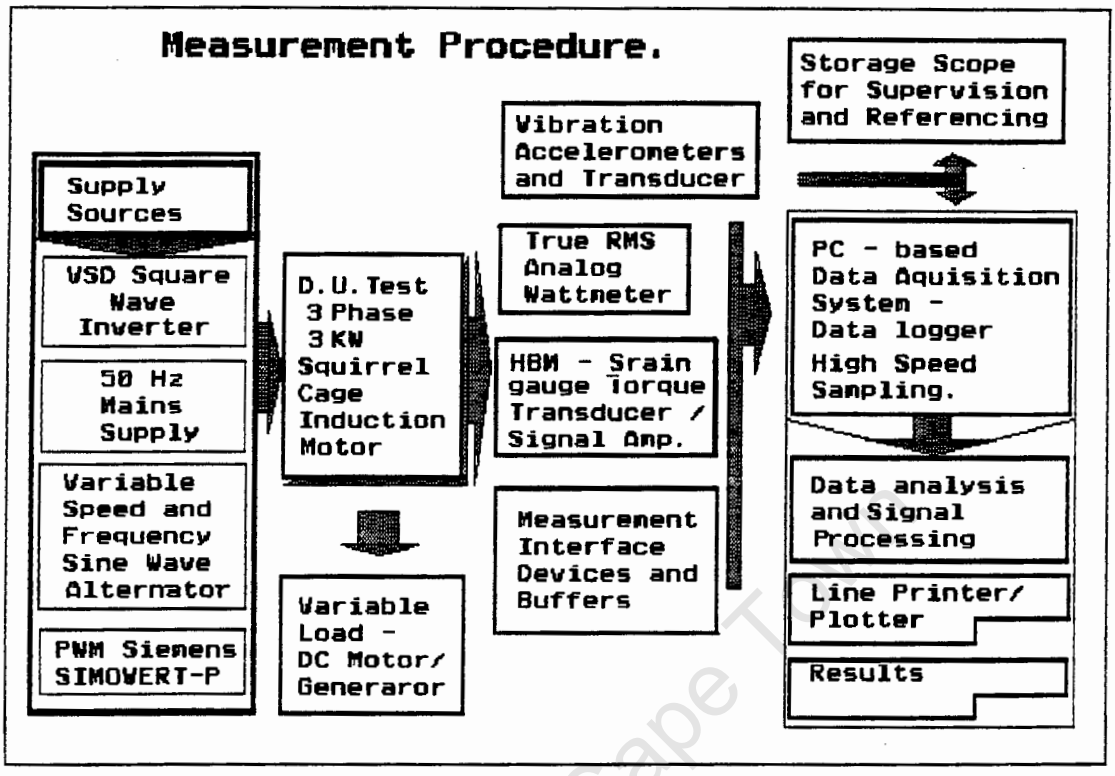


**Fig. 2.2** Flow chart, testing and data acquisition procedure. All instruments and devices are indicated.

An IBM compatible PC-based data acquisition system is used to sample all measurements. The A/D and D/A card PC30-D, a maximum throughput of 200 kHz with supplied software STATUS-30 V2.00 was installed on an 12-MHz IBM/286 computer. A maximum of 16 channels, 12 bit resolution could be sampled, either configured for DMA (Direct Memory Access) or rotational sampling. The sampling frequency and the number of samples to be logged could be set up. Logged data was saved as text file and then imported to additional support software (Quattro Pro) and then manipulated to extract information. Some information on the PC30-D card and the STATUS-30 software is attached in **Appendix 2.1.**

The frequency spectrum could be obtained via an implemented FFT (Fast Fourier Transform), or a Chirp-Z transform to pre select a specified frequency range. Depending on synchronization of the signal, windowing functions (Rectangular, Blackman Harris, Hamming, Hanning windows) were selected to reduce effect of cluttering harmonics if a non integral number of periods of a

specific sample were logged (the effect of spectral leakage).

To improve the analysis of voltage source inverter-fed motors and to analyze different methods of modulating variable frequency signals with their respective harmonic content a simulation package PWM_SIM was written in Turbo C/C$^{++}$ to simulate different modulation techniques, their respective line currents and to investigate the respective frequency spectrum. The effect of varying the leakage reactance can also be simulated. The simulation of the line current is an approximation as used in [1.4], it is assumed that the inductance is much larger than the resistance. The program is suited for teaching purposes and the analysis of modulation techniques. Information of crest and distortion factors are also displayed. Information on the software PWM_SIM is attached in **Appendix 2.2.**

## 2.3 Equivalent Circuit of Inverter-Fed Induction Motors.

Accurate equivalent circuit parameters are required to predict the steady state performance of inverter-fed induction motors. The parameters for the fundamental and parallel time harmonic equivalent circuits are determined for the induction motor. The equivalent circuit, with V/f characteristic as maintained by inverter drives is determined by a method outlined in [2.4]. Four tests, the standard locked rotor and no load test were performed for sinusoidal excitation at 50 Hz and 25 Hz at constant V/f ratio. Equivalent circuit parameters as a function of frequency (V/f constant) for that specific circuit are then derived.

A T-type equivalent circuit is used, (Fig. 2.3). This equivalent circuit takes into account the temperature of the windings, iron and mechanical losses at each frequency and the skin effect in the rotor circuit.

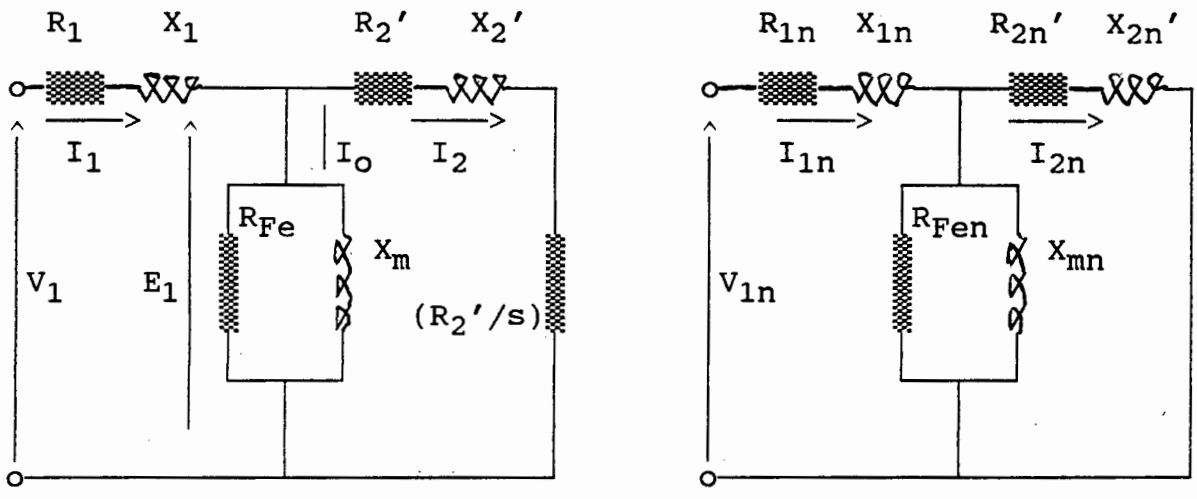


(a). (b).

Fig. 2.3 Equivalent circuits. (a) for fundamental harmonic (b) for n-th time harmonic.

The following symbols are used for equivalent circuit parameters under sinusoidal excitation:

$R_1$ = Stator winding resistance.
$X_1$ = Stator winding leakage reactance.
$R_m$ = Series resistance corresponding to core losses
$X_m$ = Mutual reactance.
$R_2'$ = Rotor winding resistance referred to stator side.
$X_2'$ = Rotor winding leakage reactance referred to stator side.

Under non-sinusoidal excitation the subscript "n" (higher time harmonics order) is added.

The fundamental slip is expressed as:

$$s = \frac{N_s - N}{N_s} \qquad ...(2.1)$$

where $N_s$ is the synchronous speed of the fundamental, N is the rotor speed.

The slip $s_n$ of the rotor for higher time harmonics is approximately equal to unity. i.e.

$$s_n = \frac{n \pm (1-s)}{n} \qquad ...(2.2)$$

where $n = 6k \pm 1$ (k=1,2,3...).

The frequency for the $n^{th}$ harmonic in the rotor is:

$$f_{2n} = s_n * n * f_1 = [n \pm ( 1 - s )] f_1 \qquad ...(2.3)$$

The slip of the rotor is $s_n \approx 1$, and rotor frequency for higher time harmonics is $f_{2n} \approx n f_1$.

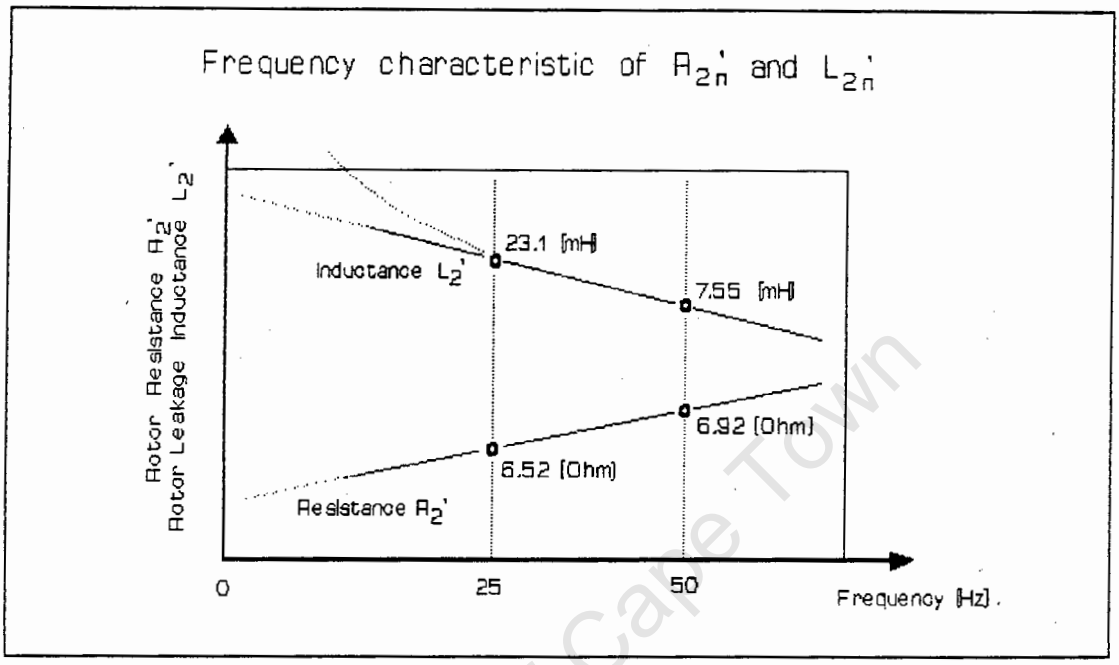


**Fig. 2.4** Secondary resistance and leakage inductance frequency characteristics measured in the motor operating range.

The measurements taken are displayed in Fig. 2.4 and also correlate with data presented in [2.5]. The rotor parameters are frequency dependant in both stator, and rotor circuit but especially in the rotor due to the skin effect in the squirrel cage bars.

To estimate the equivalent circuit resistances and reactances it is necessary to make no-load and locked rotor tests. To perform an accurate no load test the dc motor drives the induction motor at synchronous speed (locked with a mains synchronized stroboscope) to overcome all windage and friction losses. The total power then supplied to the induction motor were stator and iron core losses. For the equivalent circuit calculations uncertainties on mechanical losses could thus be eliminated. The temperature of the windings was kept at 75°C.

As the total mutual flux linkage and thus torque is influenced by the rotor position, the locked rotor test was performed at rated current and the rotor turned anti-clockwise by the dc motor. For each test 256 data points were sampled and the average calculated.

A more detailed analysis and derivation of the parameters is attached in **Appendix 2.3.**

**The following equivalent circuit frequency dependant parameters were calculated, (Appendix 2.3).**

$R_1 = 6.87 \quad \Omega$
$X_1 = 0.0081 * 2\pi f_1 \quad \Omega$
$R_m = 37.08 \quad \Omega$ at 50 Hz
$X_m = 0.591 * 2\pi f_1 \quad \Omega$
$R_2' = 6.92 \quad \Omega$
$X_2' = 0.0075 * 2\pi f_1 \quad \Omega$

$R_{1n} \approx R_1$
$X_{1n} = n * X_{1n}$
$R_{2n}' = 0.029 * f_{2n} + 5.24$
$X_{2n}' = 0.598 * f_{2n}^{-1.11}$
$X_{mn} = n X_m = 0.591 * 2\pi nf_1 \quad \Omega$

It must be noted that the series resistance corresponding to core losses is also dependant on the fundamental exciting frequency. This is outlined in paper [2.4].

The load is modelled with a separately excited 5 kW dc-generator. The armature windings are connected to a resistor bank. By varying the field excitation the e.m.f. generated increases, and so the load. A near linear load-speed relationship is obtained at constant field excitation.

## 2.4 Electric Input Power.

Before using any nomenclature it is important that all terms are clearly defined and understood to avoid any ambiguity while referring to data, measurements and calculations.

Moreover, since the power measured (i.e. voltage and current) is not always sinusoidal a concise but brief investigation into non-sinusoidal power signals has been

made. Sinusoidal and DC power transfer are merely special cases. For non-sinusoidal conditions different criteria are laid down as outlined and discussed below. Clearly, monitoring of inverter drives, where power measurement forms an integral part, is affected by time harmonics and is discussed in this project.

A design description, component data sheets, specifications and detailed circuit diagrams of the true r.m.s. power meter are shown in **Appendix 2.4.**

The classical phasor representation was developed as an analytical instrument for time varying sinusoidal voltage and current signals.

For sinusoidal signals:

$$v(t) = V_m \cos(wt + \phi) \qquad ...(2.4)$$

$$i(t) = I_m \cos(wt + \sigma) \qquad ...(2.5)$$

where $V_m$ and $I_m$ are the peak values of voltage and current respectively, $\phi$ and $\sigma$ are the phase angles.

From the phasor representation the complex (apparent) power has two mutually orthogonal components, namely real (active) and fictitious (reactive) power. These definitions of power are valid for sinusoidal voltages and linear loads.

$$S = V \cdot I^* = V \cdot Ie^{j\sigma}$$
$$= V \cdot I \cos(\Theta) + V \cdot I \sin(\Theta) = P + jQ \qquad ...(2.6)$$

where $V = |V|e^{j\phi}$ is the voltage phasor, $I = |I|e^{j\sigma}$ the current phasor with I* the conjugate, P is the active power, Q the reactive power, and $\Theta = \phi - \sigma$ the phase shift.

For a general power measurements in the time domain of all different waveforms all components must be defined.

Current is subdivided into two orthogonal components namely active $i_a(t)$ and fictitious $i_f(t)$. The active current is in phase with the voltage across the conductance G such that

$$i_a(t) = G * v(t) \qquad ...(2.7)$$

The fictitious current is the difference between the loading current and the active current.

$$P = I_a * V \qquad ...(2.8)$$
$$F = I_f * V \qquad ...(2.9)$$

A general definition of power for:

i). non-sinusoidal - and
ii). aperiodic voltage and current waveforms.
iii). nonlinear loads.

in the time domain a load related definition is proposed in the paper [2.1].

It is further stipulated that only real time voltage and current should form input data to power measurement and the actual power should not depend on the analysis of the waveform itself.

In the paper [2.1] the powers are defined of two real orthogonal components - loading, active and fictitious power were the fictitious power is subdivided into reactive and deactive power. This is required for fictitious power compensation control [2.1].

---

Clearly in the application of variable speed drives the signals are periodic in the steady state (not during transients) i.e.:

$$f(t) = f(t + T) \qquad ...(2.10)$$

To calculate eg. efficiencies the main variable of interest is the average power:

$$P = \frac{1}{kT} \int_{-kT}^{+kT} p(t)\, dt \qquad ...(2.11)$$

where k = integral no. of periods and $p(t) = v(t).i(t)$

The loading or apparent power S is determined as the product of the effective or r.m.s. (root mean square) values.

$$S = V_{r.m.s.} + I_{r.m.s.}$$

where the r.m.s. shaft voltage and currents are:

$$V_{r.m.s.} = \sqrt{\frac{1}{T} \int_0^T v(t)^2} \qquad ...(2.12)$$

$$I_{r.m.s.} = \sqrt{\frac{1}{T} \int_0^T i(t)^2} \qquad ...(2.13)$$

Solving the integral for sinusoids the result is established:

$$V_{r.m.s.} = V_{peak} / \sqrt{2} \qquad ...(2.14)$$

$$I_{r.m.s.} = I_{peak} / \sqrt{2} \qquad ...(2.15)$$

Clearly all higher harmonic components are included in this integral and any periodic signal can thus be decomposed into discrete sinusoidal components, i.e.:

$$I_{r.m.s.} = \sqrt{ ( I_{1rms}^2 + I_{2rms}^2 + I_{3rms}^2 + \dots ) } \qquad ...(2.16)$$

$$V_{r.m.s.} = \sqrt{ ( V_{1rms}^2 + V_{2rms}^2 + V_{3rms}^2 + \dots ) } \qquad ...(2.17)$$

The classical reactive power is obtained as:

$$Q = \sqrt{S^2 - P^2} \qquad ...(2.18)$$

The power factor cos θ for sinusoidal voltage and current is defined as:

$$Pf. = \cos \theta = \frac{\text{Active power}}{\text{Apparent power}} = \frac{P}{S} \qquad ...(2.19)$$

## 2.5 Output Power Measurement.

In the application of VSDs it has been measured that at especially low speed operations the torque is

pulsating and subsequently an oscillating speed (notably in low inertia systems) is present.

An accurate method to establish the mechanical output power (measured at the machine shaft) could be done by an analogue procedure as used by Lindsay [2.2] to determine the DC power supplied to a thyristor supplied DC - machine. Neither speed nor torque are truly constant over time. It is however generally assumed that speed and torque is constant which is a good approximation, for higher frequency operation and especially for high inertia arrangements.

Thus defining the average output power:

$$P_{avg} = T_{avg} \cdot w_{avg} \qquad [Nm.rad/sec] \qquad ...(2.21)$$

where

$$T(t) = T_0 + T_1.\sin(w_T) \qquad ...(2.22)$$

$$w(t) = w_0 + w_1.\sin(w_w) \qquad ...(2.23)$$

were $T_0$ and $T_1$ giving the dc and oscillating torque magnitudes respectively with $w_T$ the oscillating frequency of the torque, $w_0$ and $w_1$ the dc speed and oscillating speed amplitudes respectively with $w_w$ the oscillating frequency of the speed.

But torque and speed are at the same frequency and in phase $w_T = w_w$, so that

$$P(t) = w_0.T_0 + w_1.\sin(w).T_1.\sin(w) \qquad ...(2.24)$$

From trigonometric identities:

$$P_{avg} = w_0.T_0 + 0.5\ w_1.T_1 \qquad ...(2.25)$$

The true average values for torque and speed can be obtained by low pass filtering the signals respectively.

## 2.6 Instruments and Measuring Devices.

### 2.6.1 Wattmeter.

The active power, r.m.s. voltage and currents are acquired from the wattmeter described in **Appendix 2.4.** The power factor, reactive and apparent power are calculated according to the definitions outlined in Section 2.4.

The induction motor connected in delta, but the voltage measured is the phase voltage to fictitious neutral. Multiplying by √3, the phase to phase voltage magnitude was determined. Only the power for one single phase has been measured and the machine is assumed to be almost perfectly balanced, which is the case in present motors. The voltage signal is converted to a true r.m.s. signal. The line current is measured with a Techtronix current probe, the signal then amplified to reduce the effect of noise and also converted to a true r.m.s. signal as discussed in **Appendix 2.4.**

### 2.6.2 Voltage.

To sample and measure the voltage on inverter-fed motors is difficult because of the floating dc bus intermediate state and VSD reference neutral with respect to mains neutral. The signals measured must thus be isolated from the actual PC-based data acquisition system.

A fictitious neutral has been created by connecting phase A, B and C in star. A frequency independent potential divider with the ratio 100:1 gives an accurate loggable voltage signal. Any phase can be selected via a rotary switch and the signal is buffered via a precision isolator. The frequency is also derived from the know V/f characteristic, which was measured with the frequency option of the Fluke 8086A multimeter.

### 2.6.3 Current.

The current is measured via the Techtronix (Hall effect) current probe, the signal then amplified to improve signal to noise ratio. The current signal is also converted to a true r.m.s. signal for processing. The measured values are calibrated with a Fluke 8086A multimeter.

### 2.6.4 Torque.

The torque is an integral factor in determining the output power and thus efficiency. The torque is obtained from the HBM torque transducer, where the signal is measured on an axial shaft via strain gauges. The actual signal is transmitted via sliprings to a HBM measurement amplifier. A load cell was mounted on the load to verify

the actual torque measured. The signal is obtained via a differential amplifier with good Common Mode Rejection Ratio (CMRR).

The torque signal is passed through (i) a LPF (Low Pass Filter) as discussed in Section 2.5 with a 3 dB frequency of 10 Hz and (ii) through an HPF (High Pass Filter) to measure the torque ripple. The 3 dB cutoff frequency is 75 Hz. The HPF signal is passed through a true r.m.s. converter to measure the torque pulsations.

The measured torque quantities are (i) average torque, (ii) ripple torque, (iii) actual instantaneous torque T(t).

Circuit diagrams for the load cell configuration, the filters for the HBM torque signal and information on the HBM torque transducer are shown in **Appendix 2.5.**

### 2.6.5 Speed.

Speed measurement was performed with a permanent magnet dc tacho generator. The voltage signal was passed through an LPF to filter out any noise that would be present due to interference and then buffered by an operational amplifier voltage follower. A second frequency proportional to r.p.m. signal was used to ensure accurate calibration as frequencies can be measured accurately.

### 2.6.6 Temperature Sensors.

As indicated in Fig. 2.5 temperature sensors ($T_1$ to $T_4$) were embedded in the stator laminations at three different positions, closest to the drive end, the center of the lamination stack and closest to the non drive end. A fourth sensor close to the supply connector box measures the ambient temperature that ventilates the frame cooling ribs. The temperature profile along the z-axis could be estimated and the heating time constant and temperature rise over time for different excitation sources could be determined.

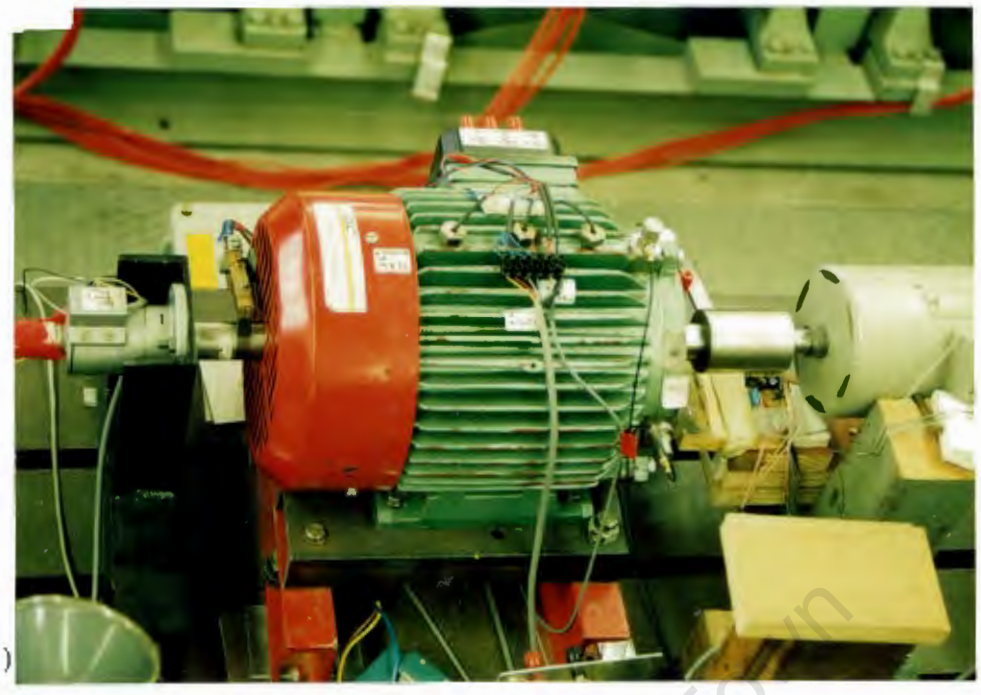

(a)

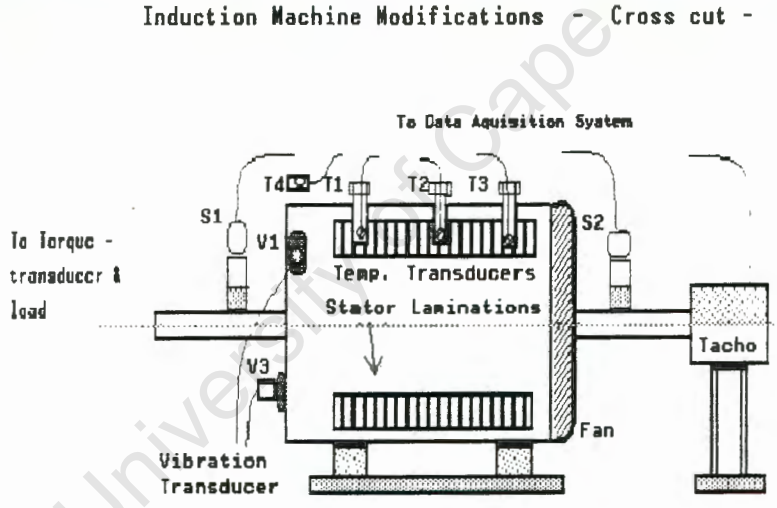


(b).

**Fig. 2.5** Induction motor modifications (a) Motor view, (b) Longitudinal view.

### 2.6.7 Shaft Voltage.

The shaft voltages induced are measured via carbon brushes fitted across the rotor shaft outside the covers and bearings. This is the only non-destructive method possible in industrial applications. The signal is then

amplified by a differential amplifier with suitable CMRR. The shaft voltage signal is passed through a r.m.s. converter. The peak voltage is measured with a Fluke 8024B multimeter at steady state conditions and the maximum value over 30 seconds is recorded.

The voltage drop across the surface between the steel and carbon surfaces is assumed to be relatively small because no current flow across the surface junction.

The two brush positions, S1 and S2, are indicated in Fig. 2.5. A circuit diagram is depicted in **Appendix 2.6.**

### 2.6.8 Vibration Measurement.

Vibrations are measured in all three principal directions, dimensions, thus along the x-, y-, z-coordinates as shown in Fig. 2.6. Piezoelectric accelerometers are fitted on the stator frame , with a layer of bees wax, a thin film of insulation material and the accelerometer mounted on a magnet (contact sensors).

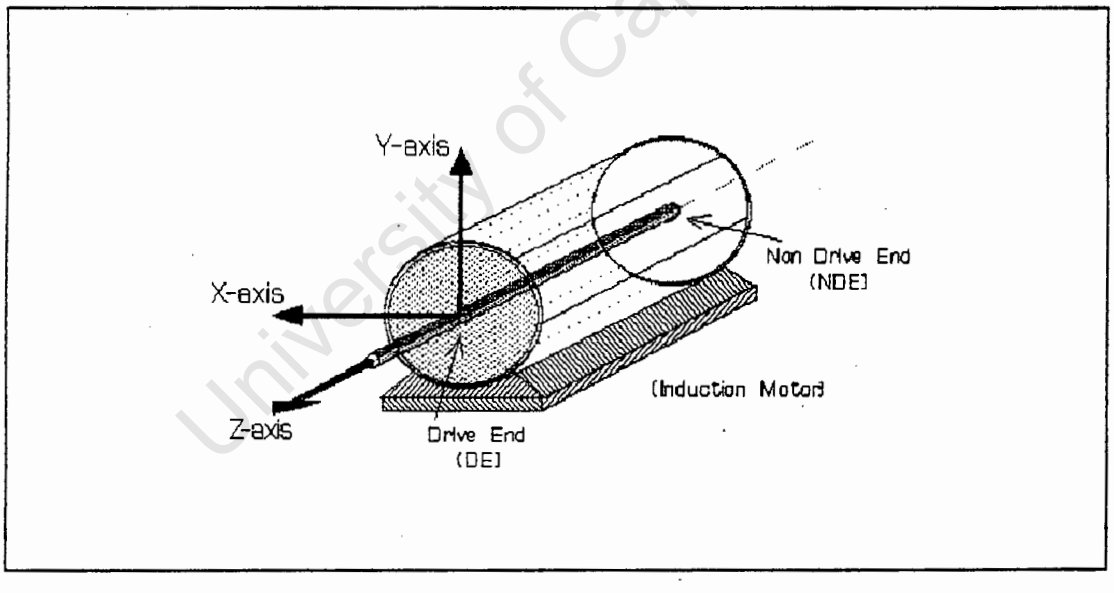




**Fig. 2.6** Vibration components measured, principal measuring coordinates.

Generally the output of the accelerometer is passed through an integrating circuit to give a signal proportional to vibration velocity [2.3]. The signal is then processed via filters, averaging circuits, r.m.s. circuits, peak value and pulse indicators.

Piezoelectric accelerometers (for x-, y-, z- axis), vibration preamplifiers (z-axis) from Bruel & Kjaer and charge preamplifiers from Klag-Swiss (x-, y-axis) were used in measuring vibrations. The preamplifiers were calibrated according to the accelerometer specification to give a proportional voltage signal in [m/sec$^2$]. This x- and y- signals was processed through a true r.m.s. to dc converter to give the equivalent r.m.s. acceleration. (z- direction excluded).

The acceleration signals was sampled at 50 kHz (512 samples) and the respective frequency spectrum analyzed via a fast Fourier transform (FFT) algorithm.

Information on the frequency response of the accelerometers and relevant circuit diagrams are attached in **Appendix 2.7.**

### 2.6.9 External Trigger.

As shown in Fig. 2.1 an external trigger is attached at the shaft to enable the measurement of rotor position with time. This is necessary to ensure that vibrations are sampled for at least one revolution and then processed by a FFT. To determine the torque as a function of position it is also required to have the rotor position over time. The pulses are fed into a synchronizing circuit that can then enables the sampling on active high for 1 to 4 pulses. The number of periods can be preselected. The trigger to the synchronizing circuit can be preselected, such as rotor position, current or voltage zero crossing. To avoid multiple triggering during jittered zero crossing, a negative hysteresis band is incorporated in the circuit. A circuit diagram is attached in **Appendix 2.6.**

## 2.7 Alternative Methods to determine Efficiencies.

The efficiency values determined from measured input and output power includes uncertainties and inaccuracies due to equipment limitations. The difference in efficiencies measured under different excitation sources can be small, eg. less than 1% , and to measure powers with a superior accuracy of 1% is very difficult. In the thesis [2.7] the thermodynamic approach was considered as

an alternative method, measuring the airflow and air temperature of an enclosed induction motor to determine the increase in losses under different excitation sources. To achieve good accuracies in measuring total losses, another promising method was suggested by [2.8], where it is recommended to place the whole induction motor in a thermally isolated oil bath. The energy loss of the induction motor could then be determined from the temperature rise of the oil, were the increase in temperature would have been precalibrated against a known energy transferred to the oil.

## 2.8 Variable Frequency - Variable Voltage Supply Units.

All measurements were performed with different excitation sources with known frequency content. In this project only voltage source inverters, i.e. square wave 6-pulse and PWM were used (Table 2.2). The inverters could be configured for two different operating ranges as shown in Fig. 2.7, namely in the (a) synchronous characteristic $V_r/50$ (0 Hz to 50 Hz) and (b) subsynchronous characteristic $V_r/87$ (0 Hz to 100 Hz) range. The respective airgap flux density was kept constant by keeping the voltage to frequency ratio constant (V/f, constant torque). For frequencies beyond the respective setting the drive is operating in the field weakening range, were the rated torque must be reduced. An initial voltage offset (voltage boost) K could be selected to overcome the resistance at low frequencies.

A VSI implies that a dc voltage appears at the input, ideally with a very small internal impedance. A PWM controls both frequency and voltage by the applied modulation technique. The dc bus for a PWM drive is thus fed by a full diode bridge. In the square wave inverter the V/f constant is controlled separately. The frequency is controlled via the switching frequency of the dc to 3 phase circuit. A feedback circuit controls the dc bus link voltage by means of a fully controlled rectifier, to keep the V/f ratio constant over the operating range.

Limitations on the inverter operation were that the square wave inverter could not be operated in field weakening range for the synchronous configuration. The

sinusoidal generator set was not stable for the subsynchronous configurations for frequencies exceeding 50 Hz.

For all inverter drives the slip compensation was disabled to avoid inherent designed control action to take place during experiments. Slip compensation increases the internal drive frequency proportional as the load increases. Experiments under steady state operation at constant frequency are conducted. The speed range and torque limits are set to extremes (min / max) values respectively.

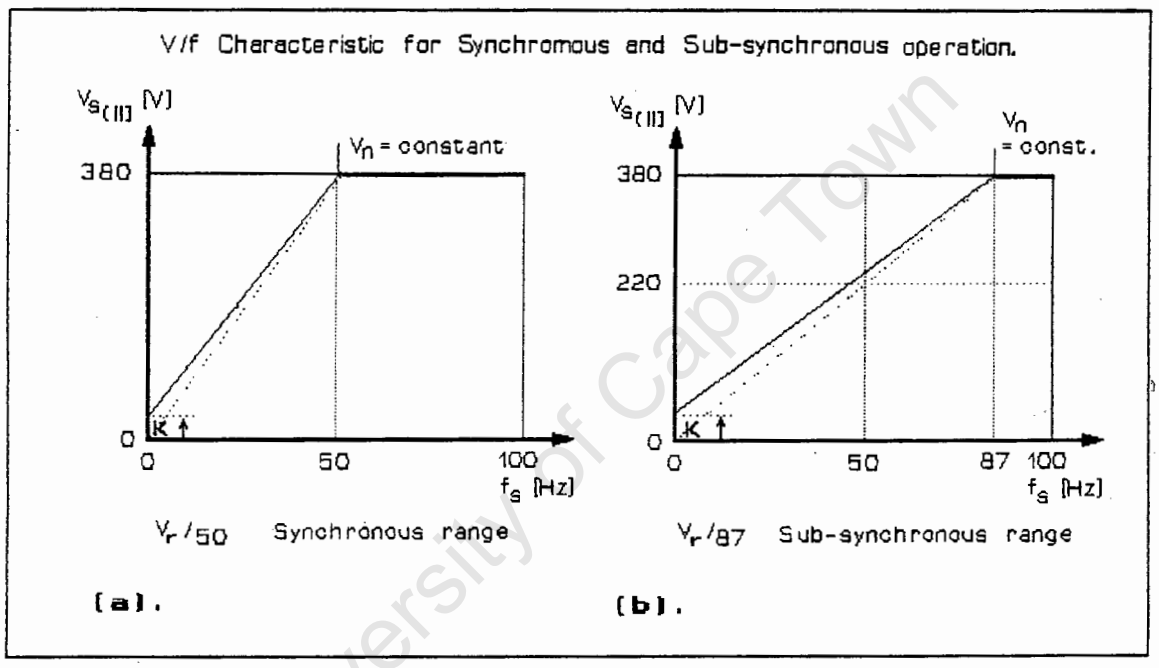


**Fig. 2.7** Voltage/frequency characteristics (a) Synchronous range $V_r/50$ and (b) Subsynchronous range $V_r/87$.

### 2.8.1 Square Wave Inverter.

A 6-Pluse Square Wave inverter is used to investigate the effect of lower time harmonics, as the $5^{th}$ and $7^{th}$ harmonic are very dominant. The VSI Danfoss VLT 5, rated at 5.5 kW is used with external speed control. An equivalent circuit diagram is shown in Fig. 2.(?).a.

### 2.8.2 PWM Inverter.

A Siemens Simovert-P PWM inverter (with pulsed resistor device for braking purposes) is used to investigate the electrical and mechanical performance under an inverter with higher harmonics. The modulation

technique used is sinusoidal PWM, and the drive is rated at 16 kVA.

### 2.8.3 Sinusoidal Excitation.

Variable frequency, variable voltage sinusoidal excitation is obtained with a Ward-Leonard set driving a dc motor output power that in turn powers a synchronous generator output power. The variable frequency can be obtained by varying the armature voltage or controlling the separate field excitation of the dc motor. The variable voltage is controlled by the field excitation of the synchronous alternator. At constant synchronous generator field excitation, a fairly constant V/f ratio is obtained as the synchronous generator is accelerated and the speed increased.

**Table 2.2** Design data of inverters.

| Quantity | PWM Inverter Siemens 6SE1116-2A | Square Wave VSD Danfoss VLT 5 |
|---|---|---|
| Supply voltage | 380/415 V | 380/415 V |
| Drive pf. cos Θ | 0.9 lagging | ≥ 0.8 lagging |
| Output voltage | 15 - 380/415 V | 0 - 380/415 V |
| Efficiency | ≥ 96 % | 91 % |
| Output frequency | 2 - 100 Hz | 0 - 100 Hz |
| Frequency range | $V_r/50$, $V_r/87$ ($2\text{-}100_{F/Weak}$, 2-100) | $V_r/50$, $V_r/87$ ($0\text{-}55_{max}$, 0-100) |
| Rated Output | 16 kVA | 5 kW |
| Rated Current | 25/23 A | 11 A |
| Enclosure | IP 54 | IP 54 |
| Cooling | Forced air cooling | Air, oil cooled. |

# CHAPTER 3. LOSSES, EFFICIENCY AND POWER FACTOR.

## 3.1 Review of Research.

An abundance on literature is available on additional losses of inverter-fed induction motors. Selected papers which in the authors opinion are the most relevant have been reviewed and are also used as reference in this chapter and following chapters.

Paper [3.1] is one of the pioneering papers written in 1968, and is cited in almost all papers relating to losses in induction motors originating from higher time harmonics. A method for calculating losses arising from harmonic currents is shown. An approximate equivalent circuit for the- fundamental and higher harmonics is used. Losses are separated into various separate components, including zigzag losses, stator and rotor end losses and other stray losses. All losses are expressed by mathematical equations. Conclusions are drawn from as series of tests performed for different excitation sources and found that tests and calculated data correlate desirably.

The paper [3.2] investigates additional losses due to time harmonics in the supply, with specific reference to losses due to skew and end leakage fluxes. Methods to calculate these losses are developed and verified with actual measurements taken.

In [3.3] harmonic losses and peak currents are calculated for various operating conditions. It is shown that the fundamental current component is controlled by the load, and the harmonic currents are primarily limited by the leakage inductance and independent of the load condition.

Theoretical performance aspects of PWM supplied motors are studied in paper [3.4]. Emphasis is made with respect to stator losses and winding insulation lifetime. The creation of low frequency parasitic torques is also described and criteria set for them to

occur with specific excitation patterns and machine designs.

Factors affecting ac drive efficiency is investigated in [3.5]. The constant V/f strategy is modified and shown that efficiencies can be optimized using asynchronously generated PWM.

In [3.6] losses from a square wave voltage and 6 pulse current source inverter are calculated. An equivalent circuit, considering the skin effect is used. Stray iron losses due to m.m.f. and permeance harmonics, leakage and skew leakages are considered. Performance of voltage and current fed inverters are compared.

In paper [3.7] characteristics of VSDs (sine, square wave, PWM) are compared. General influences on the performance are discussed. Pulsating torques for six step VSI are graphically explained and the performance capability of standard motors is discussed. The possibility to customize drives and motor units is considered.

A model based on the motors design parameters (rotor bars), power rating between 1 kW and 1000 kW (for iron and space fundamental losses) has been developed in [3.8] to estimate time harmonic dependant losses. A bandwidth of 100 Hz to 20 kHz is considered. Losses are estimated separately and design specifications are considered (rotor bars).

In paper [3.9] torques and losses are calculated for PWM and auto sequentially commutated (ASC) CSI supplied medium sized induction machines. Losses are calculated as a ratio to nominal fundamental loss for all harmonic components. Each harmonic loss component is multiplied by a constant depending on the individual skin effect of a specific current harmonic. It is shown that harmonic losses at no load and rated load are almost equal. Torque ripples as a function of rated torque are calculated and presented. The measurements are however performed on medium sized 45 kW and 25 kW motors.

In paper [3.10] additional losses for different types of inverters (CSI, PAM, PWM) are calculated according to some standard and empirical formulas taking account

of stray losses and the current displacement due to higher supply time harmonics. A comparative study of losses for different ratings of standard machines has been performed.

The paper [3.11] discusses a method to calculate the performance of inverter-fed induction machines. Performance for low speed operation with - and without initial voltage boosting, to overcome the winding resistance, were performed. Parameter variation with respect to frequency is analyzed for a single cage rotor (machine rated at 7.5 kW) and found to be significant. It is furthermore found that the output torque is insignificantly affected by higher time harmonics.

In paper [3.12] experimental results of iron losses caused by alternating and rotating magnetization of various frequencies and flux densities are measured.

A method to analyze rotor current, fluxes, voltages and losses is developed in [3.13]. All calculations are done separately for each harmonic. The derived results are used to calculate power, efficiency of a motor. An analysis is performed for a current source inverter-fed induction motor and compared to sinusoidal excitation.

In paper [3.14] a brief discussion of losses in voltage and current fed inverters is undertaken. Calculations for losses in separate components (core losses, rotor losses, stator losses etc.) are performed for different pulsing patterns and the calculated results are compared to measured values. The relative increase in losses compared to sinusoidal excitation is provided for a squirrel cage induction machine, rated at 15.3 kW.

In paper [3.15] additional time harmonic losses in the motor and inverter are described. Losses in the inverter a highlighted as they should be considered as losses being part of the actual drive unit.

In papers [3.16, 3.17] a simulation of performance (efficiency, power factor, stray losses) of double cage induction rotor machines is performed in for sinusoidal, PWM and Square Wave supplies. Results are

listed for a 5.5 kW and 7.5 kW double cage induction motor.

In paper [3.18] directly measured inverter and machine efficiencies are obtained with a digital sampling system. A very good accuracy could be obtained. Tests were performed over a wide range of frequencies for PWM excitation. In the field weakening range the efficiencies are reduced, as the supply was a quasi block voltage supply.

In paper [3.19] The influence of time harmonic frequencies on losses in inverter-fed induction machines is examined. Special emphasis is given to very high switching frequencies (15-25 kHz). Theoretical models indicate the loss - frequency dependance. Some experimental measurements indicate similar trends.

## 3.2 Inverter Output Voltage.

The rich harmonic content of inverter outputs as shown if Figs. 3.1, 3.2, 3.3 and 3.4 relative to the fundamental may have significant effects on the motor performance, mainly on the efficiency and the power factor of the induction motor.

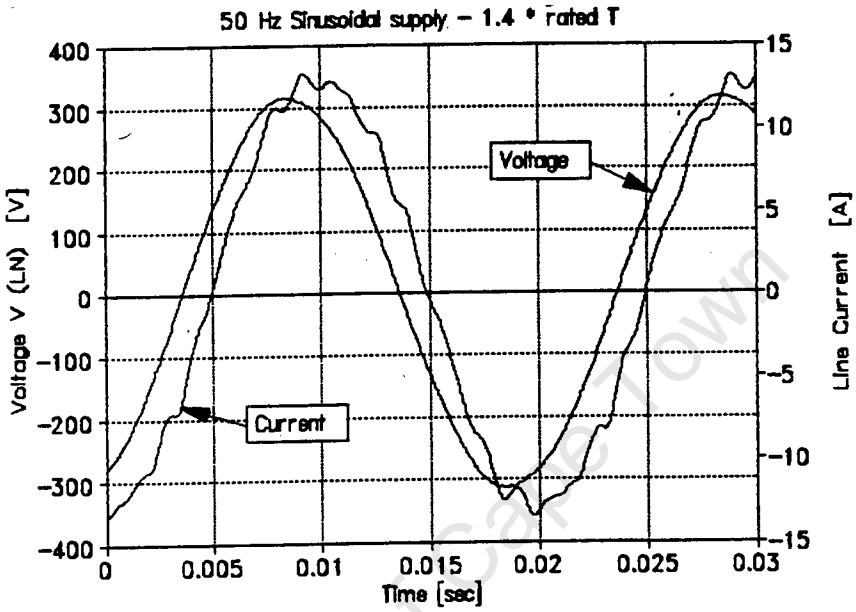


Fig. 3.1 Voltage and current supply under sinusoidal excitation. ($V_r/50$), Load condition.

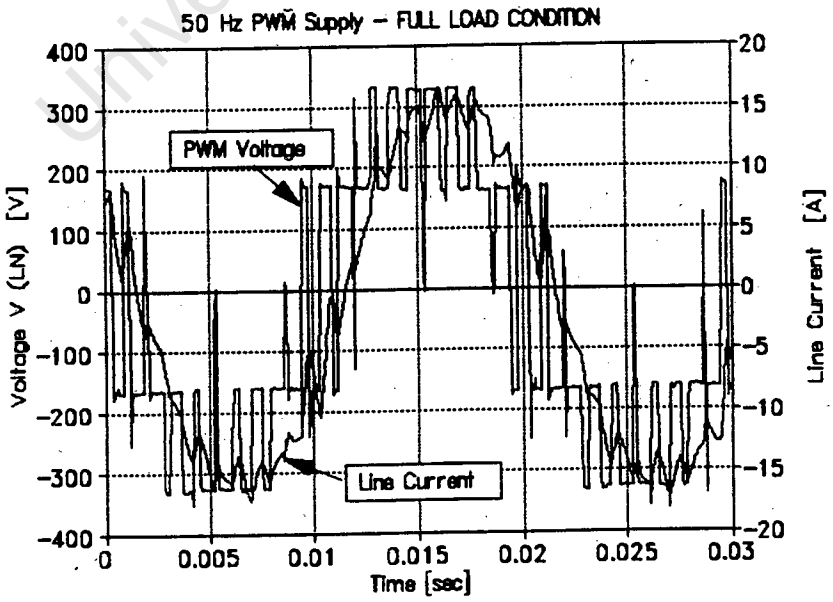


Fig. 3.2 Voltage and current supply under PWM excitation. ($V_r/50$), Load condition.

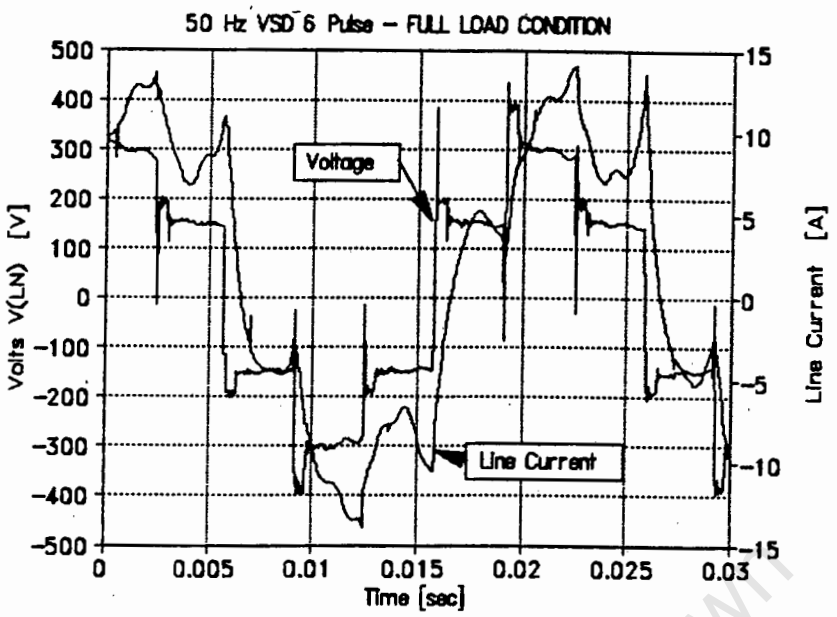


**Fig. 3.3** Voltage and current supply under square wave excitation. ($V_r$/50), Load condition.

The line voltages $V_a$, $V_b$, $V_c$ contain only odd harmonics, $n = 6k \pm 1$ for $k = 0, 1, 2, 3...$ The sign indicates the direction of the phase rotation. In case of 3 phase systems the triplen harmonics are co-phasal and thus absent. It is assumed that the phases are balanced and thus the fundamental and higher harmonics are balanced but shifted 120° in phase which each other. For delta connected motors (as in the thesis) the line and phase voltages are identical. As triplen harmonics are absent no circulating currents exist in the windings, which otherwise would contribute to additional heating. For star connected motors with floating neutral the phase voltages are the same as the inverter output phase voltages with triplen harmonics removed.

The current signal for sinusoidal excitation under load condition has a superimposed harmonic oscillating current due to saturation in the stator slots (9 slots per pole) and resulting permeance waves in the airgap. These are present in the associated frequency spectrum in Fig. 3.4.a at approximately 600 Hz and 800 Hz. A third harmonic component, although insignificantly small, is present in the frequency spectrum. This originates from very small phase unbalances.

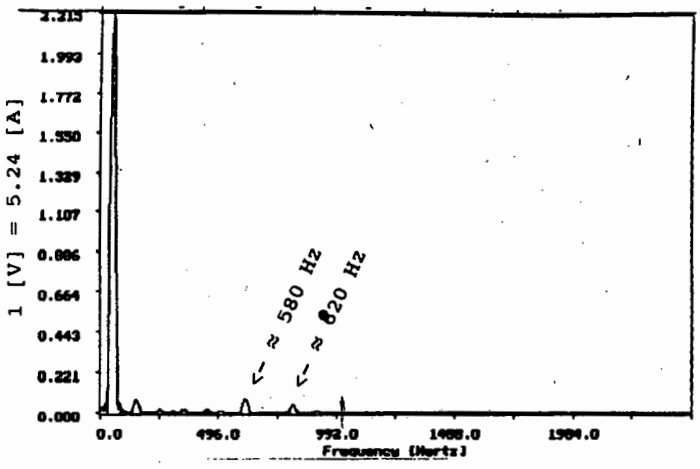


(a).

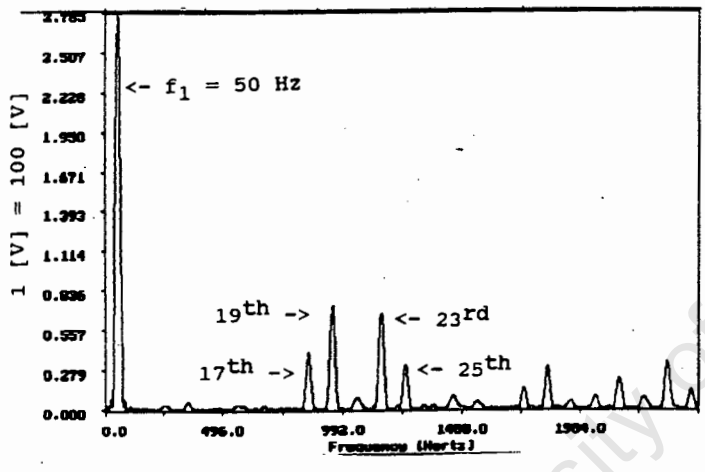


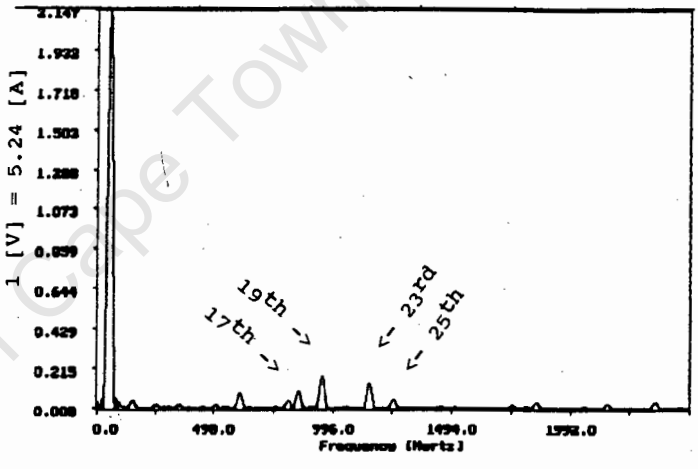


(b).

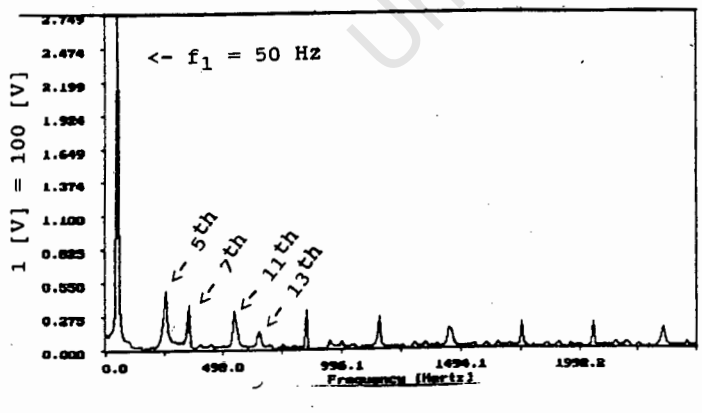


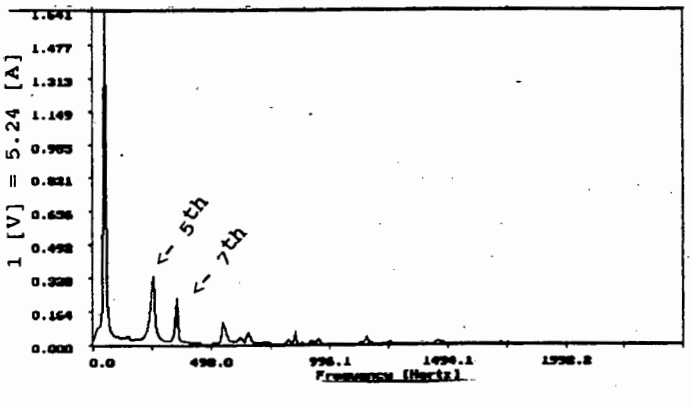


(c).

Fig. 3.4 Voltage and current frequency spectra of Figs. 3.2, 3.3 and 3.1 under load condition, for (a) Sinusoidal, (b) PWM, (c) Square wave excitation.

The order and magnitude of the predominant current harmonics depends on the inverter design as well on the motor design. Generally low order harmonics are (n = 5,7 11,13) present in square wave inverters and higher order harmonics (n = 17,19, 23,25 etc.) as sidebands in PWM inverters for a modulation frequency $f_m$ of 21 times the fundamental frequency.

Additional voltage and current signals, their respective frequency spectra under no load conditions are given in **Appendix 3.1.**

In balanced 3 phase induction motors the airgap contains odd positive sequence components (3k + 1) [k=0,1,2,..] thus 1, 7, 13, 19, ..., the negative sequence components of (3k + 2) thus 5, 11, 17, 23, ... and (3k + 3) are the zero sequence triplen harmonics.

Each harmonic current present in the input current produces a rotating m.m.f., with the same number of poles as the fundamental field, but rotating at higher synchronous speed than the fundamental. Losses and torques are produced in the same way as by the fundamental component.

## 3.3 Losses of Inverter-Fed Induction Motors.

The losses in induction motors consist of winding (copper) losses in the stator and rotor core losses, rotational losses and stray losses. The winding, core and stray losses are increased by additional higher time harmonics present in inverter supplies. Rotational losses. i.e. friction, windage and ventilation losses are independent of harmonics. Analysis of increased losses requires assessment of the inverter output voltage frequency components via any method, eg. digital implemented Fourier transform as used in Fig. 3.4.

Additional losses can be divided into fundamental frequency losses and high frequency losses induced by higher time harmonics. These higher time harmonics in the supply create m.m.f. harmonics in the rotor.

High frequency (stray) losses have the following subsequent components [3.20].

(i). Surface losses in stator and rotor.

(ii). Pulsation losses in stator and rotor teeth.

(iii). Losses in the squirrel-cage winding.

(iv). Losses due to skewing in uninsulated cast aluminium squirrel-cage windings.

### 3.3.1 Winding (copper) Losses.

Winding losses are substantial in both, stator (primary) and rotor (secondary) side as harmonic currents contribute to the total r.m.s. input current.

The skin effect in the stator windings, especially for round wires with small diameter is negligible and can be neglected. If the primary conductor depth is appreciable (e.g. Roebel's bars) for larger machines, the skin effect must be taken into consideration.

The skin effect, especially in cage type windings, influence the rotor losses considerably. Slot imbedded bar conductor resistance and inductance varies according a general pattern. The resistance increases approximately proportional to the square of the frequency and the inductance inversely proportional to the square of the frequency, according [3.19]. At even higher frequencies the effect is proportional or inverse proportional to $\sqrt{f}$ for resistance and inductance respectively because the skin depth is small compared to the conductor size, [3.19]. The frequency with respect to the rotor is given by equation (2.3).

The stator **harmonic current** can be represented by a well known approximation:

$$I_n \approx \frac{V_n}{\sqrt{\{ (R_{1n} + R_{2n'})^2 + (2\pi\ n\ f_1\ (L_{1n} + L_{2n'}))^2 \}}} \qquad ...(3.1)$$

For medium and large power motors:

$$(R_{1n} + R_{2n}) << 2\pi\ n\ f_1(L_{1n} + L_{2n'}) \qquad ...(3.2)$$

i.e. the reactive terms (leakage) are much larger than the resistive parameters at higher frequencies. Accuracy is thus maintained [3.11]. This is especially the case in the rotor due to high frequency harmonics with nearby unit slip. For voltage source inverters it is thus evident that Joule's losses are inversely proportional to the leakage reactance square, since

$$I_{1n} \approx \frac{V_n}{2\pi\ n\ f_1(L_{1n} + L_{2n'})} \qquad ...(3.3)$$

It must be realized that formula (3.3) is very approximate. The total winding losses in the rotor and stator are calculated from the fundamental and the sum of all higher harmonic elements considering the skin effect in the motor parameters, i.e.:

$$P_1 = 3 \sum_{n=1}^{\infty} I_{1n}^2\ R_{1n}\ K_{r1} = \Sigma\ P_{1n} \qquad ...(3.4)$$

$$P_2 = 3 \sum_{n=1}^{\infty} I_{2n}^2\ R_{2n'}\ K_{r2n} = \Sigma\ P_{2n} \qquad ...(3.5)$$

As in practice the leakage reactance will decrease by the deep bar effect, the harmonic currents will increase. Due to high frequency currents in the rotor the skin effect causes the rotor resistance to increase.

The resistance multiplication factor due to the skin effect can be represented as :

$$K_{r1n}(m,f_{1n}) = R_{ac}(m,f_{1n}) / R_{dc} \qquad ...(3.6)$$

$$K_{r2n}(m,f_{2n}) = R_{ac}(m,f_{2n}) / R_{dc} \qquad ...(3.7)$$

were m = number of conductor sets, $f_{1n}$ and $f_{2n}$ are the frequencies in the stator and rotor respectively, $f_{1n} \approx f_{2n}$, $R_{ac}$ = ac current resistance, $R_{dc}$ = dc current resistance.

The factors $K_{r1n}$ and $K_{r2n}$ depend on machine design and material used, but detailed information can be found in literature.

In papers [3.4, 3.3, 3.9, 3.18] the skin effect is determined analytically considering conductor size, windings and slot dimensions.

The end ring resistance also increases due the skin effect, i.e. the way the currents enter the ring [3.19].

The reduction in the leakage reactance is much less than anticipated, as only the slot teeth portions are affected considerably. Harmonic currents tend to increase the saturation of the magnetic paths and thus reduce the leakage reactances $X_1$ and $X_2$ as said, thus increasing the fundamental harmonic currents and thus fundamental winding (copper) losses. The variation of leakage is also strongly dependant on motor design details, [3.8].

The total winding losses $P_w$ are:

$$P_W = P_1 + P_2 \qquad ...(3.8)$$

Losses in the rotor bars are the main contributor to additional losses [3.1].

In the paper [3.19] a frequency dependant loss approximation for stator ($P_{1n}$) and rotor ($P_{2n}$) losses is derived to be proportional to:

$$P_{1n} \alpha V_n^2 * f_n^{0.3} \qquad ...(3.9)$$

$$P_{2n} \alpha \frac{V_n^2}{f_n^{1.2}} \qquad ...(3.10)$$

Relations (3.9) and (3.10), although approximate, clearly indicate that the harmonic rotor conductor losses are significantly reduced as the time harmonic frequencies increase. Only a small resistance increase due to harmonics occurs in the stator, with typical wire size such that little skin effect occurs.

The amplitude of the harmonic currents is fairly independent of operating conditions, but a small increase (5% to 10%) in current amplitude under full load as compared to no load condition has been observed on the frequency spectrum, given in **Appendix 3.1.** It is however generally assumed and stated that only the fundamental component is load dependant [3.15], [3.5] as for n > 1 the slip $s_n \approx 1$ and remains constant.

The marginal increase in harmonic current amplitude originates from secondary effects, such as the approximation $s_n = 1$ for higher harmonics. In fact, the fractional slip for the $5^{th}$ and $7^{th}$ harmonic are 6/5 and 6/7 respectively. As the harmonic order increases the slip approaches unity as discussed.

Losses are influenced by parameters such as material, temperature, slot shape and short circuit end ring values. A deviation of up to 25% in relative losses can be present [3.8] which highlights the importance of considering inverter compatible designed machines.

### 3.3.2 Core Losses.

A number of important factors must be considered, the main flux core losses due to time harmonics are very small and can be neglected in approximate calculations.

If the skin depth in the core is small compared to the lamination thickness the penetration depth is approximately one skin depth [3.19]. The leakage paths are altered by the redistribution of the conductor currents due to the skin effect. Eddy currents induced in the iron produce a reaction field that opposes the inducing fields with larger effect at higher loads.

A well established equation to determine the **eddy current** and **hysteresis losses** for fundamental harmonic is:

$$P_{Fe1} = P_E + P_H = ( k_E * B^2 * f_n^2 + k_H * B^2 * f_n ) * V_{CV} \qquad ...(3.11)$$

where $k_E$ = eddy constant
$k_H$ = hysteresis constant
$V_{CV}$ = Core volume
B = Magnetic flux density in core
$f_n$ = frequency of induced harmonic.

In a paper [3.11] the total core losses including harmonic losses are expressed as follows:

$$P_{Fen} = P_{Fe1} \sum_{n=1}^{\infty} \left[\frac{V_{1n}}{V_1}\right]^2 \left[\frac{f_1}{f_{1n}}\right]^{0.7} \qquad \ldots(3.12)$$

were $P_{Fe1}$ is the iron loss due to the fundamental frequency (3.11), $V_1$ the fundamental stator voltage, $f_1$ the fundamental stator frequency, $f_{1n} = nf_1$.

Square wave inverters have lower frequency harmonic components than PWM inverters, but the inverter supplied voltage amplitude is comparable.

According to (3.12) the iron losses for the $5^{th}$ harmonic are twice as high as the losses for the $7^{th}$ harmonic for square wave inverter. The $7^{th}$ harmonic iron loss has a similar magnitude as the $20^{th}$ and $22^{th}$ harmonic iron loss, at an amplitude of 0.2 of the fundamental voltage amplitude. This clearly indicates that losses for PWM inverters are very dependant the pulsing and modulation pattern implemented.

### 3.3.3 Stray Losses.

Stray load losses (Heller and Hamata [3.20], Chapter 9.), (Alger [2.9] pp.123 - 192) due to increased induced harmonic currents (and permeance waves - dependent on motor design) become much more dominant in inverter-fed motors. These increased additional eddy current losses are due to increased leakage fluxes and high frequency pulsations of these fluxes. The loss magnitudes in small induction motors with relative small magnetic circuits will be smaller than the winding and rotor-cage losses.

Stray losses, paper [3.11], given in equation (3.12) can be determined if the fundamental stray losses $P_{str1}$ are known by following empirical relation.

$$P_{str} = P_{str1} \sum_{n=1}^{\infty} \left[\frac{I_{1n}}{I_1}\right]^2 \left[\frac{f_{1n}}{f_1}\right]^y \qquad ...(3.12)$$

were $P_{str1}$ stray losses due to the fundamental frequency

$I_1$ fundamental stator current
$f_1$ fundamental stator frequency
$n$ Harmonic $n^{th}$ component.
$y$ exponent assumes a value between 1 ... 1.5, depending on machine rating and construction.

The stray losses due to the fundamental frequency according to IEC Standards are $P_{str1} = 0.005\ P_{out}$. Stray load losses $P_{str1}$ according to [2.4, JEC 1979, Japan] at output P [Watt] is considered to be approximately equal to:

$$P_c = 0.005 \frac{P^2}{P_r} \qquad ...(3.13)$$

were P is the load condition and $P_r$ the rated output.

Equation (3.12) implies that the stray losses are proportional to the harmonic frequencies and proportional to the square of the $n^{th}$ current harmonic.

Stray losses under to PWM excitation with prominent frequency components at higher frequency ($21^{st}$ harmonic sidebands) have higher stray losses than under Square Wave excitation. Substituting a value of y = 1.2 in (3.12) the losses between the $5^{th}$ harmonic and the $20^{th}$ harmonic stray loss increase approximately six times for the same harmonic amplitude.

### 3.3.4 Rotational Losses.

Friction, windage and ventilation losses are independent of harmonic content of the supply. It is generally assumed that losses are proportional to the rotational speed. This implies for lower speed operation reduced rotational losses and for subsynchronous speeds a relative increase, especially due to increased

ventilation losses for fan self-ventilated motors, where the fan load is proportional to the square of the r.p.m. speed.

## 3.5 Influence of Higher Time Harmonics on the Efficiency.

Motor efficiencies increase with increase in rated motor power, which thus implies that the per unit loss for larger machines decreases. This has been investigated in eg. paper [3.10].

The PWM modulation technique generates near sinusoidal currents ($5^{th}$, $7^{th}$ harmonics are eliminated) at up to synchronous speeds, but at higher frequencies (thus higher voltage) to maintain the V/f ratio, quasi block voltages are generated. In the field weakening range quasi block voltages are modulated which then could have low order time harmonic components ($5^{th}$). This is shown in **Appendix 3.2.**

In six pulse square wave inverters a block voltage with dominant low order harmonics ($5^{th}$, $7^{th}$) are present over the whole operating range as the dc bus voltage is controlled to keep the V/f ratio constant. It must also be pointed out that the weak field excitation range is reduced by high leakage reactances.

It is thus evident that the efficiency in the field weakening range for PWM inverter-fed motors is reduced due to:

(i) lower order current harmonics present.

(ii) increased losses due to higher pulsing frequency.

The efficiencies for the PWM inverter-fed induction motor in the constant torque range increases as the design-rated operating conditions (i.e. rated output, 3-kW in this case) are reached.

The relative decrease in efficiency with operating frequency in Square Wave inverter-fed motors will not be as dominant as for PWM drives, as the harmonic content remains constant and only the frequency increases. (This could not be measured but is predicted for the field weakening range).

For the subsynchronous characteristic inverter configuration ($V_r$/87 - 0 Hz to 100 Hz) the efficiencies increase as the operating frequency rises. Thus the relative p.u. losses decrease as the voltage and frequency rise and the supply configuration is near rated conditions. The low frequency voltage boost selected will affect the performance in the low speed operating range. As the voltage boost to overcome the resistance at low frequency (V/f ratio) during the measurements was very low (K ≈ 2%), the pullout torque at low speeds is far below rated torque [3.11]. The efficiency is thus reduced considerably at low fundamental operating frequencies as seen from Fig. 3.7.

To keep the airgap flux at a constant level as the frequency is increased, the ratio E/f (see Fig. 2.3) must remain constant, were E is the air gap e.m.f. As the stator voltage $V_1$ and fundamental frequency $f_1$ decrease, the total impedance of the motor is reduced as well. Consequently the relative stator current $I_1$ and the relative stator winding losses increases. If the ratio V/f remains constant the voltage drop across $R_1$ increases relative to the applied stator voltage, as the voltage is reduced. The pull out torque is proportional to $(E/f)^2$ and for constant torque operation additional voltage boost is required at low speeds to overcome the voltage drop. The slip will then be reduced and efficiencies at low operating speeds will increase.

The efficiencies at higher loads increase initially to a maximum, which is near the designed rated power (± 10%). It is clear as the harmonic losses at rated load are almost as high as under no-load conditions, because the harmonic currents are hardly effected by load conditions [3.1]. It can be observed from Fig. 3.5 that the losses at high load currents (loads) for PWM and square wave excitation do not increase more significantly as compared to the increase in losses with load current for sinusoidal excitation. This validates the fact that losses due to higher time harmonics are relatively load independent.

(a).

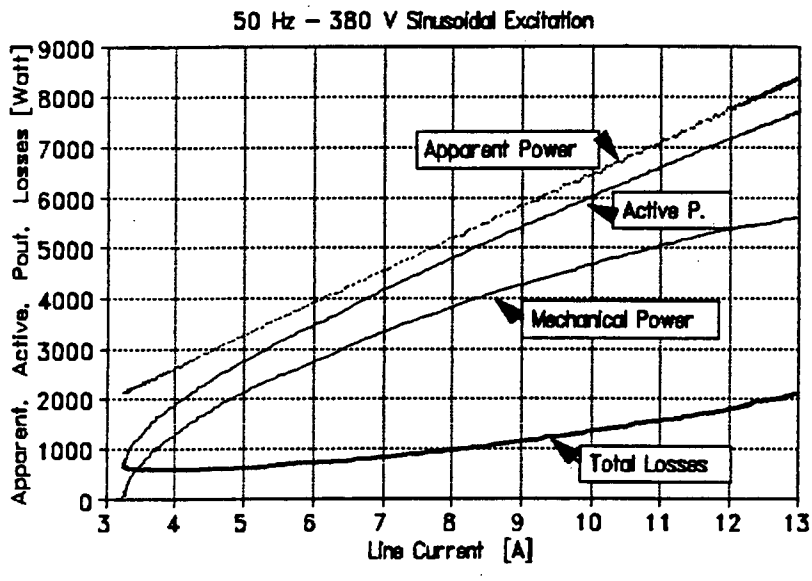


(b).

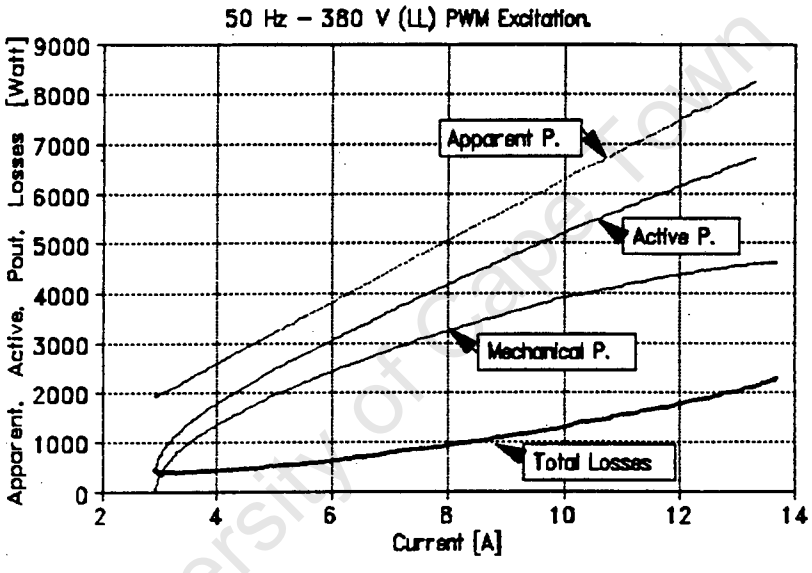


(c).

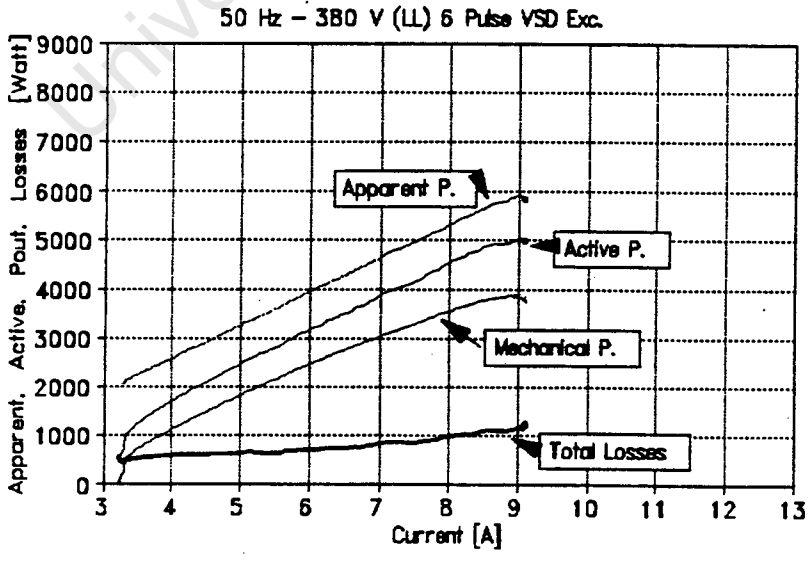




**Fig. 3.5** Input Power (Apparent and Active), Output Power and Losses for inverter excitation: (a) Sinusoidal, (b) PWM, (c) Square Wave excitation.

The performance measurements at maximum efficiency for each specific load test with different fundamental frequency were taken. The accuracy of the measurements can be said to be in the region of 1%. The intensive calibration procedures and repeatable measurements give sufficient confidence. Furthermore were all measurements taken with the same equipment and general trends can clearly be deduced from Figs. 3.6 and 3.7.

**Table 3.1** Efficiency and Losses compared to Sinusoidal excitation (configured for $V_r/50$), for different excitation sources.

| Freq. [Hz] | Efficiency in percent | | | Reduction in Efficiency, compared to Sine Exc. | | |
|---|---|---|---|---|---|---|
| | Sine | PWM | SQWave | PWM | SQWave | (%) |
| 10 | ---- | 52.4 | ---- | ---- | ---- | |
| 20 | ---- | 62.35 | 62.13 | ---- | ---- | |
| 30 | 75.3 | 72.9 | 70.3 | 2.4 | 5.0 | |
| 40 | 78.2 | 74.93 | 74.4 | 3.27 | 3.6 | |
| 50 | 80.1 | 79.4 | 78.8 | 0.7 | 1.3 | |
| 60 | 78.7 | 76.0 | ---- | 2.7 | ---- | |
| 70 | 76.3 | 71.8 | ---- | 4.5 | ---- | |

**Table 3.2** Efficiencies and Losses for PWM and Square Wave excitation (configured for $V_n/87$).

| Freq. [Hz] | Efficiencies for subsynchr. excitation, $V_r/87$. | | | Increased losses (SQWave exc. - PWM exc.) ( % ) |
|---|---|---|---|---|
| | Sine | PWM | SQWave | |
| 10 | ---- | 42.5 | ---- | ---- |
| 20 | ---- | 53.8 | ---- | ---- |
| 30 | ---- | 60.4 | 57.8 | 2.6 |
| 40 | ---- | 64.23 | 63.3 | 1.03 |
| 50 | ---- | 68.0 | 66.5 | 1.5 |
| 60 | ---- | 70.3 | 68.5 | 1.8 |
| 70 | ---- | 73.16 | 71.5 | 1.66 |

**Table 3.3** Increase in Losses referred to Sinusoidal excitation. for different excitation sources.

| Freq. [Hz] | Increase in percentage losses for PWM and Square Wave excitation compared to total percentage losses at sinusoidal excitation. | | | |
|---|---|---|---|---|
| | Sine (total loss) | PWM (% increase) | Square Wave (% increase) | |
| 30 | 24.7 | 9.72 | 20.24 | |
| 40 | 21.8 | 15.0 | 16.51 | |
| 50 | 19.9 | 3.52 | 6.53 | |
| 60 | 21.3 | 12.68 | ---- | |
| 70 | 23.7 | 18.99 | ---- | |

For the subsynchronous characteristic ($V_r/87$) configuration the 6 pulse square wave inverter driven induction motor is approximately 1.5% less efficient as compared to the efficiencies obtained for PWM excitation. This can clearly be seen in Fig. 3.7.b.

(a).

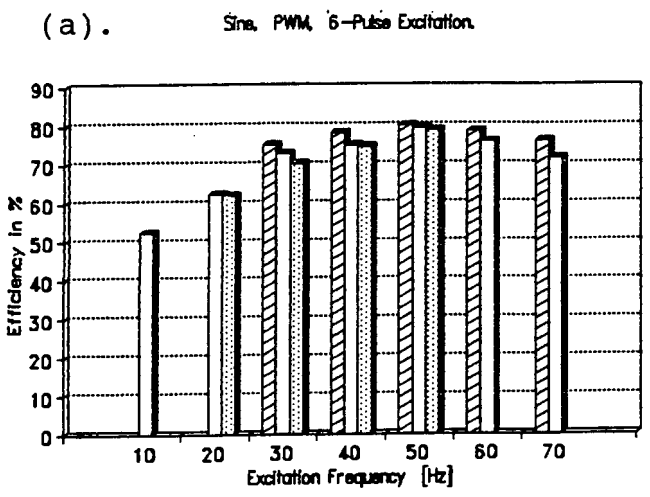


(b).

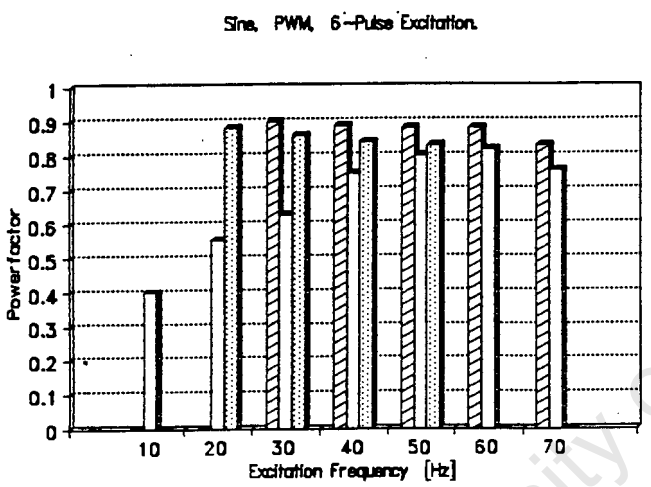


(c).

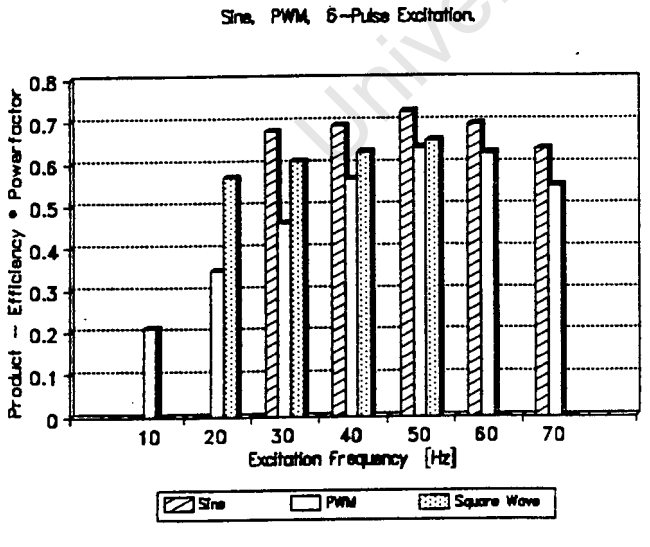


Fig. 3.6 Synchronous configuration ($V_r$/50).
(a) Efficiencies
(b) Power factor
(c) Pf. * Eff vs slip.

(a).

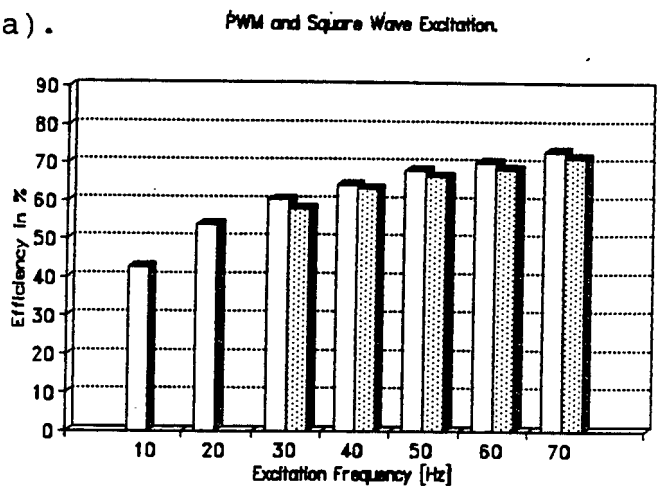


(b).

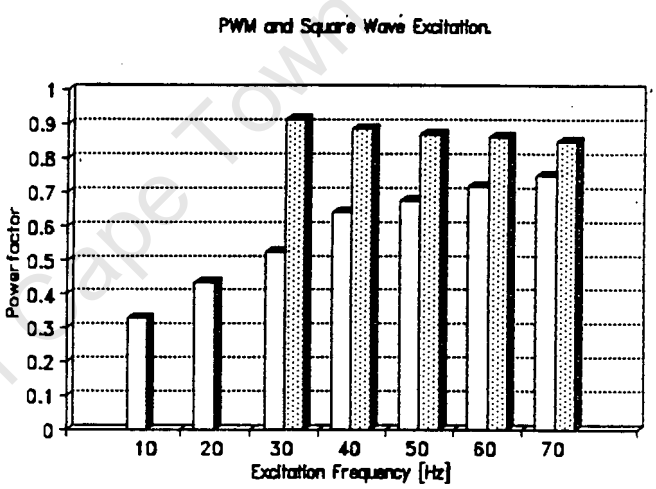


(c).

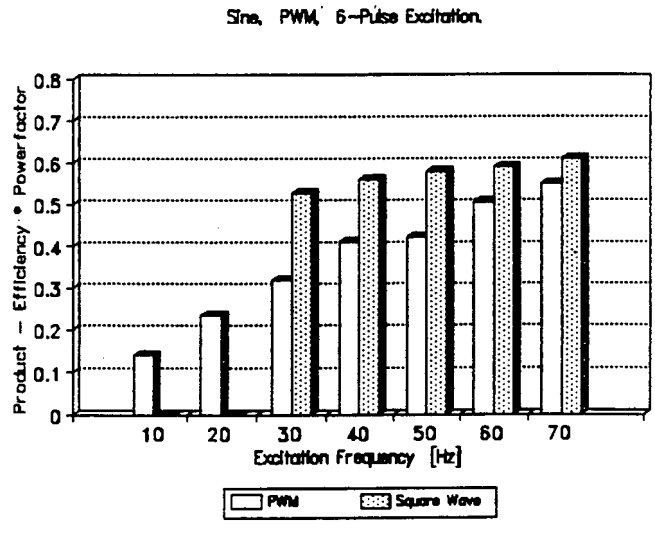


Fig. 3.7 Sub-synchronous configuration ($V_r$/87).
(a) Efficiencies
(b) Power factor
(c) Pf. * Eff vs slip.

(a).

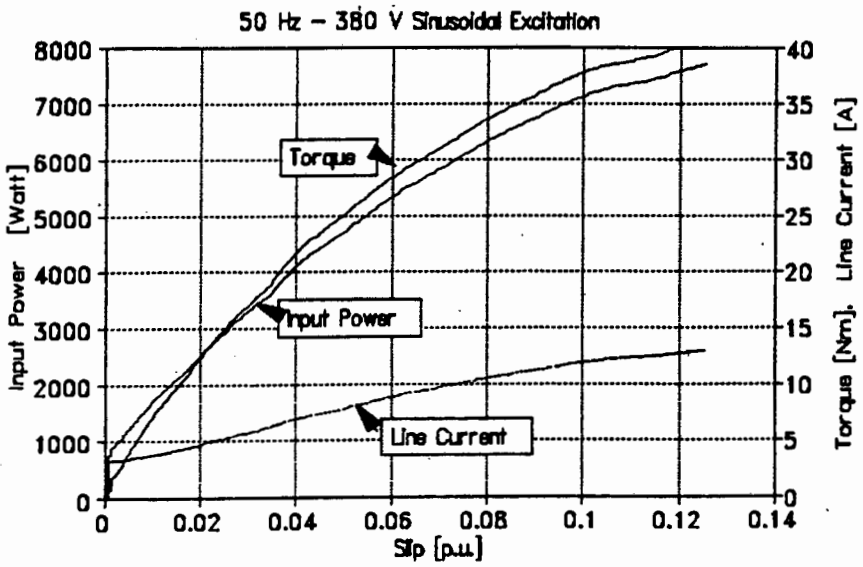


(b).

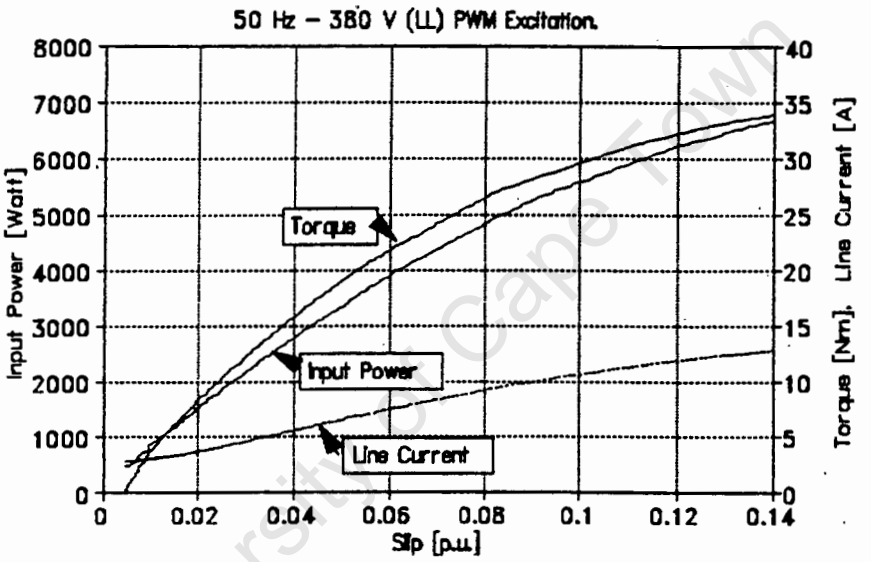


(c).

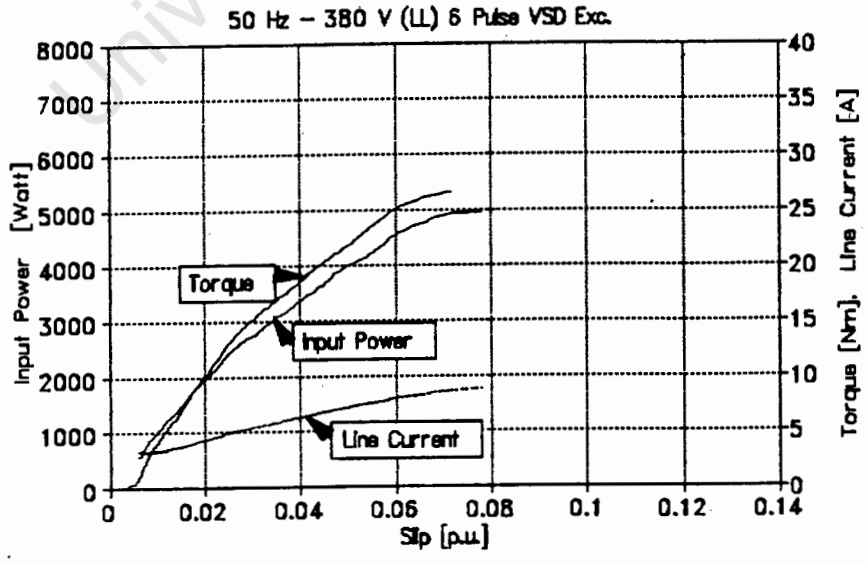


**Fig. 3.8** Performance Characteristics - Power, Torque and Current vs slip. Configured for ($V_r$/50). (a) Sinusoidal, (b) PWM, (c) Square Wave excitation.

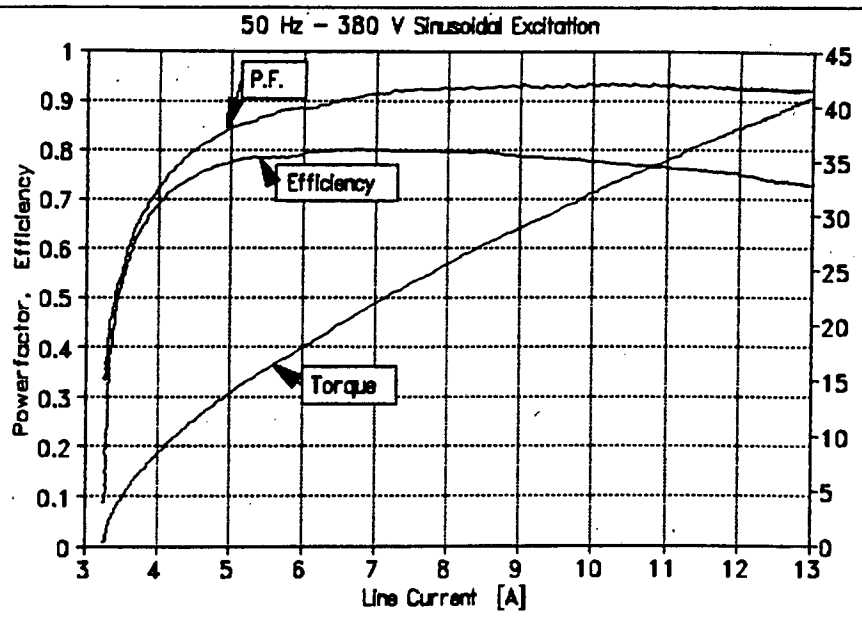


(a).

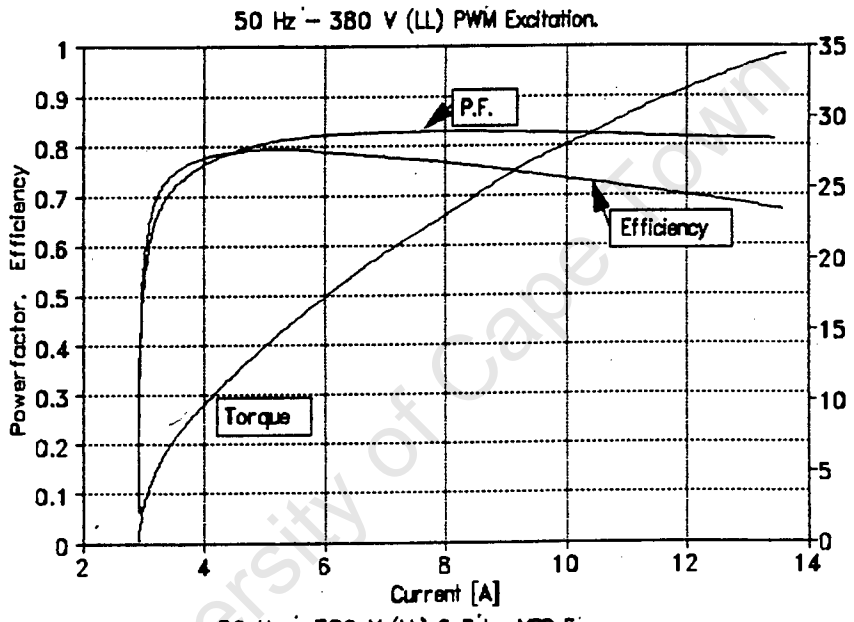


(b).

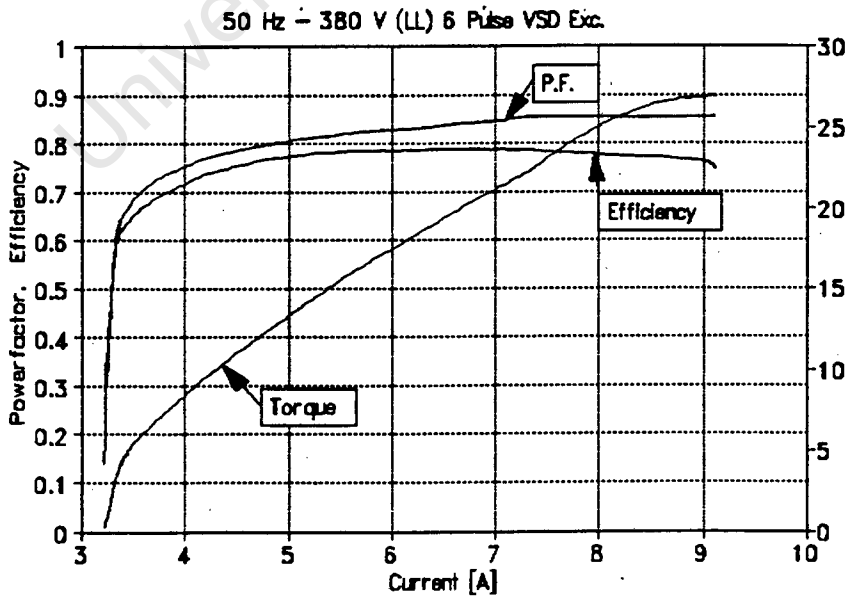


(c).

**Fig. 3.9** Load Tests - Efficiency ($\eta$), Pf. and Torque vs Current, configured for ($V_r/50$). (a) Sinusoidal, (b) PWM, (c) Square Wave excitation.

At operation above rated power the efficiency decreases steadily due to saturation and higher winding (copper) losses, both from the fundamental and harmonic currents. This can clearly be observed in Fig. 3.9.

The induction motor efficiency is reduced between 0.7% and 5% for different operating points when fed from an inverter configured for synchronous operation characteristic ($V_r/50$) as compared to sinusoidal excitation. (See Table 3.2 and Fig. 3.6). The losses due to higher time harmonics compared to the losses for sinusoidal excitation increased between 3.5% and 19%. The losses for PWM excitation for all operating points are marginally lower than those for 6-pulse square wave excitation. The results correlate well with those measured and simulated for a low power double cage induction motor in the paper [3.16, 3.17], except that the losses are almost twice as high, which is expected due to increased rotor bar losses in the double cage, which are significant. The losses would be marginally lower if the motor tested would have a non-skewed rotor.

Furthermore, compared to efficiencies calculated in a paper [3.14] for a 15.3 kW rated motor, lower efficiencies have been obtained. This is in line with measurements for a smaller machine determined in [3.10], as the p.u. losses for smaller machines is higher as compared to larger machines. This is mainly due to the increased p.u. losses arising from the fundamental component. The p.u. time harmonic losses do not vary significantly between low power and larger machines as shown in [3.10].

The efficiency $\eta$ pattern is as predicted, PWM marginally less efficient than for sinusoidal excitation and more efficient than square wave excitation.

$$\eta_{\cdot SIN} > \eta_{\cdot PWM} > \eta_{\cdot SQW}$$

were SIN indicates sinusoidal, PWM Pulse Width Modulated and SQW square wave excitation.

At low excitation frequencies it is predicted that the efficiencies will increase if the V/f ratio is boosted initially. This is the case as higher torque will be

produced and thus the ratio between input and output power increased.

In literature [3.14] it is estimated that losses due to time harmonics increase by 19% to 42% for PWM and Block-like PWM respectively as compared to sinusoidal excitation for a squirrel cage 15.3 kW induction motor. This seems relatively high. A reduction in efficiency is predicted between 2% and 4%. These trends are however comparable with measurements performed, but losses measured were not as high as predicted in [3.14]. Also the p.u. losses measured for PWM are lower as for square wave excitation. Measurements performed by Klingshirn and Jordan [3.1] show an increase of 20% in the losses (at 60 Hz) for a square wave inverter for a 20 hp motor.

An important fact to note is that the efficiency increases as the operating point gets closer to the rated conditions. It could not be investigated weather the efficiency improves for constant V/f beyond the rated 380V/50 Hz at $V_r/50$ configuration. Compared to the increasing efficiency for $V_r/87$ configuration as frequency increases, it can be deduced that the efficiency for $V_r/50$ would increase if sufficient voltage reserve would be available to keep magnetizing current (and thus the airgap flux) constant for frequencies above 50 Hz. As the V/f ratio is decreased (field weakening range) the efficiency too is reduced.

## 3.6 Influence of Higher Time Harmonics on the Induction Motor Power Factor.

The power factor (Pf) is substantially influenced by higher time harmonics in the induction motor supply. The power factor at which the drive operates from the utility supply is virtually independent of the motor power factor and drive speed because the inverter drive acts as buffer to the supply system and the power factor specified for the actual inverter (Chapter 2.) is important. It must also be noted that Pf measured is not the maximum power factor attained during the load test, but the Pf at maximum efficiency. As seen from Fig. 3.9 the Pf increases as the efficiency decreases again.

The total inductance is proportional to frequency. Furthermore, the leakage inductance is increased by skewed rotor slots. Due to the presence of higher frequency components and the parallel harmonic circuits [2.9] the harmonic circuits are superimposed to form the actual equivalent circuit. Clearly for many high frequency components the total inductance will be much larger, and consequently the power factor proportionally reduced.

$$Pf. \quad \alpha \quad \frac{1}{X_{tot}} \qquad \ldots(3.14)$$

were $X_{tot}$ is the total reactance of a motor.

This is evident from Figs. 3.6 and 3.7 . For PWM modulation with very dominant high frequency components $f_n$ ($19^{th}$ and $23^{rd}$, $41^{st}$ and $43^{rd}$ harmonic and sidebands) the power factor is very poor. The Pf for the square wave excitation is substantially higher because only the $5^{th}$ and $7^{th}$ harmonic are present at a lower frequency.

In the low operating range the Pf is very low and increases as the fundamental excitation frequency increases.

It is also observed from Figs. 3.6 and 3.7 that the Pf for PWM excitation increases as the fundamental excitation frequency increases, for both subsynchronous characteristic ($V_r/87$) and synchronous characteristic ($V_r/50$) configuration.

This can be explained because for sinusoidal PWM modulation the frequency amplitude content changes as can be seen in **Appendix 3.2.** As mentioned the modulated voltage becomes more block like as the fundamental frequency increases to keep the V/f ratio constant. In the field weakening range the Pf decreases again because the fundamental frequency increases further, but the dc bus voltage remains constant.

For Square Wave excitation the harmonic frequency content remains constant over the whole excitation frequency range. As the excitation frequencies are increased the Pf decreases, which agrees with relation (3.14), as the total reactance is proportional to frequency. This is the case for subsynchronous ($V_r/87$) and synchronous ($V_r/50$) configurations. The Pf for sinusoidal excitation goes along the same trend as for the square wave inverter, except for a better power factor of a few percent due to the absence of any harmonic components.

**Table 3.4** Power Factor for different Excitation Sources.

| Freq. [Hz] | Power Factor (p.u.) Synchr. Range ($V_r/50$) | | | Power Factor (p.u.) Subsync. Range ($V_r/87$) | | |
|---|---|---|---|---|---|---|
| | Sine | PWM | SQWave | Sine | PWM | SQWave |
| 10 | ---- | 0.4 | ---- | ---- | 0.33 | ---- |
| 20 | ---- | 0.56 | 0.88 | ---- | 0.44 | ---- |
| 30 | 0.9 | 0.63 | 0.86 | ---- | 0.53 | 0.91 |
| 40 | 0.89 | 0.75 | 0.84 | ---- | 0.64 | 0.89 |
| 50 | 0.88 | 0.80 | 0.83 | ---- | 0.68 | 0.87 |
| 60 | 0.88 | 0.82 | ---- | ---- | 0.72 | 0.86 |
| 70 | 0.83 | 0.76 | ---- | ---- | 0.75 | 0.85 |

It can be concluded that the power factor is severely affected by higher time harmonics (especially for PWM excitation) due to reasons discussed above.

The following has been observed:

(i) at low excitation frequencies ( up to 40 Hz):

$$Pf._{SIN} > Pf._{SQW} >> Pf._{PWM} \quad ...(3.15)$$

(ii) at higher excitation frequencies (40 Hz to 70 Hz):

$$Pf._{SIN} > Pf._{SQW} > Pf._{PWM} \quad ...(3.16)$$

Another factor affecting the Pf at low excitation frequency is the initial voltage boost. It is predicted that a better Pf for low excitation frequencies is obtained with higher initial voltage to overcome the resistance. This can be interpreted as the Pf for the same excitation frequency with higher harmonics ($\pm 21^{st}$), but higher voltage (compare characteristic $V_r/50$ and $V_r/87$) is significantly better.

# CHAPTER 4. TEMPERATURE.

## 4.1 Cooling and Ventilation of Inverter-Fed Induction Motors.

Due to increased losses in an inverter-fed induction motor a rise in temperature is unavoidable.

In paper [4.2] the performance aspects of an PWM inverter-fed induction motor are analyzed. Emphasis is placed on the stator copper losses, temperature rise and insulation lifetime. The creation of low frequency parasitic torques is described. A model for ac losses and the winding temperature distribution is also developed.

The necessity to derate induction motors when fed from non-sinusoidal excitation sources with a harmonic distortion exceeding 5% is emphasized in the paper [4.2].

The temperature for different operating conditions will vary depending on the higher time harmonic content in the supply voltage. Localized temperature rises are most severe where the losses are increased the most significantly. Overheating will be severe in rotor-cage bars and stator bars if square conductors are used.

The effects of increased motor temperature is multifold. It affects the winding resistance, but more important the winding insulations are exposed to additional stresses. Unless designed as eg. class F insulation, severe restrictions on the operation of the motor must be placed. The effectiveness of the lubricant in the bearings will also be reduced and the inter lubrication period of the bearings will be reduced.

The temperature distribution within the machine should be known to some extend to measure the temperature at the highest temperature location to determine weather it still falls within limiting specifications.

The operating condition, location and environment of the machine, and ambient temperature is also crucial on the heating condition of a machine. It is self evident that the ventilation effect at low speeds for self-ventilated motors is proportionally to the inverse square lower than under rated speed conditions. This is because of the reduced volume per time cooling medium, and also at high air speeds generate turbulences and are thus cooling more efficient than streamlined air flow at low air speeds. Cooling is approximately proportional to the velocity of the air. The convection heat current from the metal surface to the air is conducted away by the air flow. The convection gradient is proportional to the temperature difference between surface and ambient air temperature.

Small machines are generally all self ventilated with air as conducting medium. Metal ribs are used to increase the radiation and convection surface to ensure a maximum heat transfer. In most industry applications of small machines, totally enclosed frames are used - e.g. according to IP 54 protection. The ambient air is thus not in contact with the conduction medium (usually air for low power rating, low cost induction motors) inside the frame. An internal frame is thus generally fitted onto the end bells to circulate air inside between the frames in opposite direction as the air flow along the cooling ribs externally.

Forced ventilation and/or thermal cutout switches must be considered for low speed operations with inverter applications.



## 4.2 Temperature Rise.

The heat developed internally in the machine rises exponentially - until a steady state condition is reached, depending on various factors.

The heating time constant can be determined from a load test started at initial cold conditions. To determine a time constant analytically is difficult and experimental tests are generally carried out.

The time heating constant $\tau$ is the time in which the temperature attains 2/3 of its steady state value. The temperature as a function of time is thus:

$$T_{VSD}(t) = k_{VSD}\, T_{SIN}\, (1 - e^{(-t/\tau)}) \qquad ...(4.1)$$

where $k_{VSD}$ = Factor to include extra heating of a variable speed drive due to additional current harmonics, $T_{SIN}$ = Steady state temperature of a motor under sinusoidal excitation.

This is an over simplification, and as indicated already, the machine is not a homogeneous body and several parts with different mass, heat capacity, thermal conductivity, rate of heat production and effectiveness of cooling are present in a single unit. Hot spot temperatures must be estimated and known to be able to take required precautions.

For continuous rated machines the rise temperature time constant is not important, but rated the effectiveness of the motor cooling. Various factors are of importance for the cooling coefficient for different parts in the motor (rotor and stator surfaces, rotating rotor field coils, ventilation ducts in cores etc.) like volume of air per unit time passing the heat dissipating fins, relative peripheral speed of the rotor and air velocity in ducts.

These factors all play an important role in determining the derating of electrical machines when fed from inverters.

The temperature increases due to nonsinusoidal excitation supply are appreciable as can be seen from Fig. 4.1 and Table 4.1. The output torque was adjusted to remain constant during the test for equal test conditions. The rated torque is 20 Nm, thus the test were performed at 15% above rated condition which must be considered during the analysis. The speed - and thus ventilation - also remained almost constant for the duration. The average temperature of the three sensors T1, T2, T3 (as shown in Chapter 2.) is calculated. The ambient temperature in fact remains constant, because the measured ambient temperature $T_{amb}$ (T4) is the air blown through the fan and is thus marginally warmer.

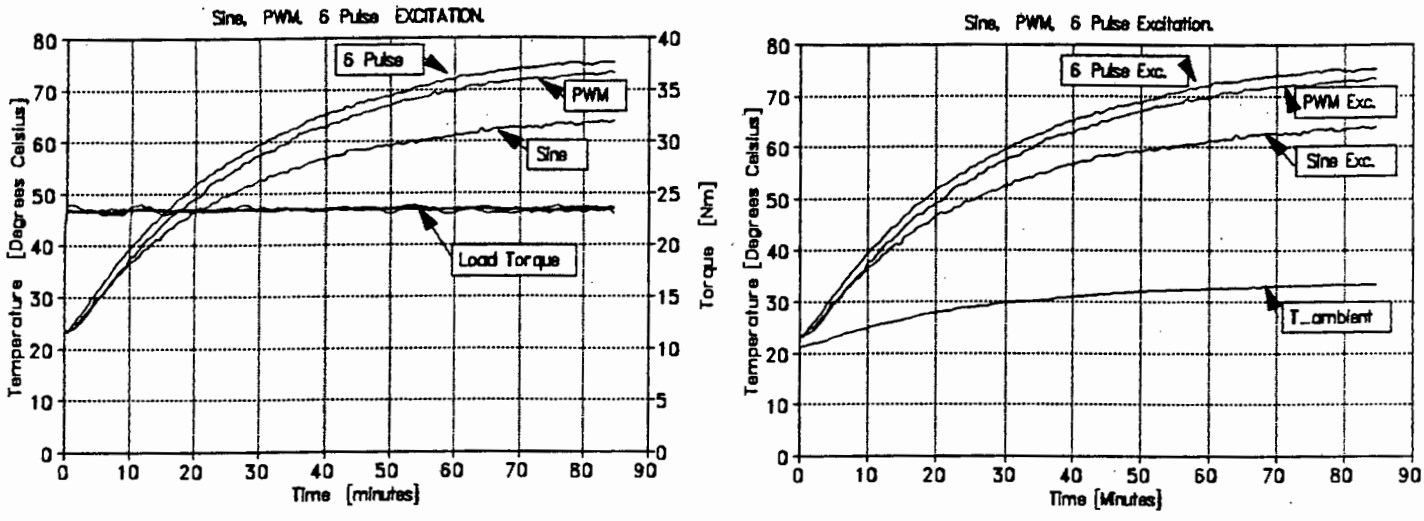


(a). (b).

**Fig. 4.1** Temperature rise characteristic for different excitation sources. (380 $V_{LL}$, 50 Hz) (a) Temperature and Torque vs Time, (b) Temperature and $T_{amb}$ vs time.

The temperature indicated is the average in the stator laminations. As shown in [4.1] the temperature in the frame is marginally lower than the core (3°C), but in the windings the temperature will be approximately 10°C higher, i.e. 10% to 20%. It can thus be assumed that specific hot spots can occur, especially due to localized losses due to inverter applications.

With inverter applications a good insulation quality is required (class F) else the life time may be reduced up to 70% as compared to sinusoidal excitation, [3.4]. This is however applicable to embedded insulated bars, were the conductor height is of importance. A more applicable problem poses the low speed operation, due to increased losses and reduced ventilation. In a paper [3.7] the winding temperatures under low frequency excitation (15 Hz) rises to above 155°C at rated torque which is clearly detrimental to the winding insulations.

**Table 4.1** Temperature rise under non-sinusoidal excitation relative to sinusoidal excitation.(At $T_{amb} \approx 33.3^{\circ}C$).

| Inverter Excitation | Temperature $T_{fin}$ [°C] | Increase in temperature compared to sinusoidal excitation | | |
|---|---|---|---|---|
| | | °C | % | $k_{VSD}$ |
| Sine | 63.96 | ---- | ---- | 1.00 |
| PWM | 73.36 | 9.03 | 14.39 | 1.14 |
| Square Wave | 75.19 | 10.98 | 17.50 | 1.17 |

In [1.2] it is estimated that with additional losses of 10% in the stator and 100% increase in losses in the rotor bars as compared to mains operation, the temperature will rise by approximately 15°C in the stator bars and by up to 60°C in the upper region of the rotor bars. The temperatures measured in the core laminations increased by approximately 9°C and 11°C for an increase in total losses of 3.5% and 6.5% for PWM and square wave excitation respectively. Considering the temperature distribution of the temperature increases estimated in [3.7] seems to agree with the measurements.

## 4.3 Temperature Distribution and Dynamics.

The temperature distribution and dynamics are specific for each machine design, depending on factors discussed in the introduction of this chapter.

The temperature profile shown in Fig. 4.2.a shows that under steady state operating conditions the temperature gradient across the stator core laminations increases substantially, between 13°C and 18°C. Moreover, the temperature gradient between T1 and T3 increases with increased losses due to time harmonic currents as shown in Table 4.2.

**Table 4.2** Temperature gradient and differences across stator core.

| Inverter Excitation | Temperature gradient across stator core. in °C | | | Increase in temperature difference in °C | |
|---|---|---|---|---|---|
| | $T_{1\_DE}$ | $T_{3\_NDE}$ | $T_{Grad.}$ | $T_{dS}$ | $T_{dSP}$ |
| Sine | 70.80 | 57.12 | 13.67 | ---- | |
| PWM | 82.33 | 64.96 | 17.33 | 3.66 | |
| SQWave | 84.22 | 66.16 | 18.06 | 4.39 | 0.73 |

$T_{1\_DE}$ = Temperature at the drive end, $T_{3\_NDE}$ = Temperature at the non drive end, $T_{Grad}$ = Temperature gradient between $T_{1\_DE}$ and $T_{3\_NDE}$, $T_{ds}$ = Average temperature increase compared to sinusoidal excitation, $T_{dSP}$ = Temperature increase under Square Wave excitation compared to PWM excitation.

The stresses on the insulation due to localized heating at the drive end will be substantially higher. This is also evident as the cooling is not as effective due to reduced air flow. The enclosed internal frame air circulation should be improved to redistribute the heat more desirable to reduce the temperature gradient.

Localized heating seems more dominant with under inverter excitation.

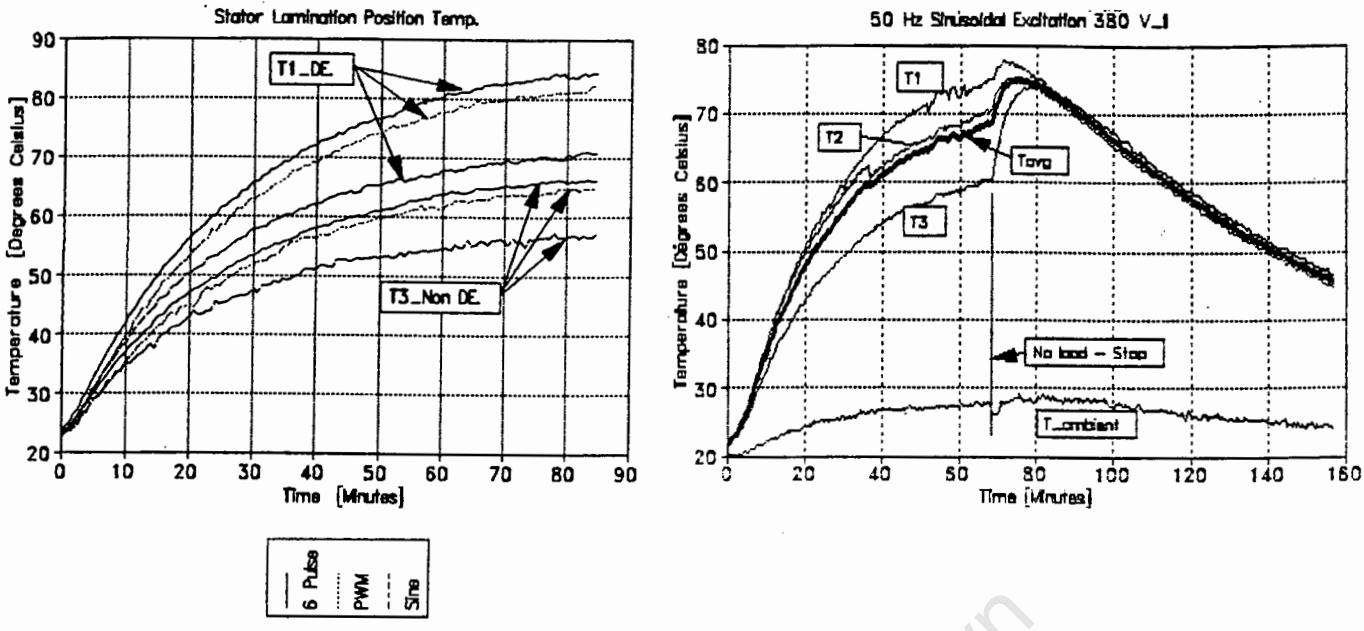


(a). (b).

**Fig. 4.2** Temperature distribution and temperature profile. (a) Temperature distribution at the drive end stator core (T1_DE) and non-drive end stator core (T3_Non DE). (b) Temperature profile - dynamic temperature redistribution.

As seen from Fig. 4.2.b, were the motor is stopped after a load run and the temperature monitored the temperature redistributes to an equilibrium temperature in the motor within approximately 8 minutes, due to the absence of self ventilation. Although no additional losses and thus no heat is generated after the motor is stopped, the temperature rises.

It can be observed that the average temperature $T_{avg}$ increases by approximately 8°C from when the motor is stopped (68°C), to the stator core maximum temperature (76°C) as the heat from the rotor and stator winding is redistributed to the stator core. This clearly indicates that the rotor and stator windings will be at a temperature of 10% to 20% higher than the core laminations. The drive end temperature is closest to the internal rotor temperature, and temperatures should thus be monitored at the drive end.

## 4.4 Temperature Decay.

The temperature decay is important to determine load cycles, especially for larger machines. A temperature decay profile without ventilation, i.e. standstill is

shown in Fig. 4.3. The temperature would decay much faster under no load conditions in the presence of the cooling effect.

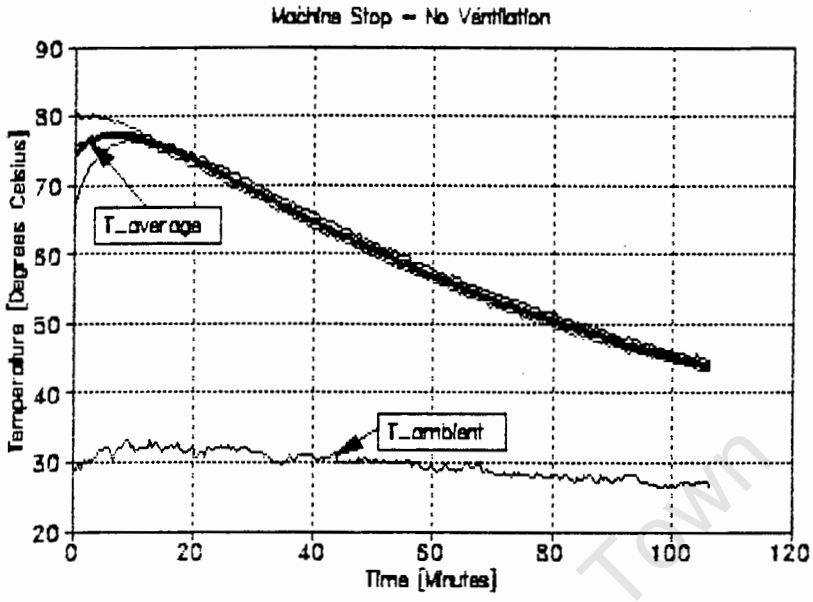


**Fig. 4.3** Temperature decay without excitation. Shown are temperatures $T_1$, $T_2$, $T_3$ and $T_{avg}$, which are at the same temperature after heat redistribution.

## 4.5 Derating and Machine Lifetime.

In inverter applications the derating is crucial due to harmonic losses in the motor, and reduced ventilation in the low frequency operating region. As can be seen from Fig. 4.4 the losses indicated depend on the inverter used and its configuration, i.e. synchronous or subsynchronous (field weakening) range, as well as initial voltage boost at low speeds. If rated torque is required at low speeds, an substantial initial voltage boost is necessary. This leads to higher losses as compared to a low voltage boost value. This is evident from the torque-voltage and losses-current relationships. i.e. the torque is proportional to the voltage square, the losses are proportional to the current square, and the current is directly proportional to the voltage.

The maximum allowable hot spot temperature is determined by the insulation class, which thus affects the continuous machine output.

The IEEE Standard suggests that no derating is required for a harmonic content of up to 5%. For inverter supplies

the harmonic content exceeds the 5% limit by far and to avoid detrimental effects on the machine, derating of the motor is required.

It is important to know the speed-airflow-contact surface relation. In papers on derating it is mentioned that the cooling effect is reduced by low speeds, but no clear guideline is given how exactly airflow at low speeds is given. It has been determined from [4.4] and [4.6] that the airflow across the cooling ribs is in the region of an exponential to an inverse quadratic with speed. (At very high speeds the airflow might in fact be reduced due to turbulences, but that is not relevant in machine applications). An estimation of losses, per unit temperature and airflow is shown in Fig. 4.5.

As discussed in Section 4.2 an increase in losses by approximately 10% could lead to a statistical reduction in lifetime of 65% [1.2].



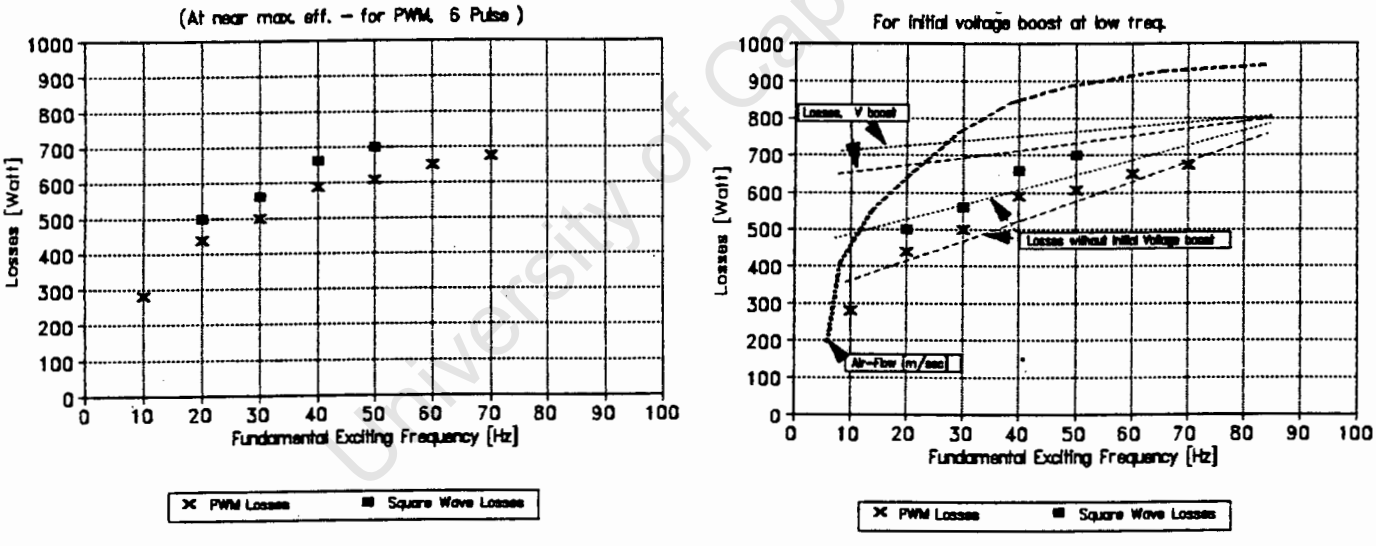


(a). (b).

**Fig. 4.4** Motor losses near max. efficiency for PWM and Square Wave Excitation. (380 $V_{LL}$, 50 Hz) (a) Losses vs Fundamental frequency of excitation, $V_r/50$ - No initial Voltage boost. (b) Losses estimated - With and without initial boost voltage .

NEMA standards stipulate a maximum allowable temperature rise of 80°C, 105°C and 125°C for totally enclosed fan cooled motors with insulation class B, F and H respectively [3.4].

Derating of inverter-fed machines depend on further important factors of machine and inverter design and configuration, i.e.:

(i). Machine design, star or delta connection, skewed or non-skewed rotor bars, position and mounting and insulation class.

(ii). Harmonic content of inverter, (PWM, square wave); whether the inverter is configured for synchronous or subsynchronous speed, the initial voltage boost of the inverter.

(iii). Ventilation and fan design.

(iv). Special design or special purpose.

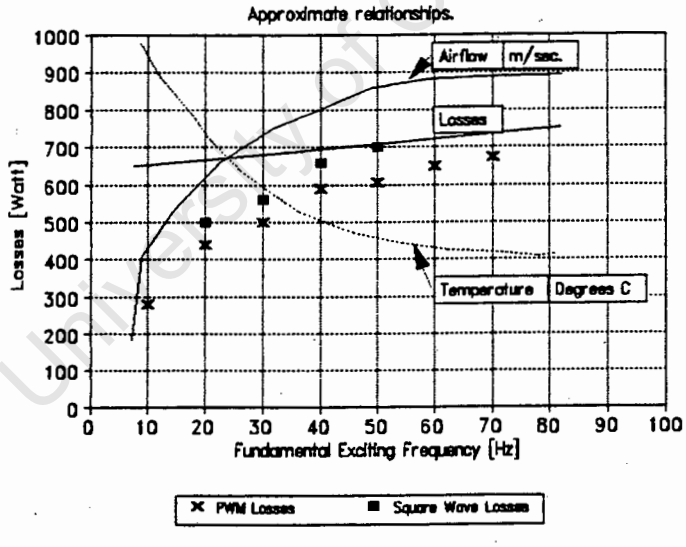


**Fig. 4.5** Estimated losses, p.u. temperature and air flow vs excitation frequency.

In industry the economic implications on the lifetime and return on value must be considered. Thus a concept of efficiency, performance, and long term economic considerations are important. Clearly the lifetime due to increased temperature will be reduced, as the lifetime can be determined according to [4.3] :

$$\text{Lifetime} = A\, e^{B/T} \qquad (4.2)$$

A,B are constants, T is the absolute temperature.

The motor lifetime is inversely proportional to temperature if time is plotted on a log scale. The rate of financial return at full load, depreciation, the cost of a larger machine, the importance of extended motor life etc. must be considered.

From an engineering point of view, derating is necessary to maintain the same life expectancy of a motor as under sinusoidal excitation which is generally used as design guideline in standard machines.

The temperature for small machines rises considerable due to inverter supplies, but still a substantial temperature margin is available before the critical temperature would be reached for a class F motor. It is therefore suggested - for small machines with class F and class B insulation to derate motors as indicated in the IEC Standards [1.1] to be certain that the motor will not overheat.

Derating guideline including the design class. The derating factor in per cent can be expressed as:

$$D_T = \tfrac{1}{2} \frac{T_{VSI}\, T_{SIN}}{T_C^2} 100\ \% \qquad ...(4.3)$$

where $T_{SIN}$, $T_{VSI}$ is the steady state temperature on the non ventilated end, at rated condition and rated load under **sinusoidal** excitation and **inverter excitation** respectively, and $T_C$ is the maximum permissible temperature for a design specification.

The derating factor indicates the percentage reduction in load by which the load must be reduced under inverter operation to keep the steady state temperature equivalent to that under sinusoidal excitation.

This implies that for a class B (130°C) and class F (155°C) insulation the machines should be derated by 17.2% and 17.6% for PWM and Square wave excitation for a class B motor. For class F insulation the motor should be derated by 12.1% and 12.4% for PWM and Square wave excitation respectively.

Applying the derating guideline on data used in Table 4.3 below for a insulation class F motor under Square Wave excitation, a derating factor of 17% is calculated according to equation (4.3). The machine load was reduced by 10.7% and the temperature was reduced by 20.1°C. If the load would have been reduced by 17% the steady state operating condition would be around 75°C equivalent to that under sinusoidal excitation.

**Table 4.3** Temperature decrease under derated operating condition.

| Torque<br>Temperature<br>Excitation: | Case 1.<br>25.75 [Nm]<br>$T_3$ [°C] | Case 2.<br>23.0 [Nm]<br>$T_3$ [°C] | Derating<br>10.7 (%)<br><br>Temp. decrease |
|---|---|---|---|
| Sine | 75 | 70.8 | 5.6(%) |
| SQWave | 105 | 84.2 | 19.8(%) |

The empirical guideline given by equation (4.3) gives a reasonable indication on the derating factor. Additional measurements should be performed to confirm the empirical equation (4.3).

It can be compared to suggested derating strategies as in the ICE standards on inverter applications [1.1]. Also the paper [4.2] recommends to derate according the output power under different supplies by a derating factor:

$$D_H = 1 - \frac{P_{OH}}{Po} \qquad \ldots(4.4)$$

where $P_{OH}$ and $P_O$ the output power of the machine under inverter supply and sinusoidal supply respectively.

# CHAPTER 5. SHAFT VOLTAGES.

## 5.1 Review of Research.

In the draft IEC standard, Project No. 2/032/2 (Guide for the application of cage induction motors when fed from inverters), it is recommended to measure the peak shaft voltage, to consider insulation of bearings if the induced peak shaft voltage exceeds 500 mV. As aware, the problem of induced shaft voltages due to non-sinusoidal excitation of small induction machines has not been investigated thoroughly. Shaft voltages and currents are mentioned as an additional effect in [1.2] and [3.10].

In paper [5.1] the induced shaft voltages and bearing currents are discussed and causes, effects and remedies are outlined. It is assumed that magnetic unsymmetrical in the winding overhangs are the main cause of induced shaft voltages.

The paper [5.2] describes causes and remedies for shaft and bearing currents flowing across the rubbing surfaces of the bearing. The cause of induced shaft voltages due to sectionalized stators is discussed.

The authors of paper [5.3] give a simplified mathematical model to ascertain shaft voltages and currents based on rotor eccentricities and sectionalized stators.

Paper [5.4] gives a explanatory and theoretical analysis discussion on induced shaft voltages due to variations in the air gap of electrical machines.

In paper [5.6] an experimental investigation is performed and possible causes given of shaft voltages induced due to inverter excitation of induction motors.

Paper [5.7] considers analysis and monitoring of shaft voltage in turbo generators.

## 5.2 The possible Causes of Induced Shaft Voltages.

It is assumed that stator and rotor laminations consist of a single segment. In paper [5.1], [5.2] induced shaft voltages due to increased reluctance in lamination segment gaps have been discussed.

Possible causes of induced shaft voltage are due to:

i). Slight eccentricity of the rotor shaft with respect to the stator circumference due to backlash in the bearings. This results in a change of shaft position relative to the stator magnetic flux. The relative airgap will also vary as function of position and time and contribute to the shaft voltage [5.4]. This eccentricity can be magnified by unbalanced magnetic pull. An e.m.f. proportional to the change of flux in space, and the difference in opposite airgaps, is induced in the shaft.

ii). Unbalanced interbar currents due to broken rotor bars (abnormal condition) which would by transformer action induce a voltage in the shaft.

iii). Time dependant current unbalances in the stator windings induce shaft fluxes and thus shaft voltages.

iv). Transformer action of the leakage flux of the stator winding overhangs in the end zone on both stator ends and currents in the end rings as shown in Figs. 5.1 and 5.2.

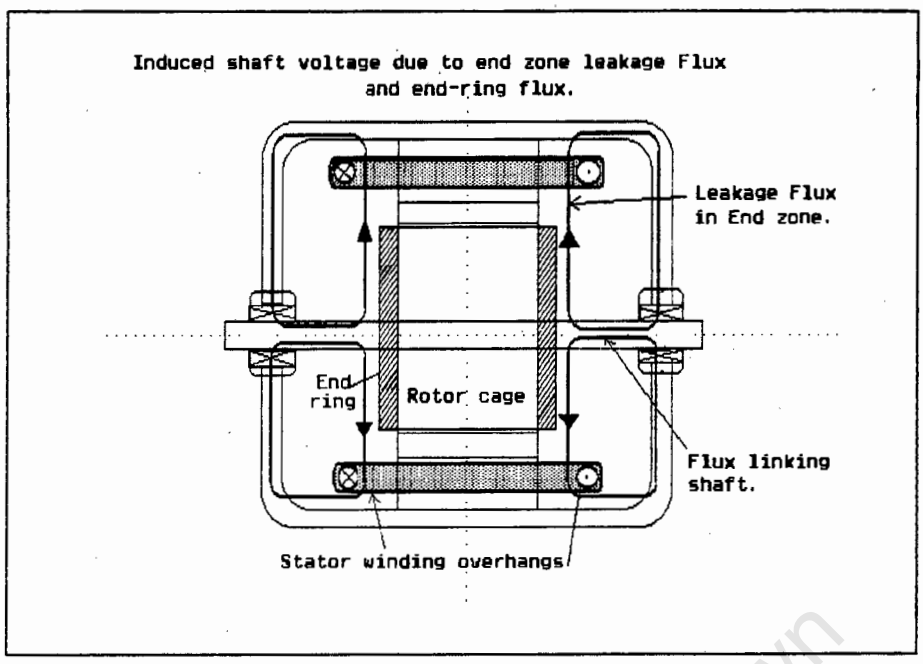


**Fig. 5.1** Schematic - Cause of shaft voltages. End zone induced shaft voltage.

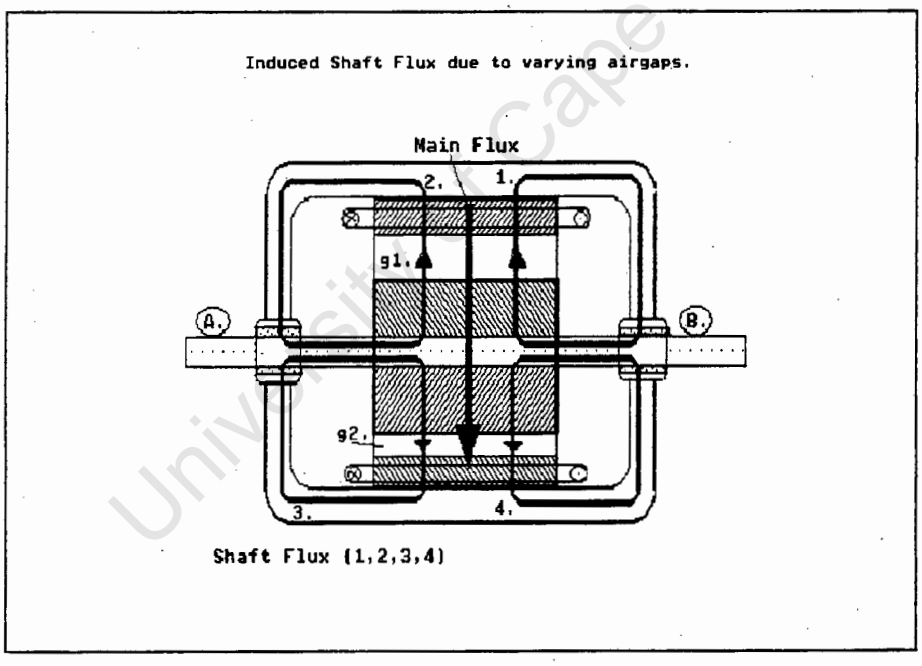


**Fig. 5.2** Schematic - Cause of shaft voltages. Motor crosscut - Flux induced due to varying air gap.

**v).** Asymmetry in magnetic circuit of the stator causes currents induced in the motor frame by the stator magnetic field.

**vi).** End ring induced excitation. [5.1]

vii). Voltages due to electrostatic charges originating from friction etc. [5.1], [5.4].

In case of inverter-fed motors, peaks in the motor input voltage and current, which occur during the commutation period, also contribute to the shaft voltage, as (vii).

Cause (i) is briefly discussed. It is assumed that stator and rotor laminations consists of one segment.

Backlash in the bearings results in the shaft to move with respect to the magnetic flux, thus inducing a voltage in the shaft.

$$e_S = - \frac{d\Phi}{dx} \frac{dx}{dt} \qquad ...(5.1)$$

were $\Phi$ is flux density, x relative position, t time.

As displayed in Fig. 5.2 the magnetic potential across gap g1. and g2. due to the main flux is proportional to the airgap, (g1. > g2.). At constant flux the magnetic potential must be equal across the gaps, which leads to the conclusion that shaft fluxes $\Phi_1$. and $\Phi_2$. across gap g1. oppose the potential and shaft fluxes $\Phi_3$. and $\Phi_4$. add the potential across gap g2. so that eventually the condition of equal magnetic potential across both gaps is fulfilled. It is thus evident that $\Phi_1$ and $\Phi_4$ create a homopolar flux through bearing number B., $\Phi_3$ and $\Phi_4$ a homopolar flux through bearing number A. [5.4]. It must be noted that eddy currents will occur in the solid metal shaft and the induction thus will be reduced.

A formula is derived in [5.4] that determines the shaft flux $\Phi_S$ analytically:

$$\Phi_S = \int_0^{2\pi} B_{S\nu} \cos(\nu x - w_\nu t - \beta_\nu)\ \delta_e\ R_S\ dx \qquad ...(5.2)$$

where $B_S$ is the induction in the shaft, $\nu$ the space harmonic component, x the airgap periphery, w frequency, $\beta$ the phaseangle, $R_S$ radius of the shaft, $\delta_e$ the skin depth

In Fig. 5.3 the homopolar flux that flows through the frame, bearing and shaft induces a bearing voltage $V_b$ across the bearing ends (point A. to C.). The current generally flows from the on side of the bearing through an oil seal to the other side and back through the oil seal on the other end (for loose liner bearings)[5.2]. The bearing current depends on the bearing type used.

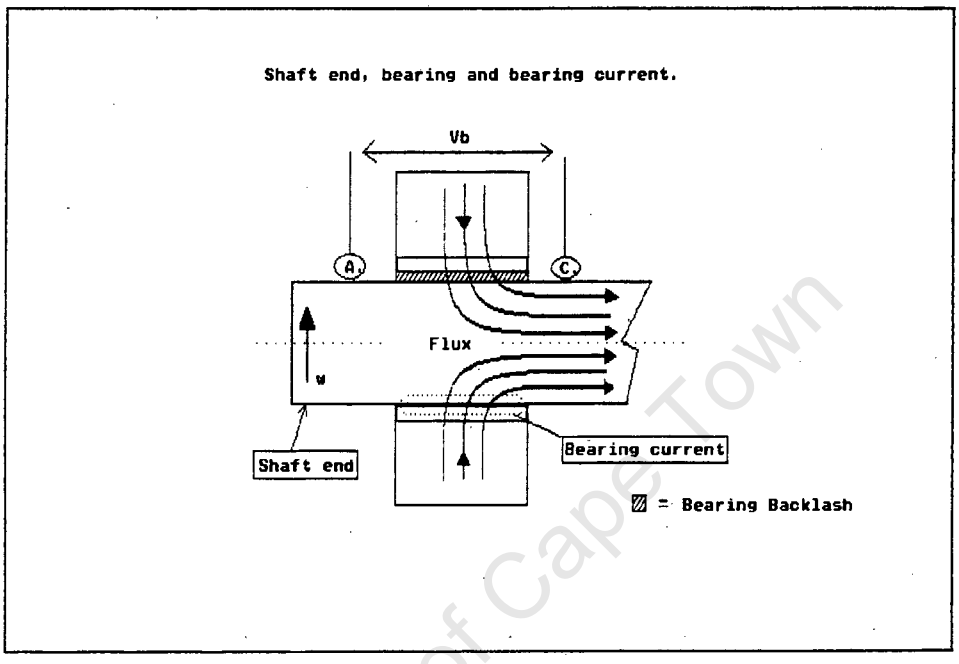


Fig. 5.3 Shaft end with bearing and bearing currents.

The voltage $V_b$ and thus the induced current are proportional to the rotor speed and flux density [5.1].

$$V_b = B\ l\ v \qquad ...(5.3)$$

where B is magnetic shaft density, l length of shaft flux path, v speed rotor change of position

$$V_b = k_i\ \Phi\ l w_r \qquad ...(5.4)$$

where $k_i$ is a constant, $\Phi$ total shaft flux, $w_r$ rotational speed of the rotor.

## 5.4 Measurements.

An experimental investigation of shaft voltage induced in an inverter - fed cage induction motor was conducted.

A 3 phase delta-connected 3-kW squirrel cage induction motor is investigated. Three different types of excitation sources have been used, all rated at 50 Hz (fundamental) and 380 $V_{LL}$ : **Mains sinusoidal**, 6 pulse **Square Wave** voltage-source inverter and **sinusoidal PWM** inverter. The motor has also been operated under unbalanced sinusoidal excitation and with increased external leakage reactance for square wave voltage excitation. Each test has been performed under no-load and rated load conditions.

The measurement apparatus and data acquisition procedure has been described in Chapter 2. Shaft voltage in this chapter refers to the voltage across the shaft ends.



**Table 5.1** Measured peak and r.m.s. shaft voltages.

| Excitation: | | LOAD | NO LOAD |
|---|---|---|---|
| Sinusoidal | Peak | 97.9 mV | 90.6 mV |
| | R.M.S | 51.0 mV | 64.0 mV |
| Square Wave | Peak | 117.4 mV | 133.5 mV |
| | R.M.S | 53.4 mV | 65.5 mV |
| Sinusoidal PWM | Peak | 132.1 mV | 117.9 mV |
| | R.M.S | 50.1 mV | 48.5 mV |
| Unbalanced Sinusoidal | Peak | 103.8 mV | 91.9 mV |
| | R.M.S | 40.9 mV | 57.9 mV |
| Square Wave (Ext. Leakage) | Peak | 96.2 mV | 96.4 mV |
| | R.M.S | ----- mV | ----- mV |

Some results are shown in Figs. 5.4, 5.5 and 5.6 as well as in Table 5.1. The scale for input phase voltage is 1 [V] = 100 [V]. The scale for line current is 1 [V] = 5.24 [A]. The scale for shaft voltage is in actual values measured.

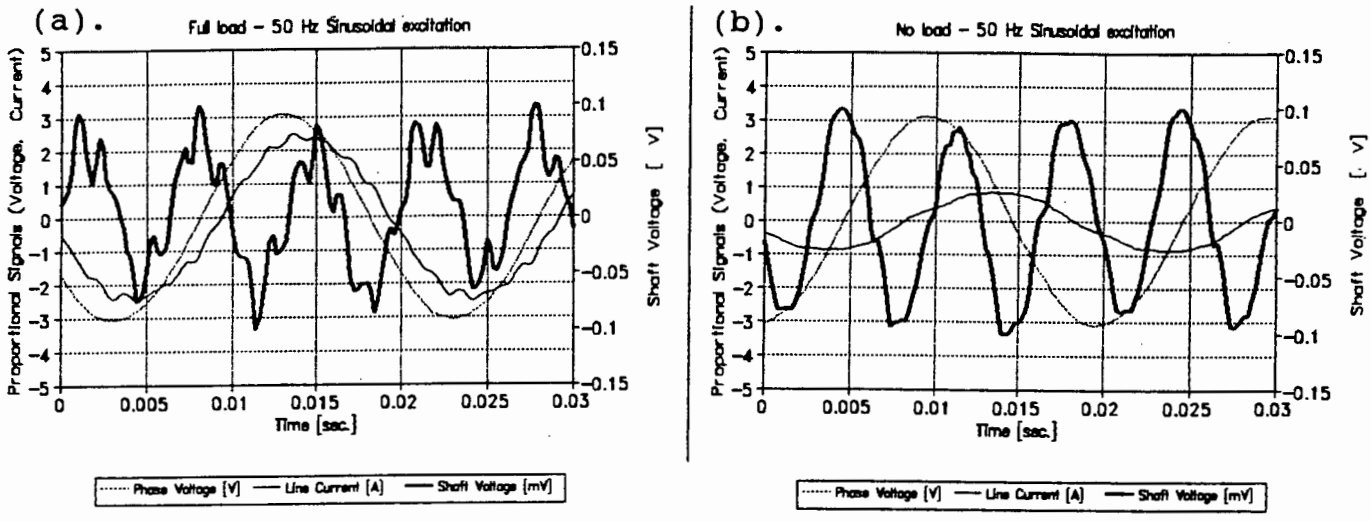


**Fig. 5.4** Shaft voltage for sinusoidal excitation. (a) Rated load (b) No load.

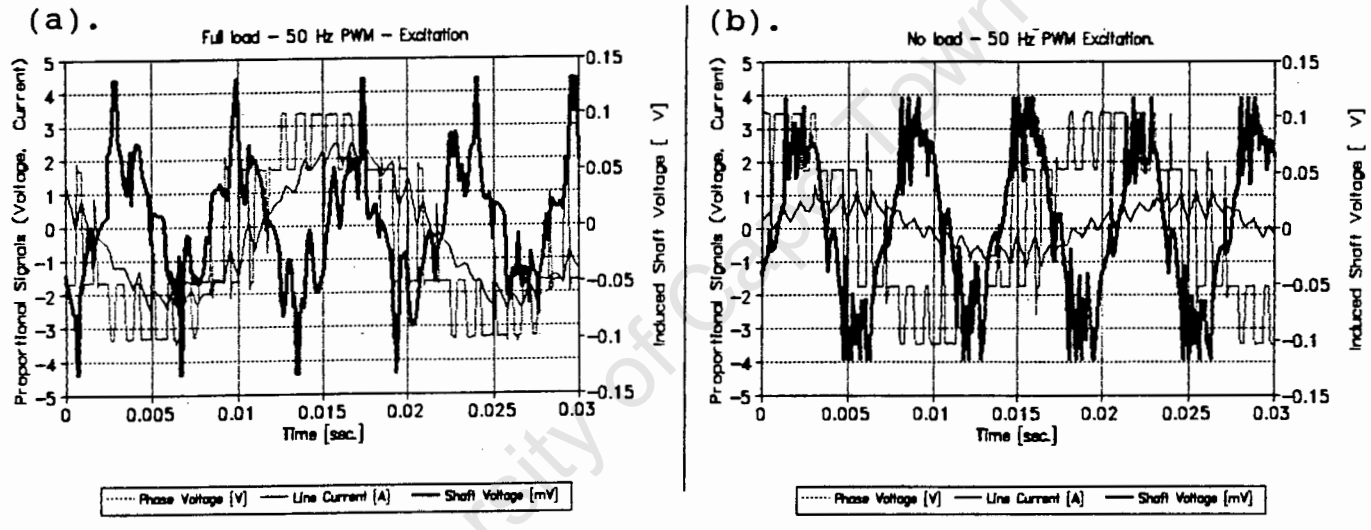


**Fig. 5.5** Shaft voltage for PWM excitation. (a) Rated load (b) No load.

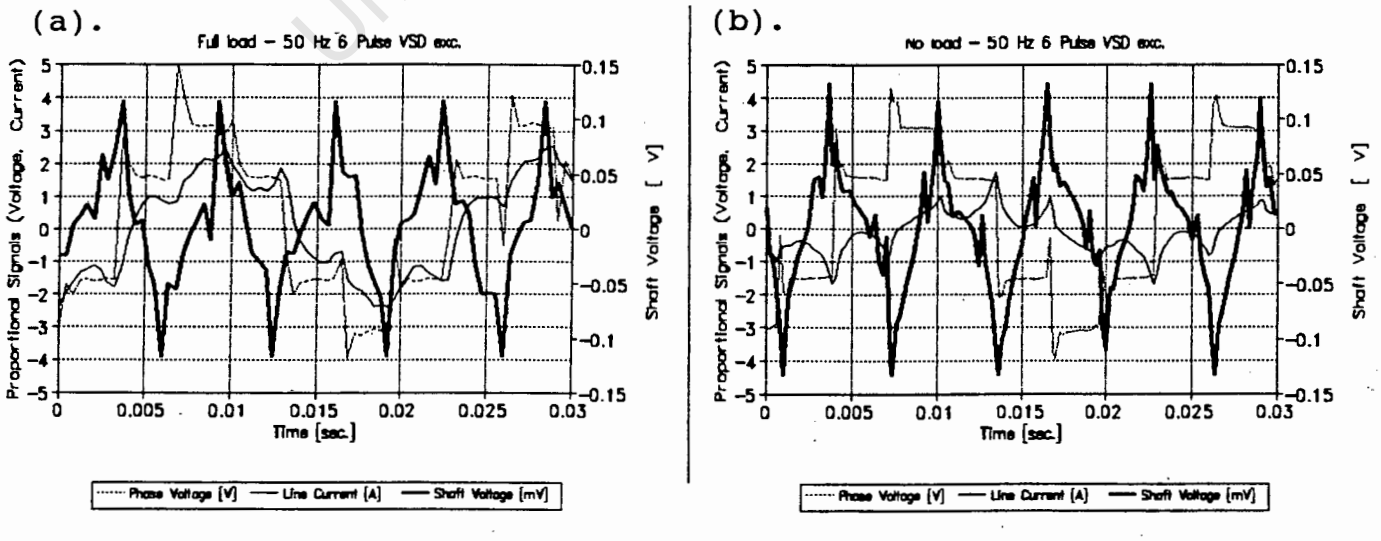


**Fig. 5.6** Shaft voltage for Square Wave excitation. (a) Rated load (b) No load.

In Fig. 5.7 the inverter-fed motor is accelerated steadily, thus near steady state operating condition. As the voltage and thus frequency is increased (increased load and current) the shaft voltage increases proportionally.

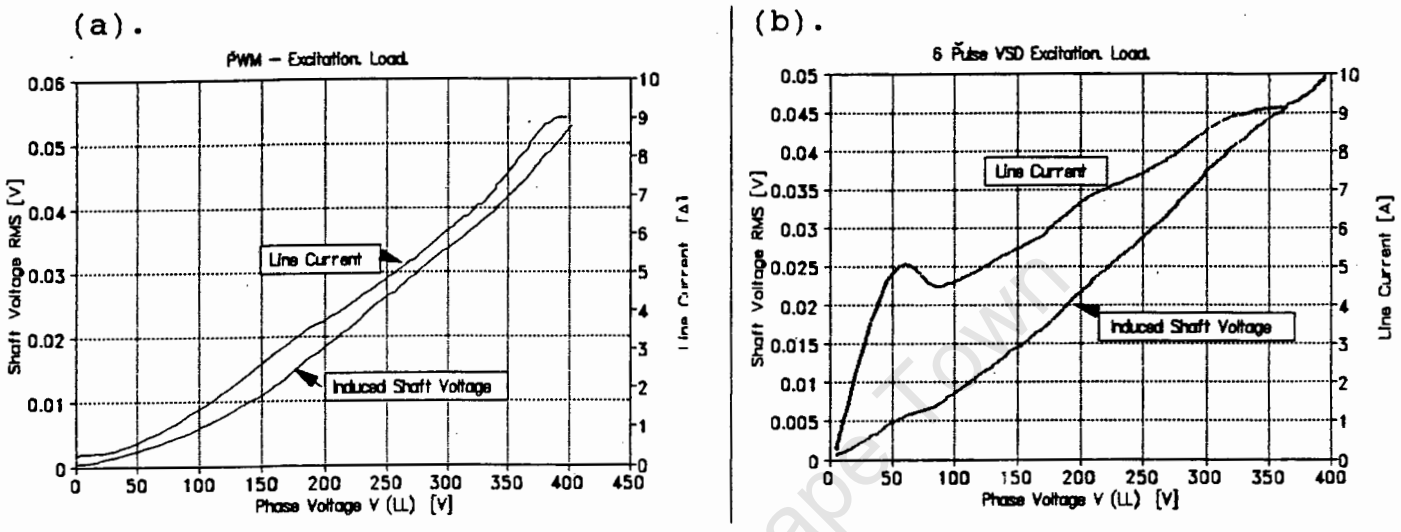


**Fig. 5.7** Shaft voltage vs Phase voltage. (a) PWM excitation (b) Square Wave excitation - (under start up load condition).

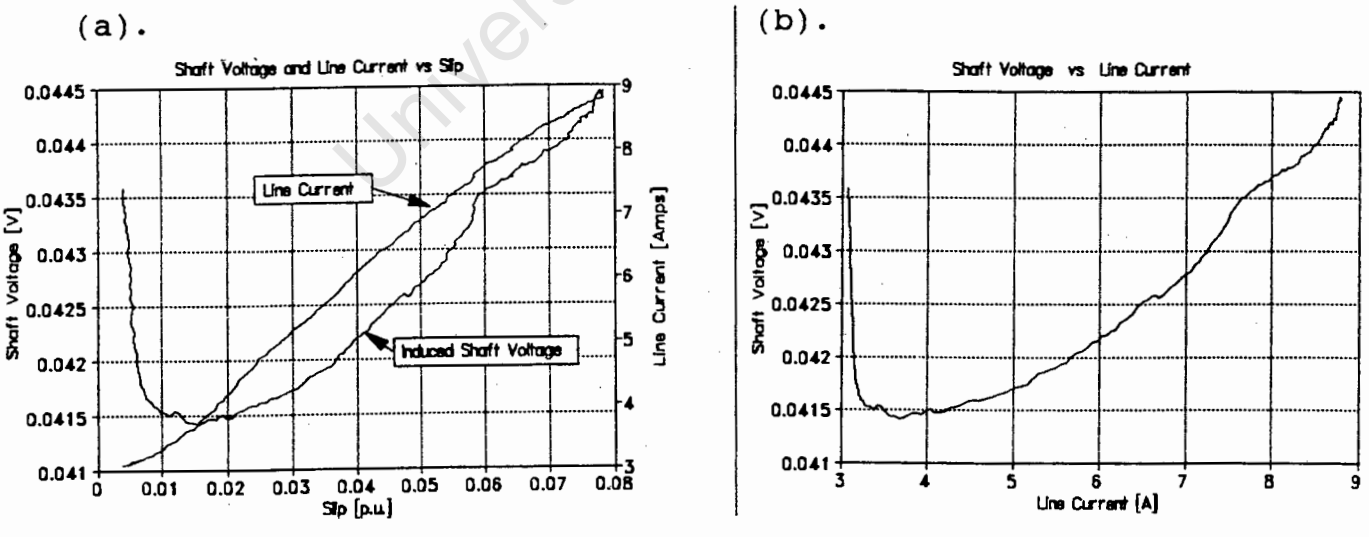


**Fig. 5.8** Shaft voltage vs operating condition for square wave excitation ($380V_{LL}/50$ Hz). (a) Shaft voltage and line current vs slip, (b) Shaft voltage vs line current.

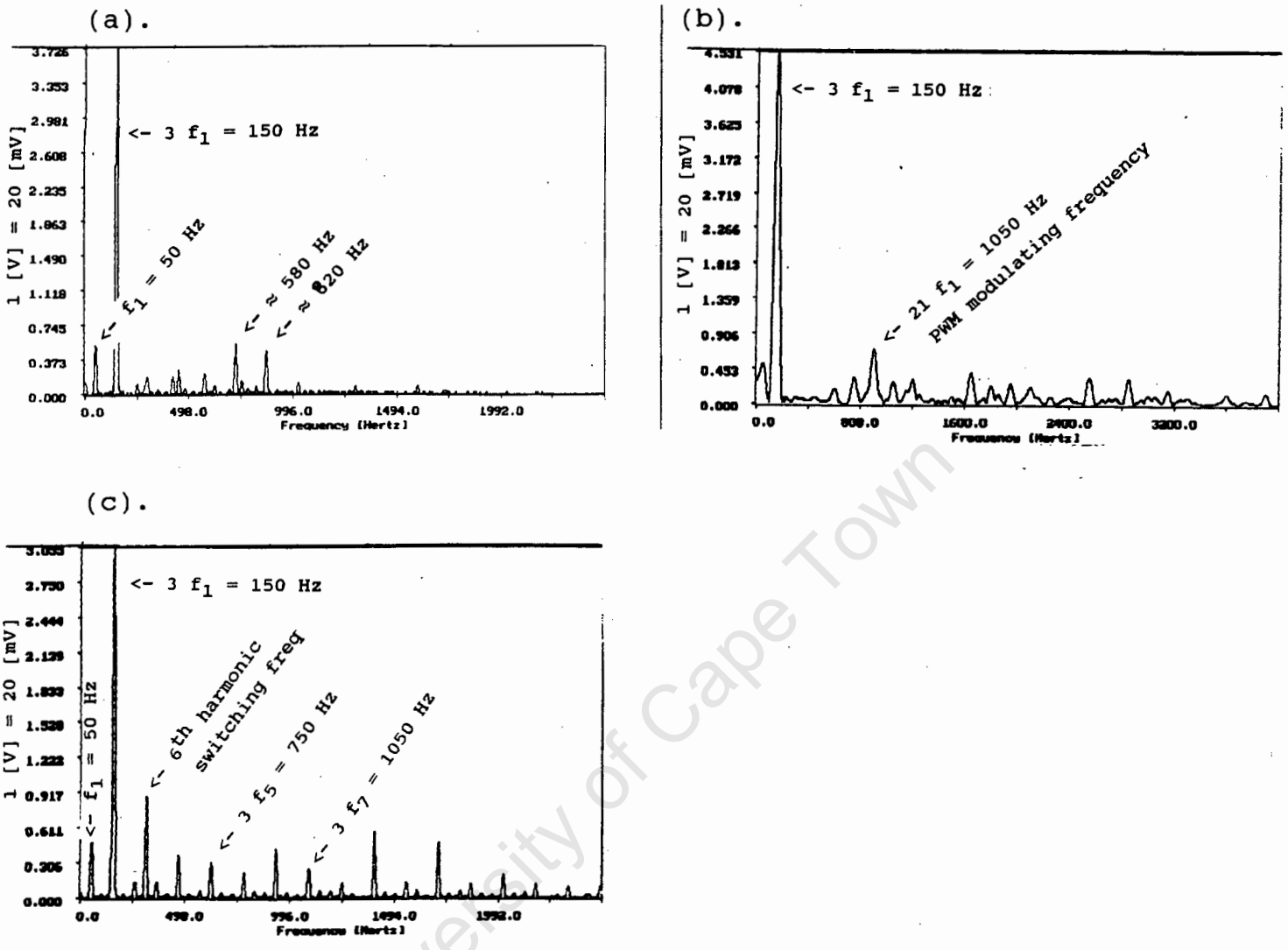


**Fig. 5.9** Frequency spectrum of induced shaft voltages under load conditions, (380 $V_{LL}$, 50 Hz). (a) Sinusoidal, (b) PWM, (c) Square wave excitation.

To investigate causes of shaft voltages further a series resistance of 7.6 Ω was inserted in line with the supply and the induced shaft voltages shown in Fig. 5.10 were measured.

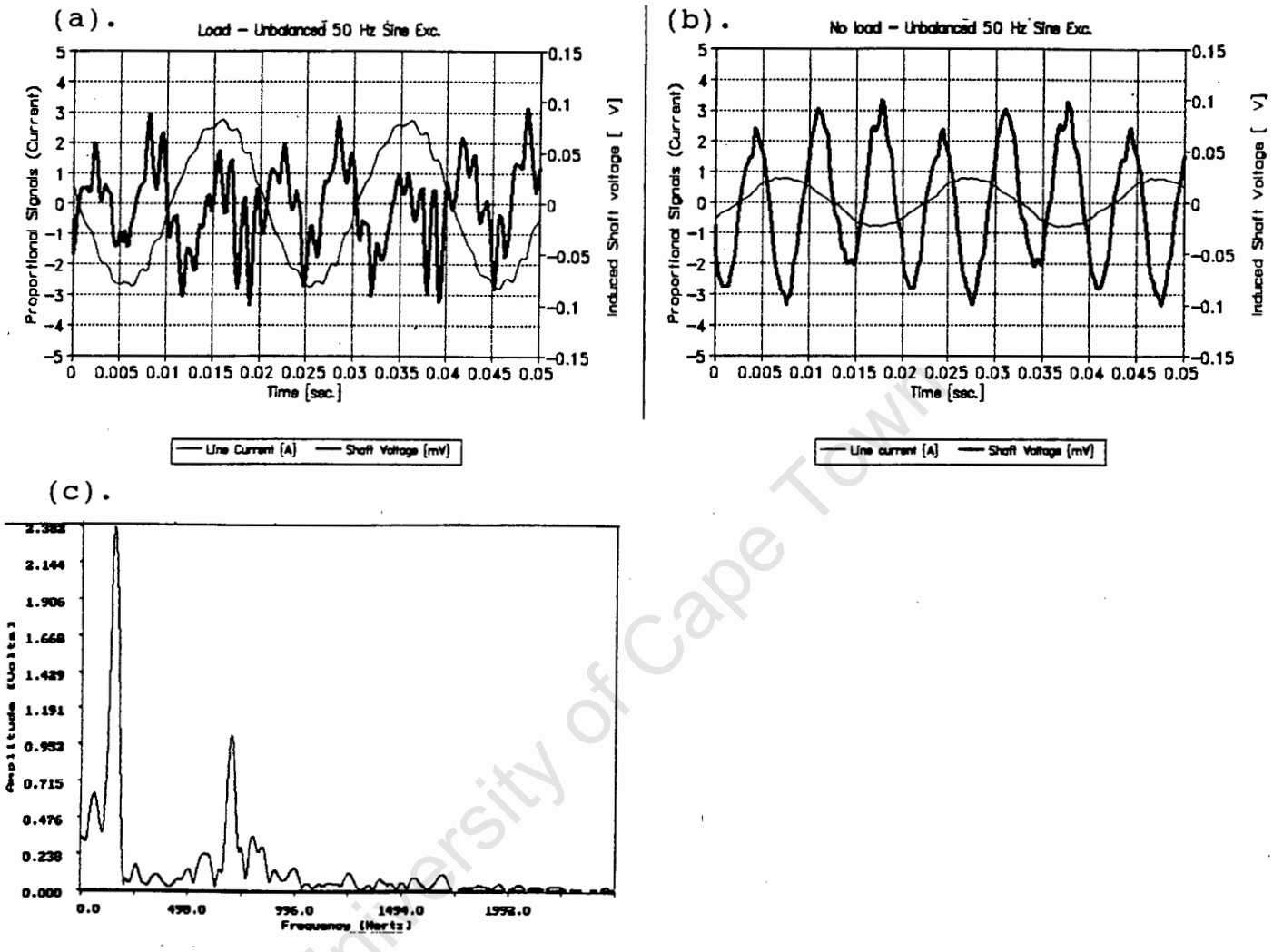


Fig. 5.10 Shaft voltage signal under unbalanced phase conditions, sinusoidal excitation (380 $V_{LL}$; 50 Hz). (a) Load condition, (b) No-load condition (c) Frequency spectrum of load shaft voltage.

The following conclusions were drawn:

i). Peak voltages induced under non-sinusoidal excitation considerably exceed those of sinusoidal excitation. At inverter commutation voltage spikes are induced across the shaft.

ii). The r.m.s. shaft voltage does not indicate any substantial increase in induced shaft voltage.

iii). The frequency of the induced shaft voltage is three times the fundamental excitation frequency; Also the higher time harmonic voltages are reflected in the shaft voltage at three times their fundamental frequency. (See Fig. 5.9).

iv). Unbalanced phase excitation increases the peak shaft voltage being induced.

v). Increasing the external leakage inductance reduces the shaft voltage peaks substantially.

vi). A linear relationship exists between the supply voltage and induced shaft voltage. (See Fig. 5.7).

vii). Changing from no load to rated load condition, the r.m.s. shaft voltage decreases initially and then increases steadily. (See Fig. 5.8).

Initial measurements indicate higher voltages between the shaft and motor frame. This could be due to increased resistance across the bearing and the current flowing in the frame - shaft circuit.

As r.m.s. induced shaft voltages are approximately independent of load condition - Fig. 5.8, it indicates that shaft voltages are mainly induced due to circulating fluxes [5.2] as briefly explained under Section 5.4.

## 5.4 Shaft Currents.

Shaft currents exist due to an e.m.f. between shaft and bearing lining. The most important cause is an ac flux linking the shaft [5.2]. Alternating shaft fluxes

and electrostatic potentials also contribute to shaft currents.

### 5.4.1 Currents due to shaft flux.

The magnetic circuit consists of shaft, bearings and frame. If a flux flows in the magnetic circuit a homopolar voltage will be induced in each bearing as the revolving shaft cuts the radial flux lines from shaft to bearing. The voltage induced in the two bearings is opposite and equal if the flux through the one bearing returns via the other bearing, which is generally the case. Such voltages will induce localized bearing currents.

The frequency of the shaft voltage will be equal to the frequency of the induced flux. For a three phase excited low power induction motor (with whole stator and rotor segments) three times the fundamental frequency will be induced. This can be deduced from the fact that for a square wave inverter the $5^{th}$ and $7^{th}$ harmonic (250 Hz and 350 Hz) are present in the shaft voltage frequency spectrum Fig. 5.9.b as $15^{th}$ and $21^{th}$ harmonic (750 Hz and 1050 Hz) respectively. Moreover, the $6^{th}$ harmonic (300 Hz) present is due to the switching frequency - 6 pulse square wave inverter which substantiates the fact that additional voltages are induced originating from the commutation process and voltage and current spikes.

If an alternating shaft voltage can thus be detected, a bearing current will be induced. Homopolar voltages across the bearings could not be measured, as it is practically inconvenient, and unpractical or impossible in real industry applications.

### 5.4.2 Currents due to ac voltages induced in the shaft.

In all multipolar induction machines the flux of each pole, after crossing the air gap flows through the yoke and splits up into two portions. The clockwise and counterclockwise flux returns via the air gap. If these two fluxes are not exactly equal, the difference flows to complete the magnetic circuit in the yoke. This difference in the flux links the shaft and will induce an alternating voltage in the circuit consisting of

frame, bearings and shaft. A shaft current will then flow.

This cause is more dominant in sectionalized stator and rotor laminations.

The shaft currents described in Section 5.4.(ii) are discussed in more detail in [5.2].

## 5.5 Effects and Physical Relevance.

The effect of bearing currents is illustrated in a paper [5.1] for a rolling type and shell type. Roller bearings have a few finite contact points thus very localized concentrated currents will flow across the contact points. For shell bearings a thin oil-film separates shaft and bearing, but a few points with thinner layer of oil will break down and will conduct, causing localized damages. Small craters will occur in the metal surface, small metal particles will be rubbed off (manifested in dark lubricating oil) thus reducing the isolation capability. A temperature increase and increased friction will result in a rapid destruction of the bearing surfaces.



**Table 5.2.** Limiting values for shaft voltages with loose liner bearings according to [5.1].

| Shaft Voltage [mV] | Effect on bearings. |
|---|---|
| < 300 | No danger. |
| 300 to 1000 | Damaging bearing currents can flow. |
| > 1000 | Detrimental effects in due to bearing currents can occur after weeks to years. |

For rolling bearings, (according to [5.1]), the limiting values are **100 [mV]** which are exceeded for peak values at nonsinusoidal excitation. See Table 5.1.

It can be concluded that in the case of using an inverter excitation, the lifetime of bearings is shorter than those used under a sinusoidal excitation. From the discussion it follows that the shaft voltage due to inverter excitation is increased due to following factors:

(i). Additional harmonics present in the supply voltage.

(ii). The commutation process in the inverter induces switching transients (e.g. 6 Pulse) superimposed on the inverter supply and induces another shaft voltage component by means discussed in this chapter.

No large difference between the shaft voltage induced by the Square Wave and PWM inverter has been observed.

## 5.6 Suggestions

It is suggested that the induced shaft voltage of a new machine under known excitation and load should be specified. At a later stage, e.g. after 1000 working hours, measurements should be repeated or should even be incorporated into a planned maintenance system. Proper knowledge of bearing type and lubricant in the machine must be available to determine limiting characteristics. Once a data base on shaft voltages and conditions of associated bearings has been established, conclusions on the state of the bearing can possibly be drawn. The effect of using different types of lubricants should also be established. (Graphite based lubricants will clearly conduct better due to its electrical properties).

A reduction in shaft voltage across the shaft end indicates that the oilfilm does not isolate properly, which is more important in shell-type bearings [5.1] and could also reveal conditions on other type of bearings. A reduction in effective voltage between shaft and frame also indicates increased damage to the bearing.

Shaft voltage compensation methods are discussed in [5.1] and [5.2].

# CHAPTER 6. TORQUE PULSATIONS.

## 6.1 The Torque of the Inverter Motors.

The higher time harmonics similar as higher space harmonics can produce asynchronous and pulsating torques.

Asynchronous torques due to higher time harmonics can be calculated similarly as asynchronous torques due to the fundamental harmonic eg. dividing the developed (electromagnetic) power by the angular frequency. In the case of 3-phase motors, higher harmonic torque n = 7, 13, 19, ... produce asynchronous torques acting in the same direction as the fundamental harmonic torque (n = 1) and higher harmonic n = 5, 11, 19, ... produce asynchronous torques in opposite direction to the fundamental rotating magnetic field.

As a result of action of stator currents and rotor currents of different frequency, pulsating torques are produced, the frequency of which exceeds significantly the fundamental frequency and the average value of them is equal to zero. The most important pulsating torques are those due to the stator fundamental harmonic and rotor higher harmonics.

Selected papers which in the authors opinion are the most relevant have been reviewed. [1.4, 1.5, 3.2, 3.4, 3.7, 3.9, 3.11, 3.16, 6.1, 6.2].

An analytical method to calculate pulsating torques, including the effect of dc bus pulsations and rotor speed oscillations is presented in the paper [6.1], using transformations in a multiple reference frame. Increased torque pulsations, especially at low rotor speeds are predicted.

The strain of an induction motor drive for electric locomotives with 16 $^{2}/_{3}$ Hz supply is investigated in [6.2] and the effect of harmonics in the dc link are determined. Magnitudes of torque pulsations and their respective frequency spectrums are calculated according to derived fromulas and are verified by measurements.

## 6.2 Asynchronous Torques.

The motor output asynchronous torque $T_n$ as a function of slip $s_n$ for synchronous speed $w_{sn}$ and supply voltage $V_{1n}$ can be approximated as:

$$T_n \approx \frac{3}{nw_s} \cdot \frac{R_{2n}'}{s_n} \cdot \frac{V_{1n}^2}{(R_{1n}+R_{2n}'/s_n)^2 + (2\pi n f_1 (L_1 + L_{2n}'))^2} \quad \ldots(6.1)$$

A more detailed analysis including the effect of losses can be found in the papers [3.3, 3.11].

The effect of asynchronous (time constant) torques on the steady state average rotor torque at different operating conditions has been considered. The torque as a function of r.m.s. line excitation current is given in Fig. 6.1. It can be observed that at rated current the torque output is reduced for inverter applications. This is clear as the harmonic components measured are portion of the r.m.s. current, but do not produce any useful torque. In Table 6.1 the rated torque (20 Nm) is tabled at respective current and produced torque at maximum efficiency, as well as the associated power factor and rotational speed in r.p.m.

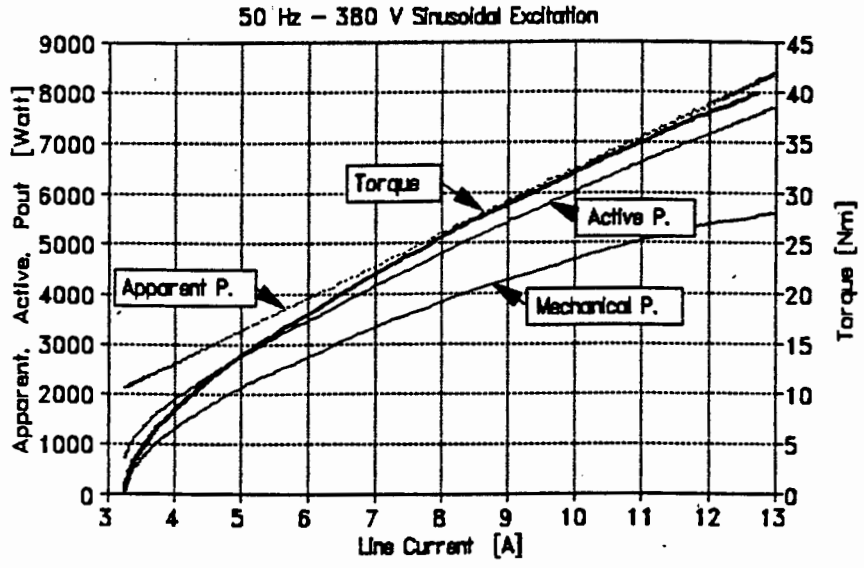


(a).

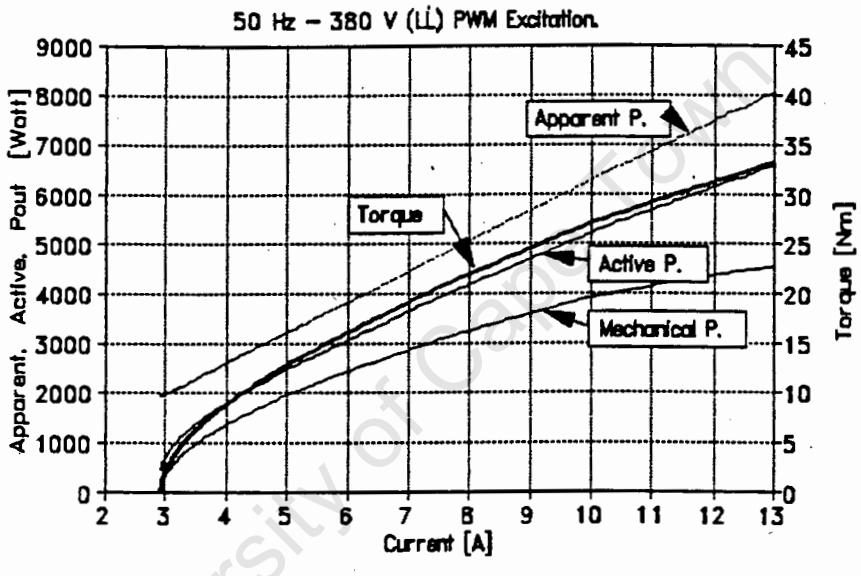


(b).

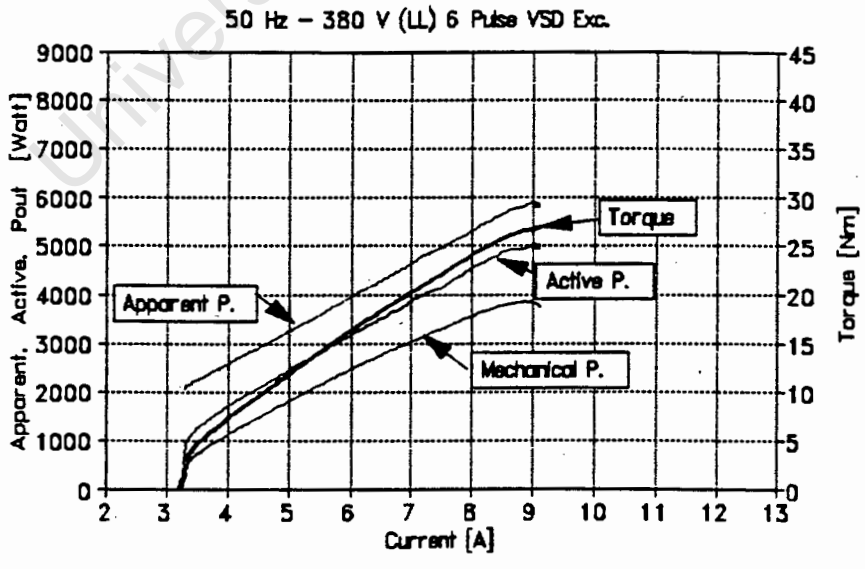


(c).

**Fig. 6.1** Input Power (Apparent and Active), Mechanical Output Power and **Torque** vs r.m.s. line current for inverter excitation: (a) Sinusoidal, (b) PWM, (c) Square wave.

**Table 6.1** Rated and associated Torque and Current, efficiency, power factor and rotational speed. (configured for $V_r/50$).

| Excitation | Torque [Nm] | Current rms. [A] | Eff.($\eta$) (%) | Power-Factor | Speed [Rpm.] |
|---|---|---|---|---|---|
| Sine. | 20.24 ▒ | 6.54 | 79.9 | .905 | 1430 |
| | 22.56 | 6.88 ▒ | 80.08 | .913 | 1443 |
| PWM. | 20.02 ▒ | 7.33 | 78.2 | .823 | 1430 |
| | 18.89 | 6.95 ▒ | 78.5 | .82 | 1421 |
| Square Wave. | 20.07 ▒ | 6.96 | 78.7 | .852 | 1431 |
| | 20.57 | 6.92 ▒ | 78.7 | .831 | 1431 |

▒ indicates rated torque or rated current respectively.

It can be concluded from measurements performed that at rated r.m.s. line current the electromagnetic torque $T_i$ developed at rated current is related according:

$$T_{iSIN} > T_{iSQW} > T_{iPWM} \qquad ...(6.2)$$

At rated torque the respective r.m.s. line current $I_t$ supplied to the induction motor is related according:

$$I_{tPWM} > I_{tPWM} > I_{tSIN} \qquad ...(6.3)$$

The increased r.m.s. current at rated torque can be explained in view of the distortion factor **DF**, which is zero for sinusoidal excitation, for square wave excitation approximately equal to 0.31 and for PWM (sinusoidal modulation) equal to 0.511 according to the simulation in **Appendix** 3.1.

The amount of voltage distortion (DF) is defined by the IEEE Standard 519 as:

$$DF = \left[ \frac{\sum_{n=2}^{\infty} V_n^2}{V_1^2} \right]^{\frac{1}{2}} \qquad ...(6.4)$$

See **Appendix 3.2.** for a simulation of data, distortion factor indicated.

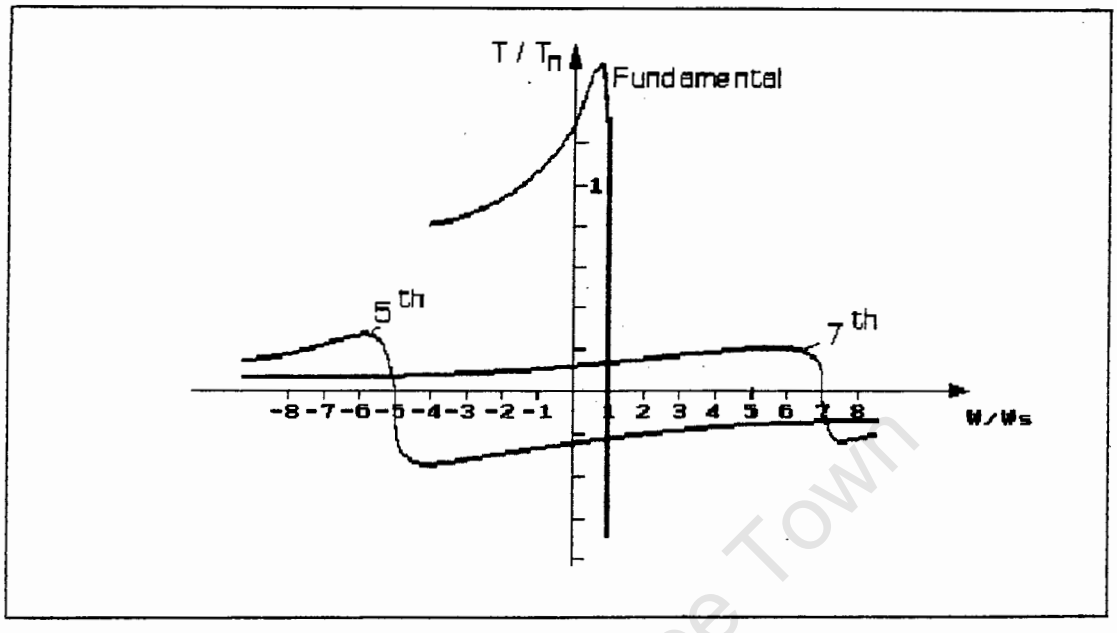


**Fig. 6.2** Fundamental and harmonic Speed Torque curves.

The asynchronous torque contains forward $T^{+}_{n}$ (n = 1, 7, 13, ...) and backward rotating components $T^{-}_{n}$ (n = 5, 11, 17, ...) ie. :

$$T = \sum_{n=1}^{\infty} (T^{+}_{n} + T^{-}_{n}) \qquad ...(6.5)$$

For a square wave VSI a negligible small negative torque would be developed in the operating region, reducing the developed torque very slightly. The torque is generally approximated for n = 1,5,7 as in [3.16]. For operation purposes the asynchronous harmonic torques produced by impressed time harmonic voltages do not affect the torque significantly, [3.16] and [4.2].

At high frequencies the motor impedance is large and thus only a very small torque producing current flows. This has been confirmed by simulation and measurement in a paper [3.11].

## 6.3 Pulsating Torques.

Inverter induced torque pulsations (also referred to as parasitic oscillating torque components) due to the

high harmonic content in the supply, are produced by the interaction of rotor m.m.f. waves and the air gap fluxes of different harmonics. These parasitic torques are in general much larger than oscillating torques produced by space harmonics [2.3, 6.2].

A harmonic component in the airgap induced by higher time harmonic voltage components in the supply, induces an rotor current of approximately the same frequency ($s_n \approx 1$). The torque then produced is in the same direction as the direction of the air gap flux.

In the case of a square wave inverter with dominant low frequency harmonics ($5^{th}$ and $7^{th}$), the $5^{th}$ harmonic (+1) rotates in the opposite directions (clockwise) as compared to the fundamental (-1)(anticlockwise), and the $7^{th}$ adds to the fundamental torque in the same direction (-1).

The electromagnetic torque pulsations can be calculated by superimposing flux and rotor current phasors.

The interaction between the fundamental airgap flux $\Phi_{g1}$ and the fundamental rotor fields $B_{r1}$ produces a steady torque as both components rotate at the same speed and same direction. The same applies for $5^{th}$ and $7^{th}$ torque components. However, the interaction between the $5^{th}$ (+1) harmonic flux and airgap field and the fundamental (-1) components results in a torque component rotating at 6 times the fundamental frequency. The same applies for the $7^{th}$ and fundamental component which both rotate in anticlockwise direction, resulting in another $6^{th}$ harmonic torque component. Thus, the $5^{th}$ and $7^{th}$ harmonics with respect to the fundamental produce a $6^{th}$ harmonic pulsating torque. The same applies to harmonic components of higher order, e.g. $11^{th}$ and $13^{th}$ would produce a $12^{th}$ harmonic torque, however at much smaller magnitude.

The interactions between harmonics of higher order can be neglected, as the flux components of e.g. $5^{th}$ and $7^{th}$ harmonics are very small.

For the calculations of motor torque pulsations, generally linerarized models have been used which assume constant speed of operation as well as constant dc-

inverter bus voltage. Harmonic torques result in oscillations of the rotor speed, and harmonic currents in the stator windings result in a variation of the inverter bus voltage.

Methods to calculate the torque pulsations as a function of various data such as excitation frequency, harmonic content of the supply voltage, dc bus voltage ripple, speed ripple are presented in many papers e.g. [3.1, 3.2, 3.3, 3.11, 3.9, 1.4].

The rectified dc bus voltage is not smooth so that current time harmonics are also existent in the intermediate dc circuit which could in turn create new torque oscillations or intensify existing harmonics. The current in the intermediate circuit is given in [2.3] and 6.2] as:

$$I_d(t) = I_{d0} + \sum_{u=2}^{\infty} I_{du} \cos (u\ 2\pi f_{sup} + \delta_{nu}) \qquad ...(6.6)$$

were $I_d$ is the current flowing in the dc circuit
$I_{du}$ alternating current in the dc circuit
$f_{sup}$ the supply frequency
$u$ the order of the harmonic in the dc circuit,
with $u = 2, 4, 6 \ldots, \infty$.

The peak value of the torque oscillations for three phase systems are given in [2.3, 6.2], consisting of three components.

$$T_a = 1.83\ p\ L_m\ I_{d0}\ \hat{I}_{du}\ \frac{1}{s\ w_1\ \tau_{ro} + 1/(s\ w_1\ \tau_{ro})} \qquad ...(6.7)$$

at frequency $uf_{sup}$.

$$T_b = \frac{\hat{V}_1^2}{w_1^2}\ \frac{1}{(L_1+L_2')}\left[\frac{1}{(6k-1)^2} - \frac{1}{(6k+1)^2}\right] \qquad ...(6.8)$$

at frequency $6kf_1$.

$$T_c = \frac{\hat{V}_1^2}{w_1^2} \frac{1}{(L_1+L_2')} \left[\frac{1}{(6k-1)^2} - \frac{1}{(6k+1)^2}\right] \left[\frac{\hat{I}_{d\tau}}{2I_{do}}\right] \quad ...(6.9)$$

at frequency $6kf_1 - uf_{sup}$.

were $T_a$, $T_b$, $T_c$.. respective peak torque pulsations due to inverter applications

$\hat{V}_1$ and $\hat{I}_{du}$... are the peak fundamental voltage and harmonic$^{th}$ dc current.

$L_m$, $L_1$, $L_2'$.. are the magnetizing inductance, stator and rotor leakage inductances at $w_1$.

p..... number of pole pairs.

$\tau_{r0}$..... rotor time constant $(L_m+L_2')/R_2'$

$k = \pm1, \pm2, \pm3, \ldots$

Harmonic components present are $n = 1 \pm 6k$.

From the equations (6.8) to (6.10) it can be concluded that:

(i). Higher p.u. torque pulsations at low speeds $w_1$ (according to $T_b$ (6.8) and $T_c$ (6.9) ) will be experienced.

(ii). Dominant torque pulsations if low order harmonics ($5^{th}$ and $7^{th}$, k=1) are present in the excitation voltage. For higher harmonics ($17^{th}$, $19^{th}$ and $23^{rd}$ $25^{th}$ as sidebands of the $21^{st}$ for PWM excitation) k will be larger k=3, k=4, thus reducing the harmonic torques considerably. The pulsating component contributed from $T_b$ (6.8) will be the largest component.

(iii). An increased effect on torque pulsations $T_a$ and $T_b$ due to dc bus voltage pulsations can be expected.

(iv). At low excitation frequencies with high voltage boost which is required for higher starting torque, thus $V_1$ is large and $w_1$ low, considerable pulsating torques can be expected according $T_b$ and $T_c$. For low voltage boost the torque pulsations will be marginally smaller, but also the starting torque will be reduced considerably.

(v). Increased leakage reactance will reduce the torque pulsations.

In a paper [3.9] an equation for the harmonic torque related to the fundamental torque is derived from a two axis equivalent. It is shown that the amplitudes decrease inversely to the order number of the harmonic torque. The harmonic torque spectrum also changes only marginally between no load and rated load condition.

The dc bus voltage on a six step square wave voltage source inverter was measured and is shown in Fig. 6.3. Under load conditions a ripple voltage of 10V to 20V and under no load conditions 20V to 30V peak to peak is superimposed on the average dc bus voltage of approximately 430V dc. The the PWM inverter dc bus voltage ripple was not be measured but will also have some voltage ripple superimposed.

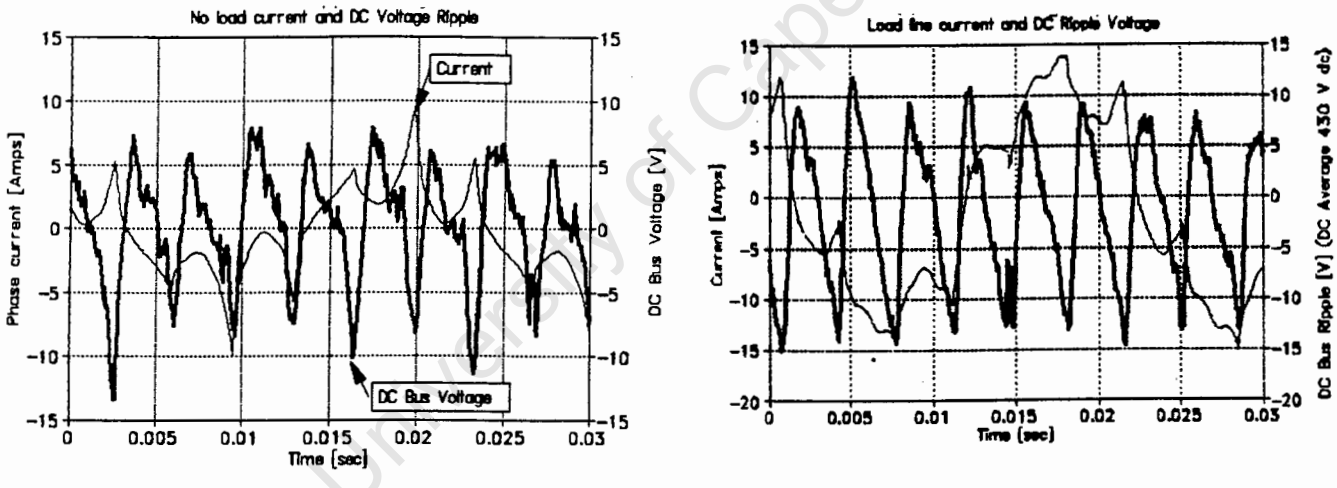


(a). (b).

**Fig. 6.3** DC bus Voltage ripple for a six step square wave VSI (at 50 Hz, configured for $V_r/50$) under (a) No load and (b) Load condition.

The frequency of the voltage ripple is six times the fundamental exciting frequency. The thyristors are switched at the same frequency which thus create a dominant $6^{th}$ harmonic voltage ripple component. The transistor controlling the dc bus voltage (Danfoss VLT 5, controlled dc bus voltage) has only a very small effect at high fundamental frequency (e.g. rated 50 Hz as in Fig. 6.3). At low frequencies the dc bus voltage must be kept low and the switching of the voltage regulator

transistor will effect the dc bus voltage to a larger extend, possibly inducing another lower frequency components due to transistor switching. Low speed torque pulsations for square wave and PWM excitation are shown in Fig. 6.10. It is also evident that the superimposed dc bus voltage ripple is larger under load conditions as compared to no load conditions.

## 6.4 Consequences of Pulsating Torques.

The important aspect of torque pulsations is to understand and identify the adverse effects caused and the influence on the mechanical performance. In the IEC standards the presence of oscillating torques is highlighted and it is recommended to analyze the torsional resonance frequency if transmission elements are not sufficiently damped.

Torque pulsations affect the mechanical performance of induction machines severely. It must be understood that a load unit interacts with a motor and adverse effects caused must be identified. Pulsating torques affect amongst others:

(i) The vibration of the frame and rotor shaft, especially if the torque pulsations are at a frequency near the mechanical resonance of the motor. The damping coefficient of steel is relatively small, and detrimental resonant oscillations can produce dangerous torsional stresses in the shaft and coupling.

(ii) Torque pulsations produces excessive bursts of speed. This is observed as jitter and is more prevailing in low inertia machines.

The amplitude of the angular speed ripple is approximated according to [1.6] as:

$$w_{rip} = k_T \frac{T_{rip}}{f_{rip} * H} \qquad \left[\frac{1}{s}\right] \qquad \ldots(6.10)$$

were $k_T$ is a constant, $w_{rip}$ is the amplitude of the angular ripple speed, $T_{rip}$ the amplitude of the torque ripple, $f_{rip}$ the ripple frequency and H the inertia of the system.

(iii). System instability may occur at low frequencies, and over a larger speed range if system parameters are not selected appropriately [6.1]. Unsatisfactory performance of feedback control systems can take place.

These effects could cause shaft fatigue, wearing of the gear teeth, and may affect the operation of the load, depending on the application. Shaft fatigue failure subsequent to shaft system torsional resonance, induced by higher harmonic torques, is common in induction motors.

The use of variable speed drives must be considered with their application. Where uniform speed of rotation is essential, such as for machine tool applications, antennae positioning, synthetic fibre spinning machines, film or web machines etc. speed oscillations which occur due to torque pulsations must be minimized. Torque pulsations can not be eliminated however, but reduced by proper modulation strategies eliminating low order harmonics.



## 6.5 Torque Pulsations over the Operating Range.

For variable speed drive applications it is important to estimate the mechanical performance with respect to torque pulsations under different load conditions over the whole operating range. As shown in equations (6.8) and (6.10) relative torque pulsations are dependent on fundamental speed. Moreover, over the whole speed some mechanical and torsional resonance may occur, thus reinforcing torque oscillations. At some excitation frequencies the interaction between higher time harmonics

and space harmonics, depending on the machine design may interact to a larger extend than at other excitation frequencies. In the subsynchronous operation region some resonance may occur, which are of importance for both the vibrational aspect as well as torque oscillations which would result in torsional stresses on shaft, coupling and load.

In the following figures the peak torque oscillations are shown under load and no-load (except PWM excitation) condition configured for synchronous characteristic ($V_r/50$) and load conditions under PWM and square wave excitation for subsynchronous characteristic ($V_r/87$) operation. The fundamental excitation frequency and rotational speed in r.p.m. are indicated.

For synchronous configuration ( up to 50 Hz).

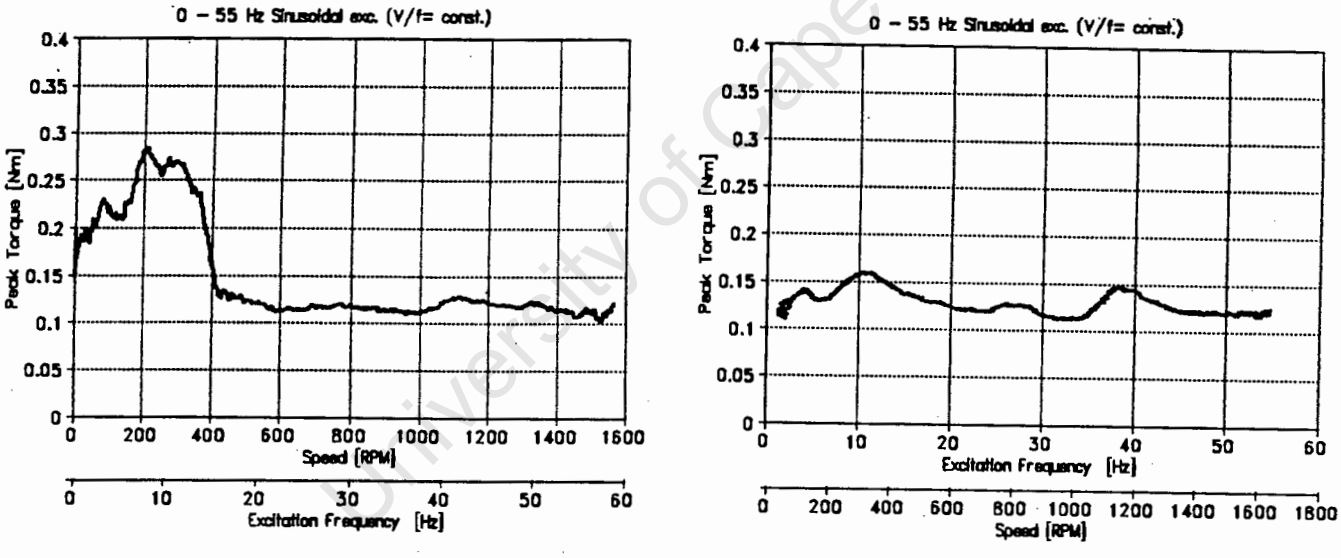


(a). (b).

**Fig. 6.4** Sinusoidal excitation ($V_r/50$) Peak Torque Pulsations vs Excitation frequency and rotational Speed. (a) No Load and (b) Load condition.

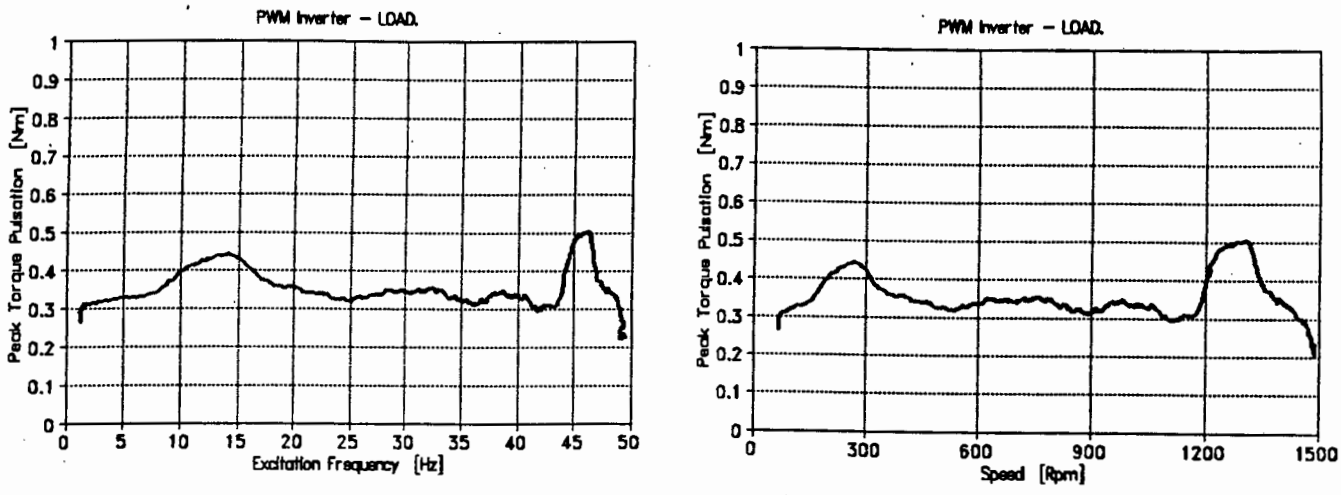


(a). (b).

**Fig. 6.5** PWM excitation ($V_r/50$) Peak Torque Pulsations vs Excitation frequency and rotational speed. (a) Torque Pulsations vs frequency and (b) Torque Pulsations vs speed.

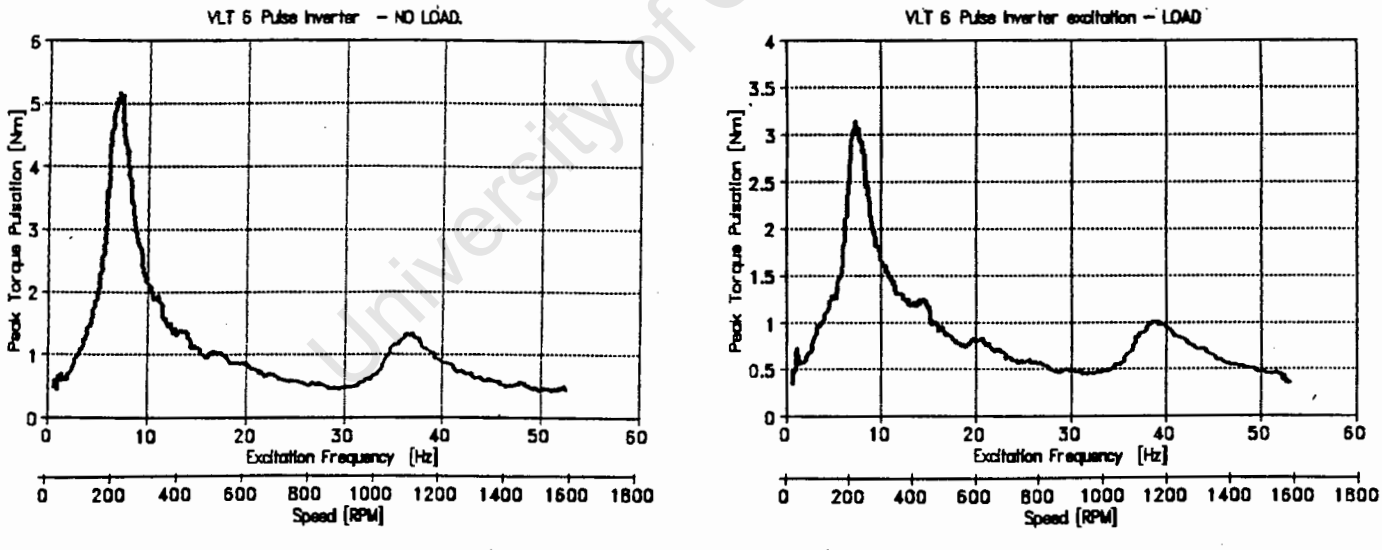


(a). (b).

**Fig. 6.6** Square wave excitation ($V_r/50$) Peak Torque Pulsations vs Excitation frequency and rotational speed. (a) No Load and (b) Load condition.

For subsynchronous configuration (up to 100 Hz).

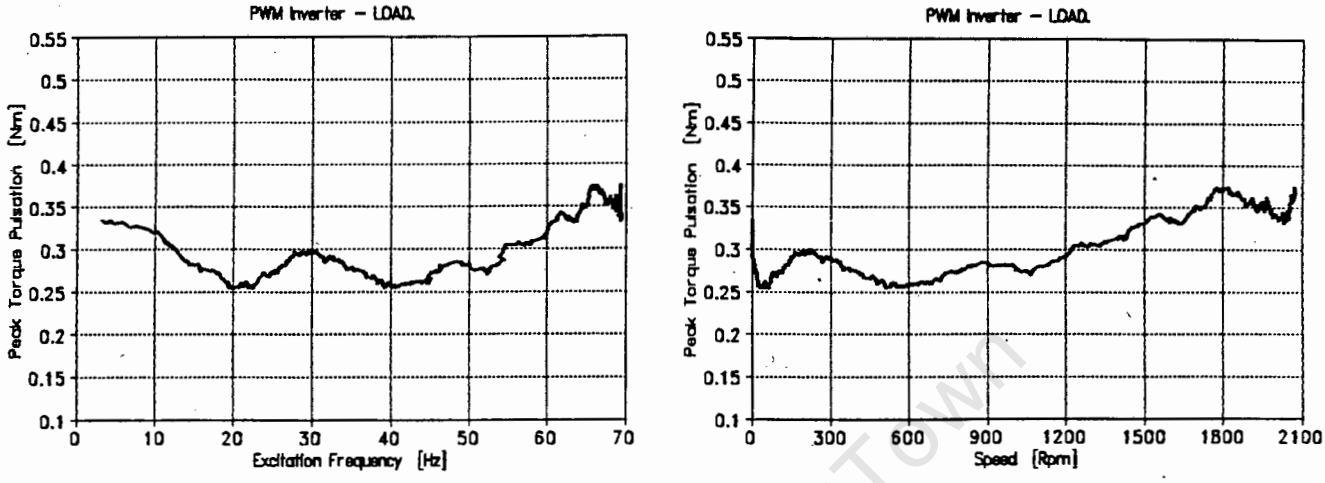


(a). (b).

**Fig. 6.7** PWM excitation ($V_r/87$) Peak Torque Pulsations vs Excitation frequency and rotational Speed under load condition. (a) Torque Pulsation vs frequency and (b) Torque Pulsations vs Speed.

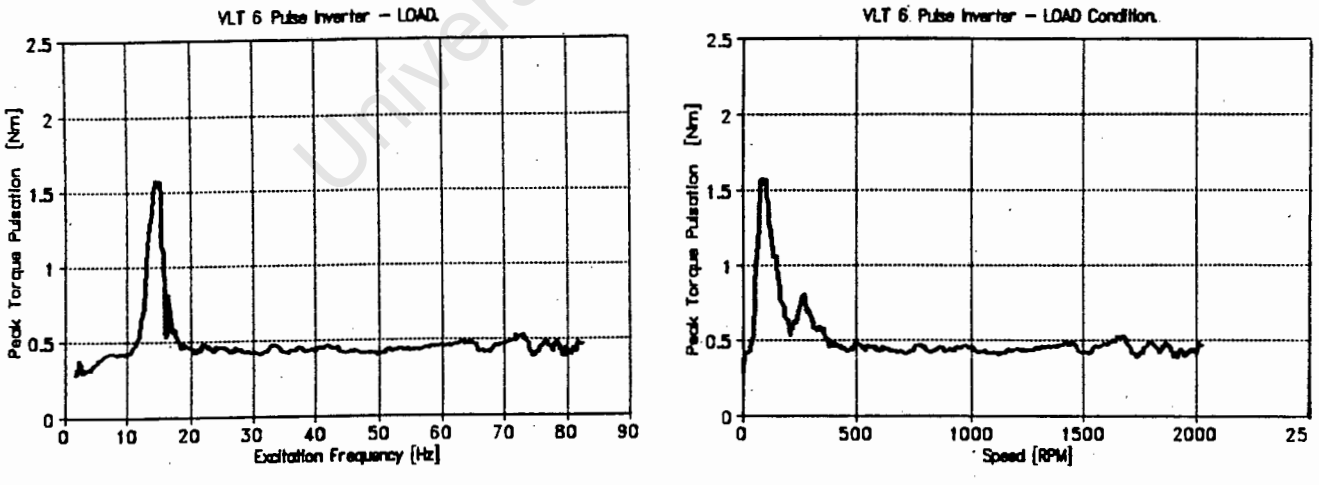


(a). (b).

**Fig. 6.8** Square wave excitation ($V_r/87$) Peak Torque Pulsations vs Excitation frequency and rotational speed under load conditions. (a) Torque Pulsations vs frequency and (b) Torque Pulsations vs speed.

Additional graphs for no-load pulsating torques for subsynchronous conditions are given in **Appendix 6.1.** Additional graphs for torque pulsations with external leakage inductance in series with the supply to filter out some harmonics is shown in **Appendix 9.1.**

It is clear that the peak torque pulsations vary considerable over the whole speed range. It can generally be concluded that under load conditions the torque pulsations are significantly reduced at low frequency ranges, and marginally reduced at higher operating frequencies. A high slip can be noticed at low frequencies under load for subsynchronous configuration. From figures **Appendix 6.1.** it is clear that a pulsating torque resonance will occur at high speeds, which is caused by the mechanical behaviour of the system.

For square wave excitation severe torque pulsations occur at low excitation frequencies in the zone around 7 Hz and 15 Hz for synchronous and subsynchronous configuration respectively. Near 37 Hz the pulsations increase again, and then decrease to a low value. The high amplitude of the torque pulsations at low speeds is also simulated in [6.1], and it is thus apparent that speed pulsations are present and enhance the oscillations, which may possibly resonate at that frequency. A crawling noise was distinctly audible at the peak torque pulsations, supporting the assumption that some resonance occurs at that low speed and configuration.

For sinusoidal and PWM excitation no considerable high pulsating torques are present, neither at low speed nor rated speed operation. An marginal increase in peak torque pulsations materializes at 46 Hz for PWM excitation. This will be due to some mechanical vibration or small resonance. Only for square wave excitation significant and unfavourable torque pulsations occur.

It can be observed from figures attached in **Appendix 9.1.** that the torque pulsations are reduced considerably at low speeds when **external** inductances are inserted in series with the supply to increase the total leakage inductance. This is in accordance with equation (6.9) and (6.10). However, another increase in pulsations at 25 Hz is evident under both load and no-load conditions.

## 6.6 Torque Pulsations at low Speeds.

As discussed in theory in section 6.5 relative large magnitude p.u. torque pulsations are expected at low speeds.

This phenomena known as parasitic asynchronous and synchronous torques have been often described eg. Heller and Hamata [3.20]. Only high torque pulsations were measured for square wave VSI's as they contain low order current harmonics. The current and torque signal under load condition at 10 Hz fundamental excitation (low speed - approximately 300 r.p.m.) with their respective frequency spectra are shown in Fig. 6.9. The current harmonics ($5^{th}$ and $7^{th}$, $11^{th}$ and $13^{th}$...) can clearly be seen. A very dominant $6^{th}$ pulsating torque is present at 60 Hz, thus confirming the results predicted.

Speed oscillations which would come about due to pulsating torques at low speeds could be observed using a stroboscope under steady state conditions and watching the fan blades jittering.

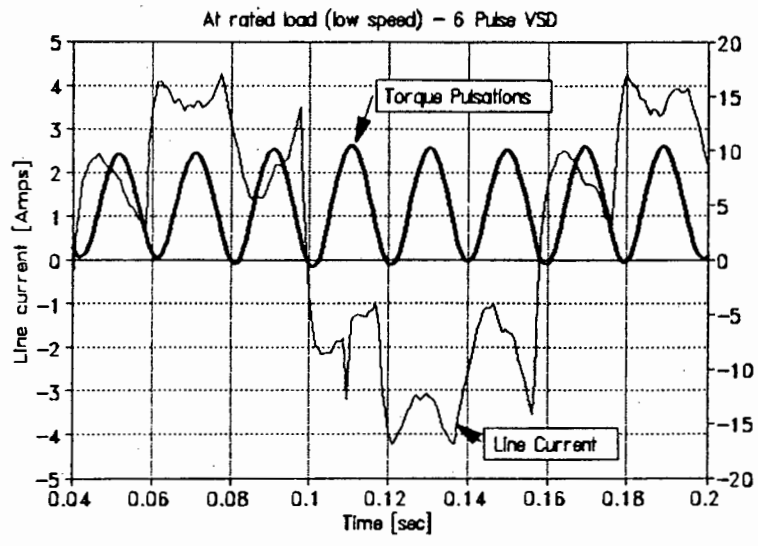


(a).

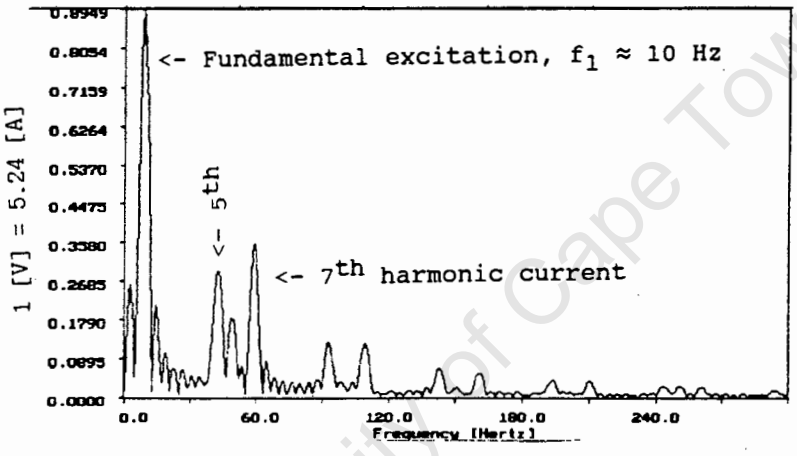


(b).

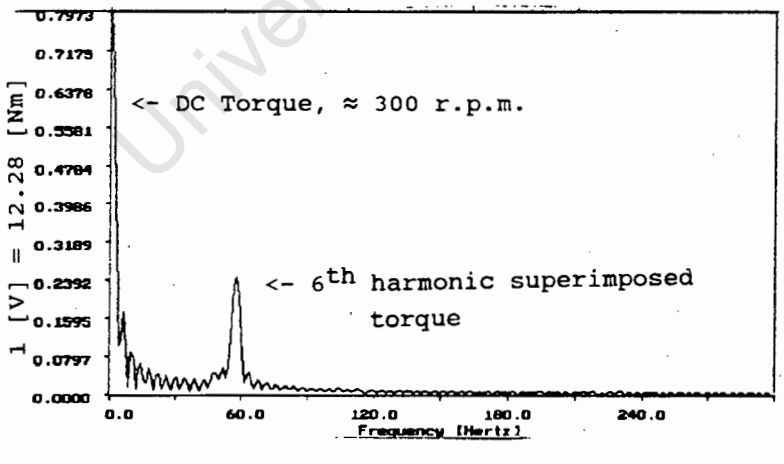


(c).

**Fig. 6.9** Low speed Torque Pulsations for square wave excitation. (a) Current and Torque signals, (b) Current frequency spectrum and (c) Torque frequency spectrum.

Due to the absence of low order time harmonics in the PWM excitation, no significant torque pulsations were observed at very low speeds as can be seen from the peak pulsations plotted as a function of speed and frequency in Figs. 6.5. and 6.7.

At an intermediate frequency of 30 Hz the steady state instantaneous torque and current were measured for PWM and square wave excitation and are shown in Fig. 6.10. (a). and (b).

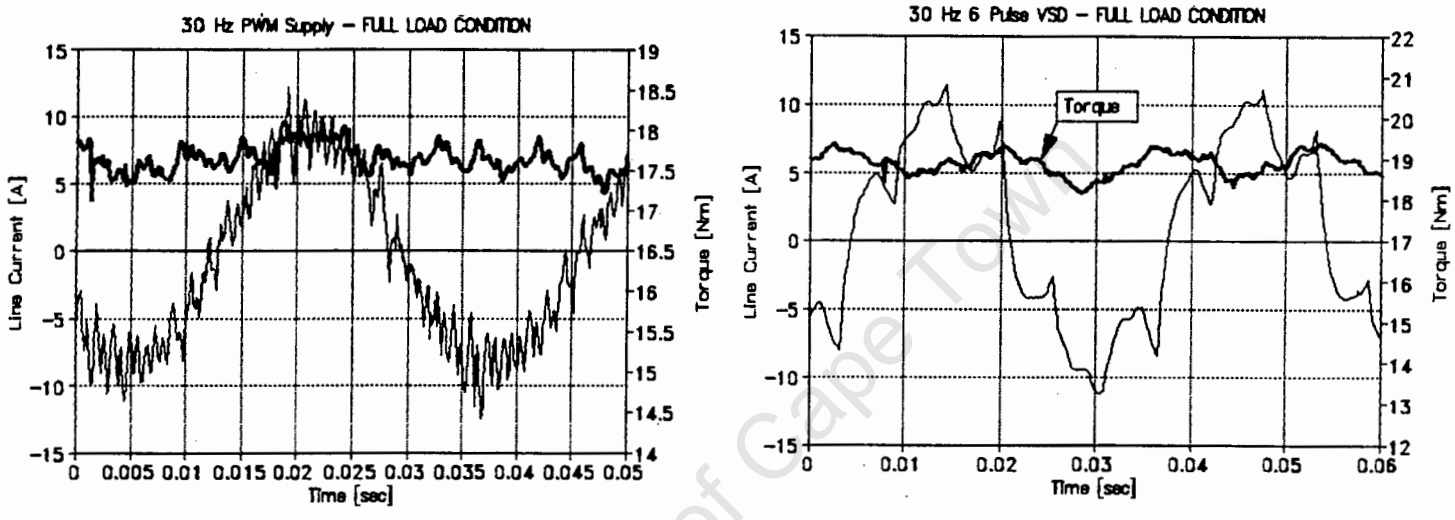


(a). (b).

**Fig. 6.10** Instantaneous Torque and Current at 30 Hz fundamental excitation under load condition for (a) PWM and (b) Square wave excitation.

The torque pulsations under PWM excitation are at relative high frequency compared to the fundamental excitation. Under square wave supply the $6^{th}$ harmonic can be detected superimposed on a low frequency oscillating torque, which may be of mechanical origin.

## 6.7 Torque Pulsations at Rated Speeds.

The influence of higher current harmonics on the parasitic torques is investigated at rated operating conditions, i.e. 50 Hz and 380 $V_{LL}$ excitation near rated torque. The instantaneous torque, current and the respective torque frequency spectrum for sinusoidal, PWM and square wave excitation at rated operation condition is shown in Fig. 6.11 (a). (b). and (c).

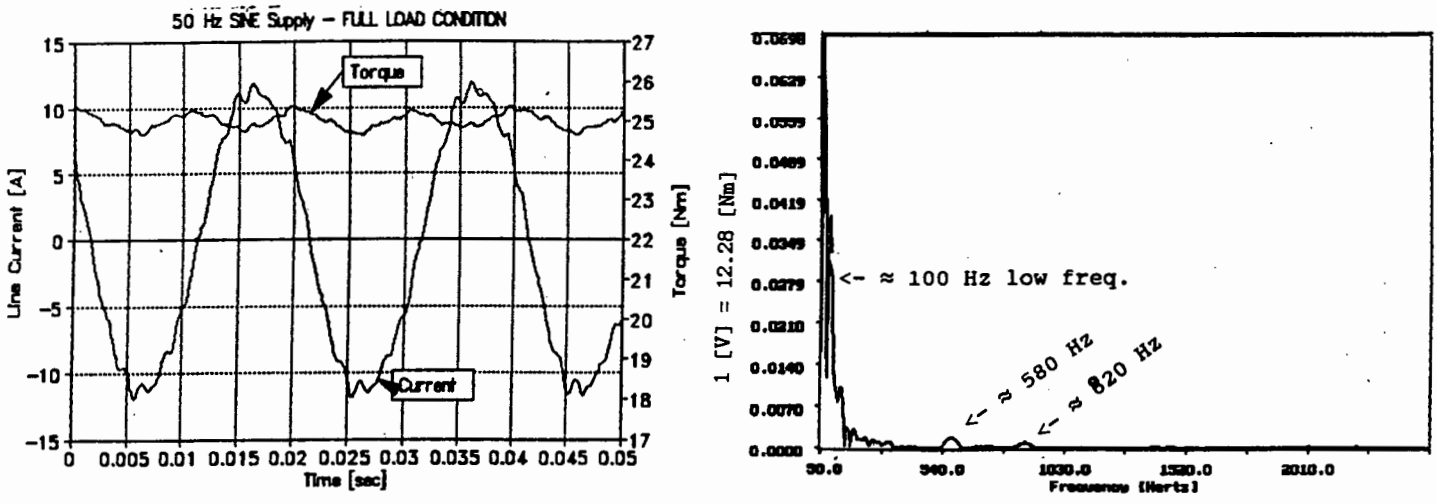


(a).

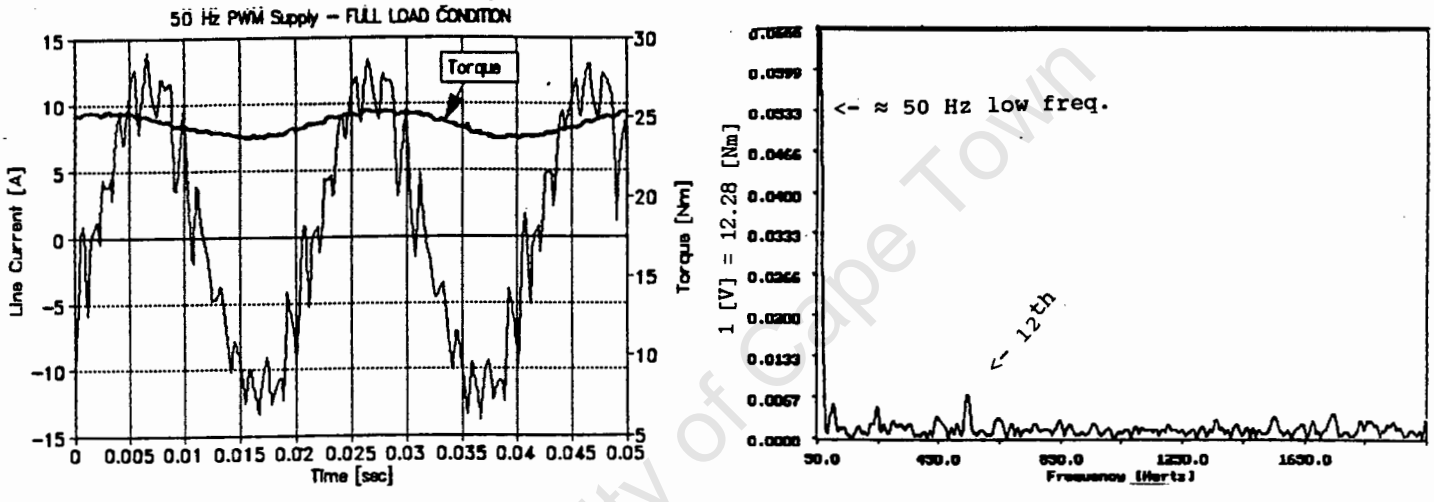


(b).

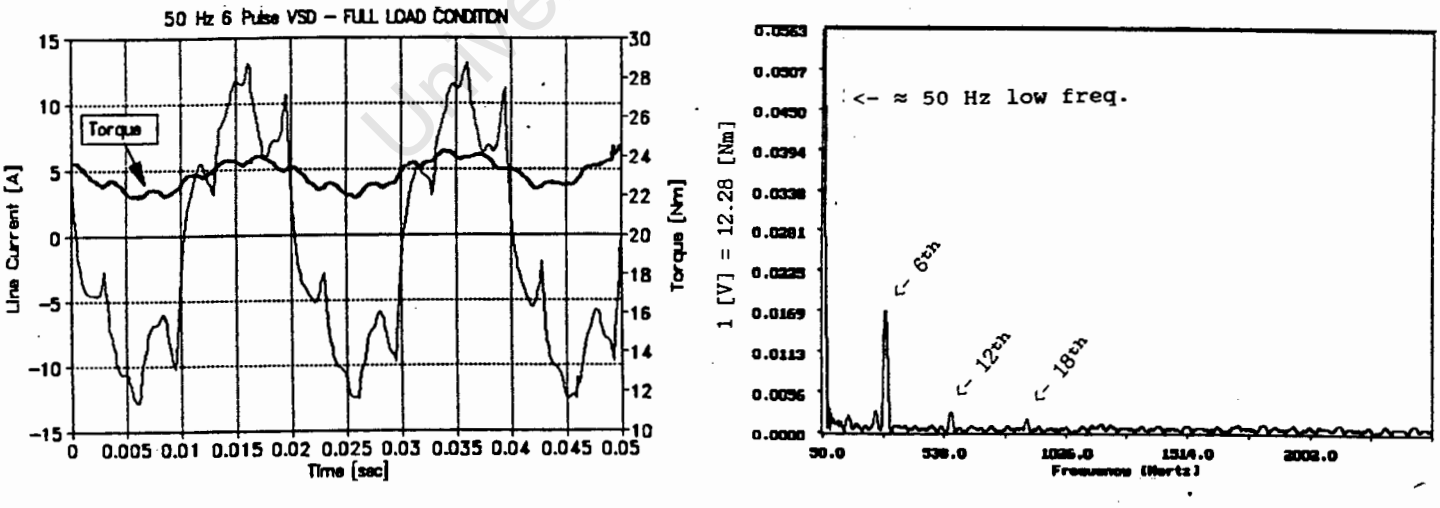


(c).

**Fig. 6.11** Instantaneous Torque, Current (left) and the respective torque frequency spectrum (right) (50 Hz, 380$V_{LL}$ for (a) Sinusoidal, (b) PWM and (c) Square wave excitation.

Under all excitation sources a low frequency oscillating torque can be observed. For sinusoidal excitation the low order torque oscillating frequency around 100 Hz is slightly higher than for PWM and square wave excitation, which is at approximately 50 Hz. For square wave and PWM excitation the magnitude of the torque oscillations seem to be marginally larger as compared to the low frequency torque amplitude for sinusoidal excitation, as seen in Fig. 6.11.

Two causes for the low speed oscillations will be briefly discussed.

(i). As the load is coupled via a stiff flexible rubber coupling (Fenner - type) some oscillations may be induced due to the interaction between the drive and the load. These oscillations are at low frequencies as the damping factor for the rubber coupling will be relatively high and motor - load interaction will be limited. Low order torque pulsations for sinusoidal excitation will most likely originate from mechanical causes.

(ii). A time harmonic stator current creates space harmonic rotating stator fields, which, on their turn, cause rotor currents in the cage of the induction motor [3.4]. These interactions are present if any of the conditions below for a cage motor are fulfilled:

$$N_1 = N_2 \pm 2p \quad \text{or} \quad N_1 = N_2$$
$$n \approx N_1/p \pm 1$$

were $N_1$ is the number of stator slots, $N_2$ is the number of rotor slots, and n the time harmonic order.

(iii) Synchronous and low frequency torques can be produced by superposition of permeance and m.m.f. harmonics [3.4]. These low frequency torques exist for both cage and slip ring motors if the conditions as before are fulfilled:

$$N_1 = N_2 \pm 2p \quad \text{or} \quad N_1 = N_2$$
$$n \approx N_2/p \pm 1$$

For the 4 pole induction machine tested $N_1 = 36$, $N_2 = 28$, ($p = 2$, 2 pole pairs). The lower harmonic numbers n to be considered for the square wave and PWM inverter are n = 5,7 11,13 and n = 17, 19 23,25 respectively.

$N_1/p = 18$; $N_2/p = 14$;

thus $N_1/p \pm 1 = 17, 19$ and $N_2/p \pm 1 = 13, 15$

Thus resulting in a match 13 in the case of the square wave excitation and a match for 17, 19 for PWM excitation.

However the condition to match the pole pair number for stator and rotor slots (synchronous torques) is not fulfilled for either type of requirement, but some interaction could still develop, even though to a smaller extend. The torque pulsations are also reduced by the rotor skew.

From the frequency spectra in Fig. 6.11 for all three supplies following observations can be made:

(i). Sinusoidal Excitation.

The low frequency torque component of approximately 100 Hz can be observed. Other parasitic torques at higher frequencies at (approximately) 150 Hz, 600 Hz and 800 Hz are present. These are due minimal unbalance and to space harmonics in the airgap and stator slot harmonics. It is interesting to note that the superimposed current harmonics due to saturation (in the slots) as shown in Fig. 3.4.a are at the same frequency as the parasitic torque components. The amplitude is however insignificantly small.

(ii). PWM Excitation.

The low frequency torque component of 50 Hz can be seen. A multiple of low frequency torque components are present, with very low amplitude. A component in the proximity of 250 Hz, 450 Hz, 600 Hz, 700 Hz, 1500 Hz are observed. The 600 Hz, $12^{th}$ harmonic torque is the largest of all higher frequency components. Compared to the other excitation sources, many high frequency components are superimposed on the average torque under PWM excitation. In the IEC standards [1.1] torque oscillations at twice the pulse frequency are predicted, i.e. at 21*50*2 Hz = 2100 Hz. The magnitudes and effects are however insignificant.

(iii). Square Wave excitation.

The low frequency torque component of 50 Hz can be seen. Dominant higher frequency torques are present near 300 Hz, 600 Hz and 900 Hz which represent the $6^{th}$ $12^{th}$ and $18^{th}$ torque component respectively. The $6^{th}$ harmonic torque can also clearly be seen superimposed on the average torque in Fig. 6.11 (c). This clearly correlates with the theory and predictions, as shown in equation (6.9).

The relative magnitude in percent at their proximate frequency with respect to the nominal fundamental torque is given in Table 6.2. Low frequency amplitudes were obtained from the graphs, as the torque frequency spectrum window starts at 50 Hz, and frequency components at eg 49 Hz would be not be detected.

**Table 6.2** Peak Torque Pulsations as percentage to nominal torque. for Sinusoidal, PWM and square wave excitation at rated operating conditions.

| Harmonic Torque: frequency [Hz] | | Excitation 50 Hz, 380 $V_{LL}$ (Percentage of full load torque) | | |
|---|---|---|---|---|
| | | **Sine** | **PWM** | **SQWave** |
| ≈ 50 | Low freq. | | 3.00 | 3.30 |
| ≈100 | Low freq. | 1.86 | | |
| 250 | | | 0.20 | |
| 300 | $6^{th}$ | | | 0.90 |
| 450 | | | 0.11 | |
| 580 | | 0.10 | | |
| ≈600 | $12^{th}$ | | 0.35 | 0.16 |
| 700 | | 0.07 | 0.12 | |
| 900 | $18^{th}$ | | | 0.08 |
| 1500 | | | 0.10 | |
| 1725 | | | 0.11 | |

The only relevant harmonics are the low frequency components of 1.86%, 3% and 3.3% for sinusoidal, PWM and square wave excitation respectively. The $6^{th}$ harmonic parasitic torque of ≈ 1% relative amplitude for square wave excitation is the only relevant higher torque portion. All other harmonics due to multiple interactions are in the region of 0.1%, except for the PWM torque component at 0.3% at ≈ 600 Hz, and are insignificant.

The frequency spectra are slightly obscured due to a Hanning window implemented and the zoom operation of the Chirp Z transform to obtain the specific frequency window.

# CHAPTER 7. VIBRATIONS.

## 7.1 Review of Research.

There are a lot of publications dealing with vibrations of induction motors. Many of them have been cited in Chapters 1. to 6. e.g. [1.2, 1.3, 2.3, 3.21].

In addition in the paper [7.1] equations for the axial forces developed due to rotor skew and displacement are developed on the basis of energy distribution are given. Experimental measurements confirm the predictions according to the derived equations.

In the paper [7.2] the natural frequencies for small to medium sized induction machines with thick stator laminations and thin frame are presented. Analytical and experimental results are compared.

The author of [7.3] discusses methods to limit the vibrations of induction machine dynamic systems.

In [7.4] equations are derived to determine natural frequencies of induction motor stators. The analytical approach includes as variables several design parameters, such as stator teeth, number of slots, Youngs modulus etc. Multiple resonances are also discussed.

In papers [7.5, 7.6] experimental procedures and apparatus are discussed to perform the test on different motor model outlined in part 2. of the paper. Results correlate with the theory developed in a companion paper [7.4].

## 7.2 Relevance of Vibrations in Inverter Applications.

In the draft IEC standard [1.1] no specific reference is made to increased vibrations of the induction motor or rotor shaft. It is clear that increased torque pulsations will affect the motor vibrations, but the increased number of magnetic exciting forces originating from higher time harmonics on the stator core and frame are not indicated in [1.1]. Critical speeds are relevant as

the operating range is covered as the motor will operate at some steady state speed within the operating range, which may cover a range from a few r.p.m. to 3000 r.p.m. - 6000 r.p.m. for 4 pole and 2 pole induction machines respectively. The frequency of the force waves are changed under VSI operation and a serious risk of resonance exists. The phenomena of resonance can occur under transient, as well as under steady state conditions if motor resonance and excitation forces coincide. Under mains excitation the critical speeds are passed relatively fast (depending on load condition) so that resonance cannot develop. Under variable speed operation however, the excitation force frequency may coincide with the natural frequency for longer periods with adverse effects to motor and system.

Vibration can be limited and managed if the natural frequencies of a machine and the driving forces are controlled. It would be impractical from a design point of view to keep all natural frequencies far above the excitation force frequencies. The easiest method would be to control the exciting forces [7.3], but this situation is complex under inverter application and measurement results will indicate the effect of higher time harmonics on vibrations. Motors are designed to have acceptable low levels of vibration, even at their natural frequencies. Motors interact with associated equipment and loads to form a dynamic system. This system may contain some interacting frequencies already and increase the number of natural frequencies of the system. Critical speeds can be unique to a specific installation, and are not always predictable in advance.

Natural frequencies of induction machines can be determined fairly accurately by calculations [7.2, 7.4] or by equivalent models [7.4].

## 7.3 Vibration Measurement.

Standard measurements use vibration velocity as reference, as vibration velocity is relative insensitive to frequency, but related to the sensation of vibration [2.3]. Due to limited equipment, only the vibration acceleration and r.m.s. vibration acceleration was measured. Band pass filters are used in some applications

to measure isolated conditions. To measure the vibrations precisely for small to medium sized machines, motors are mounted flexibly to isolate machines from their environment. Tests are performed under no load conditions at rated supply.

The quality of vibration is a single value indication the vibration severity. The vibration severity is the r.m.s. vibration velocity at selected operating points. [2.3, pp. 186].

In this project vibrations are measured on a rigid mounted machine-load set on a solid concrete and steel base isolated from the surroundings. Accelerometers with relative negligible mass compared to the motor mass, are fitted in the bearing plane as vibrations will be transferred to the frame in that plane from the rotor shaft via the bearings. Different excitation sources are used and vibration levels are compared under exactly the same operating conditions, thus valid conclusions can be drawn.

The principal directions in which vibrations are measured are the x, y, and z-coordinate as shown in Chapter 2., Fig. 2.6.



## 7.4 Oscillating and Deformational Force Waves.

Force waves of electromagnetic origin (due to interaction between rotor and stator waves) as discussed in Chapter 6. are also causing forces that act on the stator frame as well as the rotor and shaft. Further undesirable mechanical and magnetic forces are generated due to standard manufacturing inaccuracies. To highlight the importance of vibrations and resonance with inverter applications, theoretical aspects are briefly discussed.

The amplitude of the force wave varies with the square of the voltage, such that if time harmonics are very small, the resultant force waves become negligible. The frequency composition of the set of forces acting on the motor becomes richer in content.

The deformation (and noise) increases drastically if the exciting force frequency $f_r$ is near or at the natural

frequency of the motor, resulting in excessive vibration due to resonance.

In [2.3, pp. 39] the excitation force frequency as a function of slip (for transient conditions), the number of stator slots and number of pole pairs is derived as:

$$f_r = f_1\left[\frac{g\ N_2}{p}(1-s) + \begin{matrix}2\\ <\\ 0\end{matrix}\right] \qquad ...(7.1)$$

due to stator and rotor winding space harmonic interaction.

$$f_r = f_1\left[\frac{g\ N_2}{p}(1-s) + \begin{matrix}2\\ <\\ 0\end{matrix} \pm \begin{matrix}0\\ <\\ (1-s)/p\end{matrix}\right] \qquad ...(7.2)$$

due to stator winding and rotor eccentricity space harmonic interaction.

$$f_r = f_1\left[\frac{g\ N_2}{p}(1-s) + \begin{matrix}4\\ <\\ 2\end{matrix}\right] \qquad ...(7.3)$$

due to stator winding and rotor saturation harmonic interaction.

were $f_r$ is the frequency of the excitation force, $f_1$ the frequency of the fundamental excitation voltage to the stator, g any integer, $N_2$ number of slots in the rotor and s the slip.

For higher time harmonics the slip is approximated to 1 and excitation forces of higher order are 0, $2f_n$ or $4f_n$ with $f_n = nf_1$ . From equation (7.1) to (7.3) it is clear that the frequency of the exciting force is a function of slip. This explains the resonant vibration under transient conditions, as eg. on line starting of induction machines, as shown in Fig. 7.1. For inverter applications the slip for the fundamental will always be relative close to zero (≈ 10% max. depending on load condition) and the fundamental excitation frequency $f_1$ will change continuously.

For the induction machine tested, with 28 rotor slots and assuming s≈0 and g=1 the excitation force frequencies can be approximated to:

$$f_r \approx f_1 * (14 + \{0 \;/\; \pm\tfrac{1}{2} \;/\; 1\tfrac{1}{2} \;/\; 2 \;/\; 2\tfrac{1}{2} \text{ or } 4\}) \qquad ...(7.4)$$

according to (7.1 to 7.3) where $f_1$ is the fundamental excitation frequency.

These values will obviously deviate if the slip changes. At each operating point a multiple of excitation forces can exist (g = 1, 2, ...) and the chance that an existing force frequency and natural frequency of the system coincide is very likely.

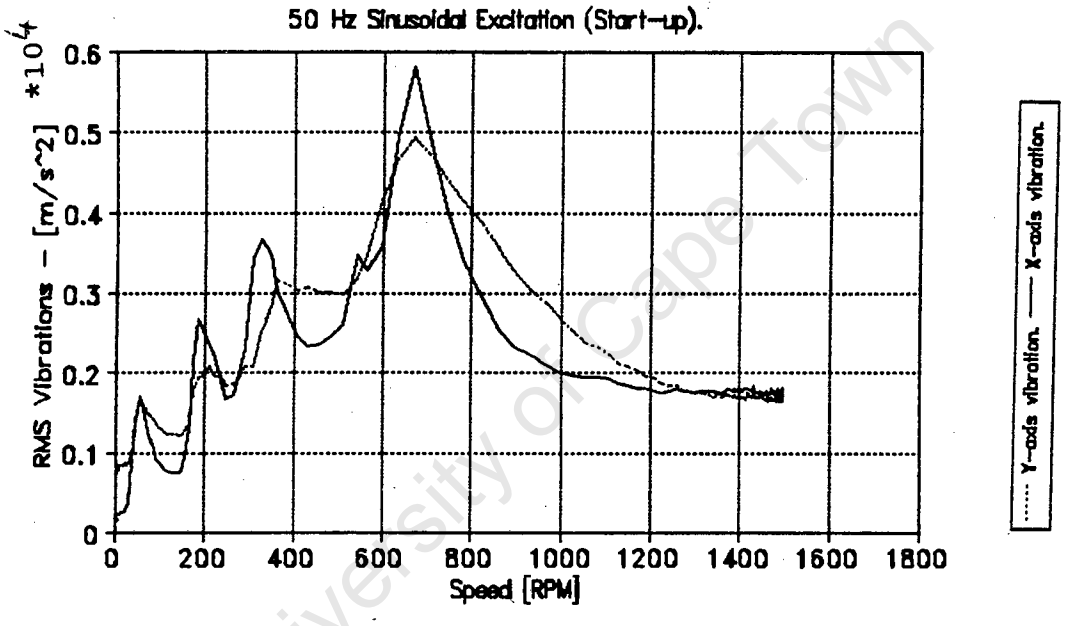


Fig. 7.1 Resonant frequencies under starting condition for sinusoidal excitation, 50 Hz, increasing the supply voltage via a variac.

The relative high starting current can be observed during acceleration under no load condition due to high slip. Critical transient vibrations can clearly be observed.

The mode number $r_v$ of the force wave is related to the number of poles and interaction between stator and rotor harmonic forces.

$$r_v = (\mu \pm \epsilon)\, p \qquad ...(7.5)$$

were $\mu = 2mg + 1$ (for stator force waves) and $\epsilon = gN_2/p + 1$ (rotor force waves), with $m$ the number of phases, $N_2$ the number of rotor slots, $p$ the number of pole pairs and $g = 0, \pm1, \pm2, \ldots$

Based on experience [2.3], low and medium powered machines are rigid against higher mode numbers greater than 6 and a velocity frequency range to be considered for the force wave $f_r$ is 10 Hz < $f_r$ < 1000 Hz.

All exciting frequencies incite different vibrational mode numbers that could lead to deformation of the stator. The vibration severity depends on the mechanical design such as machine size, damping, and on natural frequencies of the motor.

In a paper [7.5] resonant frequencies of stator frames and laminations are determined. Resonances are measured at different points on the circumference of the motor to ensure that resonances perpendicular to a specific test point are also measured. The main parasitic resonant vibrations of the stator are analyzed and are attributed to following phenomena:

(i). Dual resonances due to minor geometrical asymmetries introduce a second resonance frequency differing a few hertz from the other resonant frequency component. The smaller component is referred to as parasitic resonance.

(ii). Resonances due to harmonic excitation of the force acting on the frame. These harmonics are induced by a shaker, but harmonic forces will also be exerted by non-sinusoidal excitation and further parasitic harmonic resonances will occur in the stator.

Furthermore, shaker and teeth resonances are indicated as another source of measured harmonic vibrations.

## 7.5 Axial Vibrations.

At inverter operation an axially (z-coordinate) acting oscillating force is produced by rotor cages with skewed bars relative to the stator [1.2]. This requires consideration in bearing and coupling design. Axial forces due to skewed slots are derived analytically in [7.1], based on increased skew-leakage which results in an axial force and due to non-uniform distribution of the magnetic energy stored in the air gap. It is further pointed out that imperfect levelling of the machine produces an additional axial force proportional to the applied torque. The displacement and vibrations induced by these forces are relatively small compared to vibrations in the direction of the x-coordinate and y-coordinate (see Fig. 2.6) The vibration acceleration magnitudes are indicated on the frequency spectrum in Fig. 7.2.

**Table 7.1** Z-axis vibrations under no-load and load condition.

| Z-axis Vibrations in $[m/s^2]$ $*10^3$, and (%) increases. | | | | |
|---|---|---|---|---|
| Excitation | Load $[m/s^2]$ | No-Load $[m/s^2]$ | % increase No Load -> Load | % increase wrt. Sine under Load |
| Sine | 0.489 | 0.456 | 6.66 | |
| PWM | 0.804 | 0.708 | 11.94 | 39.1 |
| SQWave | 0.598 | 0.462 | 21.64 | 18.2 |

It can be observed that peak vibrations in axial direction increase under inverter excitation as suggested in [1.2]. Also under load conditions to axial vibrations increase, as predicted by [7.1] and discussed in this section.

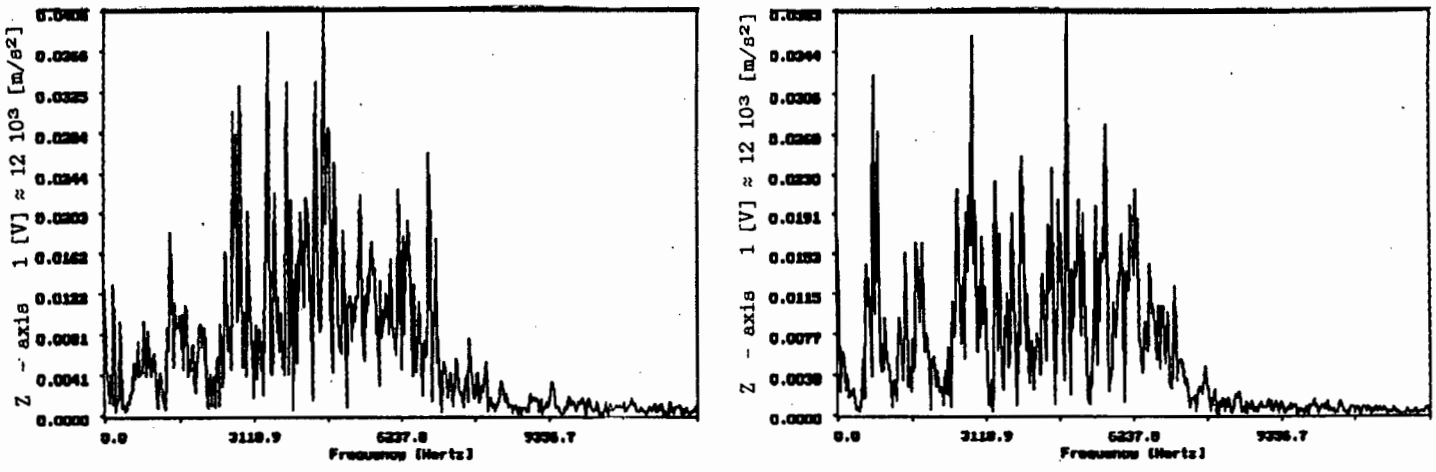


(a).

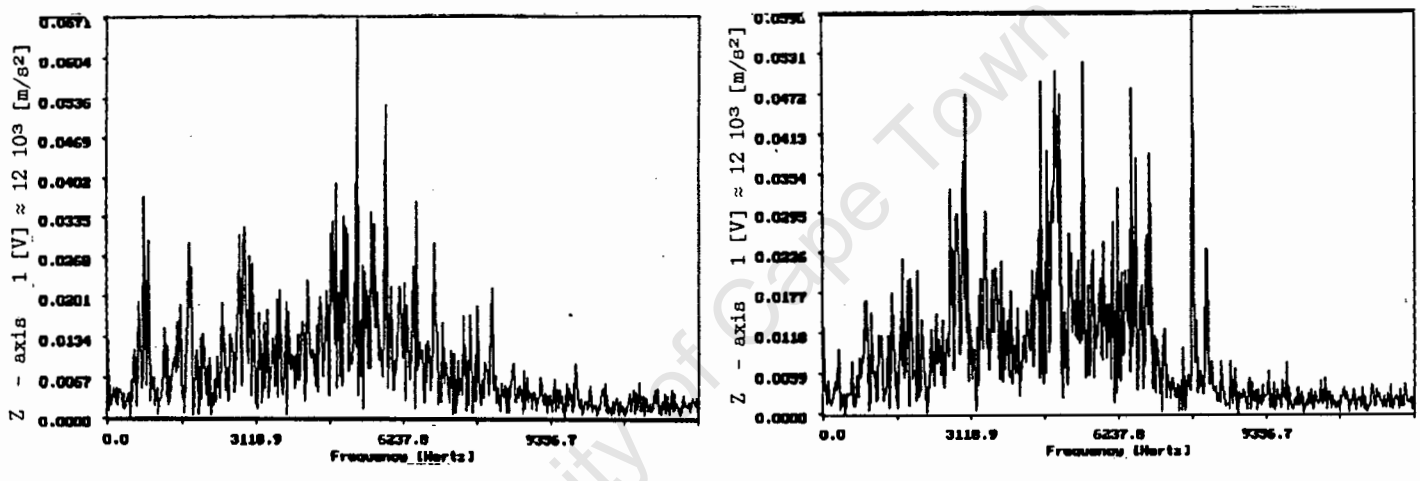


(b).

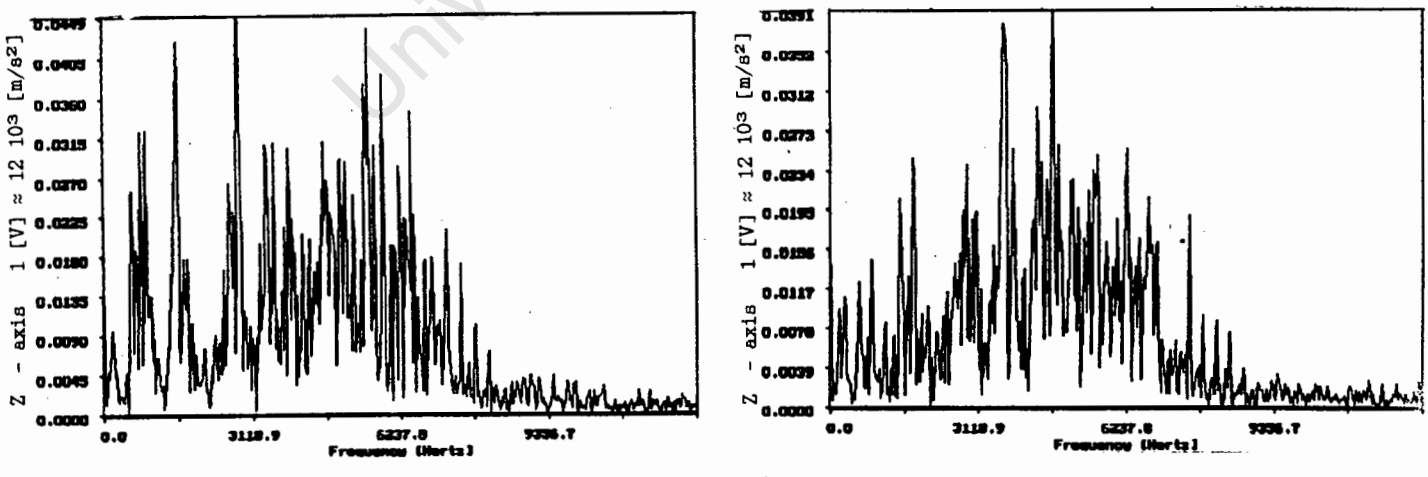


(c).

Fig. 7.2 Frequency spectra of axial vibrations - in **Z-axis** at $380V_{LL}/50$ Hz, under Load (left) and No-load (right) condition: (a) Sinusoidal, (b) PWM, (c) Square Wave excitation.

## 7.6 Critical Speeds.

For inverter applications the operating speed and excitation frequency varies continuously. It is important to avoid running the induction motor and load system near, or at a critical speed. Depending on the inverter application, motors are required to operate at different speeds for longer periods. If this is at one of the natural frequencies of the mechanical system, severe stresses are exerted on the motor, bearings, coupling and load.

This is more important for 2 pole machines for very high speed operations. However, 4 pole machines with a synchronous speed of 1500 r.p.m. (50 Hz) are often operated in the subsynchronous speed range (field weakening range) for specific utilization. It becomes crucial, not only to consider the natural frequencies and speeds of the motor, but also to consider the driven load which is generally less robust than the motor itself. Motors with large bearing span and flexible rotor shaft have a problem as they tend to have a vibrational mode number of $r_v = 1$. Reinforced shafts, which are less effective resulting in reduced efficiency and power factor [1.2] can constrain shaft vibrations in y-direction. Four pole machines would tend to have a vibrational mode number $r_v = 2$. Some vibration modes of the stator are shown in Fig. 7.2, according to [2.3, 7.2].



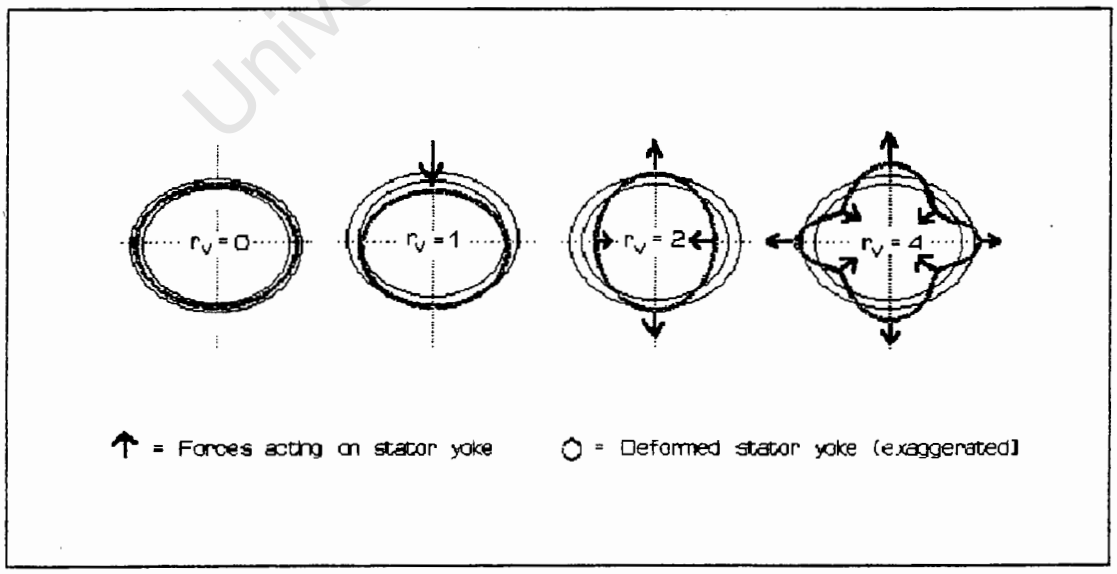


**Fig. 7.3** Deformation waves and mode numbers.

If at some speed the force frequency $f_r$ and the natural frequency coincide, noise increases and deformations are enhanced. The r.m.s. value of the vibrational velocity $v_{fr}$ is given in [2.3] as:

$$v_{fr} = \sqrt{2}\ \pi\ f_r \sum_{j}^{\infty} H_j\ P_r \qquad \ldots(7.6)$$

were $H_j$ is the system function consisting of geometrical dimensions, material of the machine and vibrational mode number, $P_r$ is the amplitude of the force wave and subscript j is the vibrational component.

### 7.6.1 R.M.S. Vibrations in the Operating Range.

The critical speeds at which increased vibration due to resonance occurs can be recognized in Figs. 7.4. and 7.5. As discussed, at some force frequencies resonance will occur as natural frequencies coincide with force frequencies.

For synchronous $V_r/50$ and subsynchronous configuration $V_r/87$ the r.m.s. vibration accelerations for each individual excitation source respectively at specific frequency differ only marginally in the range 0 Hz to 50 Hz. The same resonance pattern at approximately the same frequency occurs. Due to higher V/f ratio for synchronous characteristic excitation as compared to subsynchronous configuration, the magnitude of the force waves will be larger and thus the r.m.s. vibration is marginally higher as well.

(a).

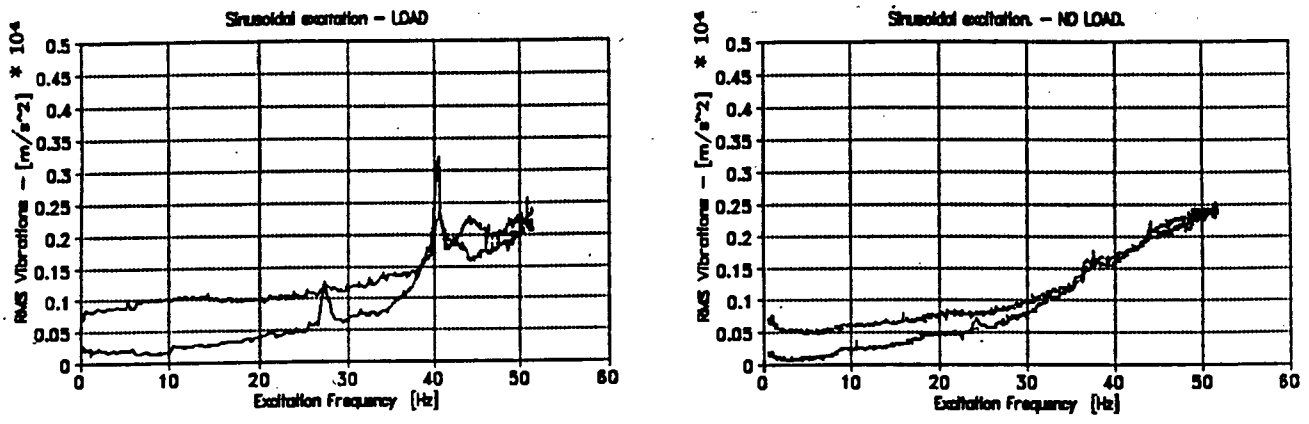


(b).

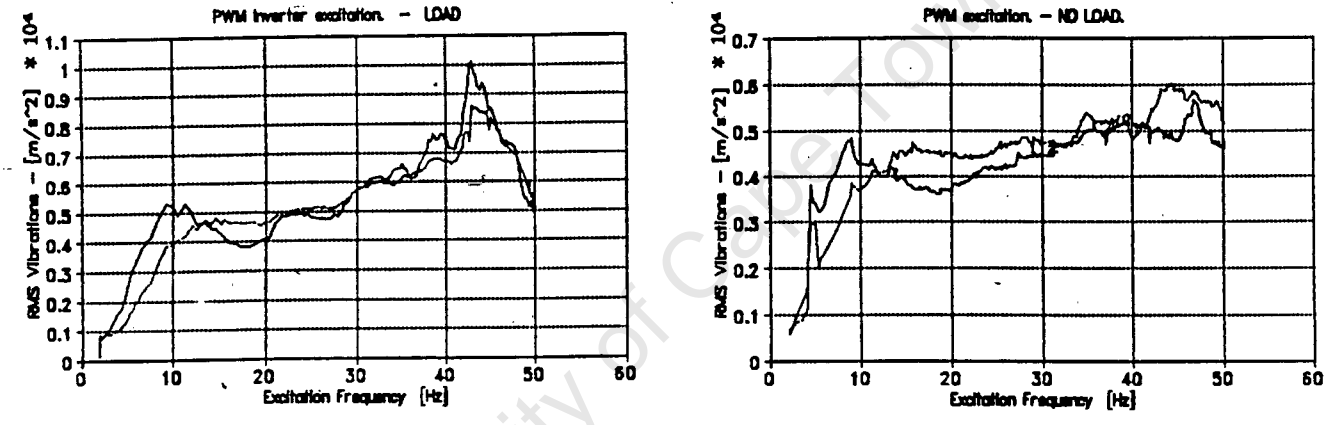


(c).

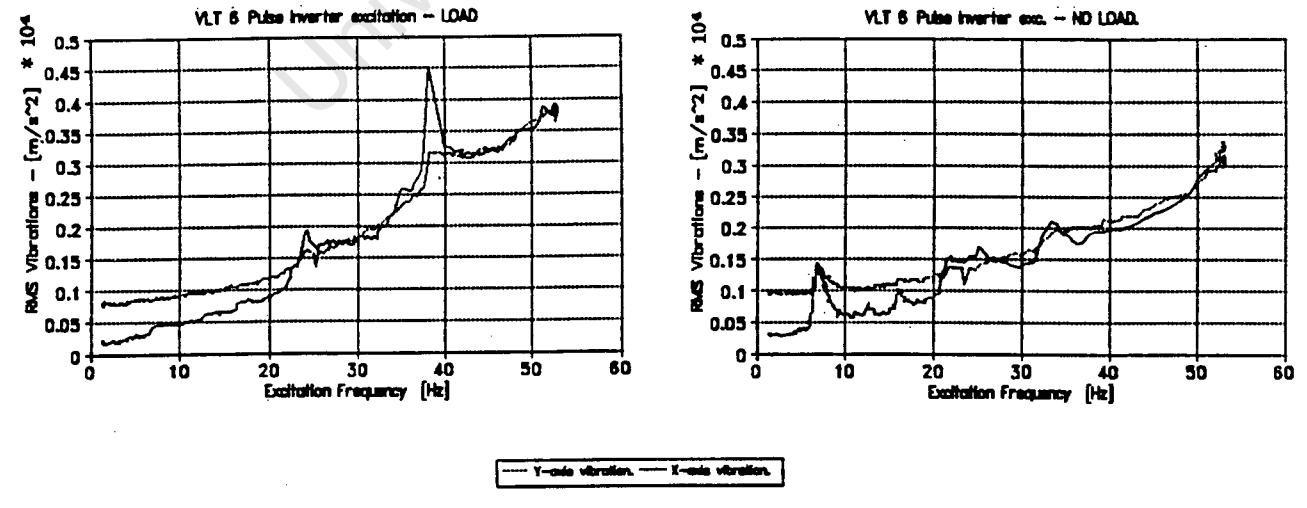


**Fig. 7.4** R.M.S. Vibrations under $V_r/50$ configuration over the operating range. (a) Sinusoidal, (b) PWM, (c) Square wave excitation under Load (left), and No-load (right) condition respectively.

(a).

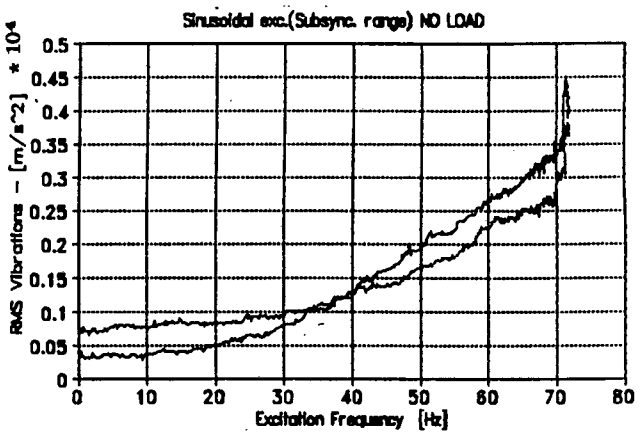


(b).

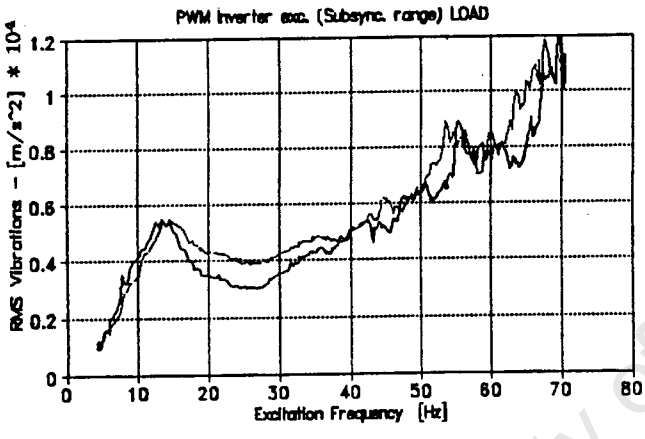


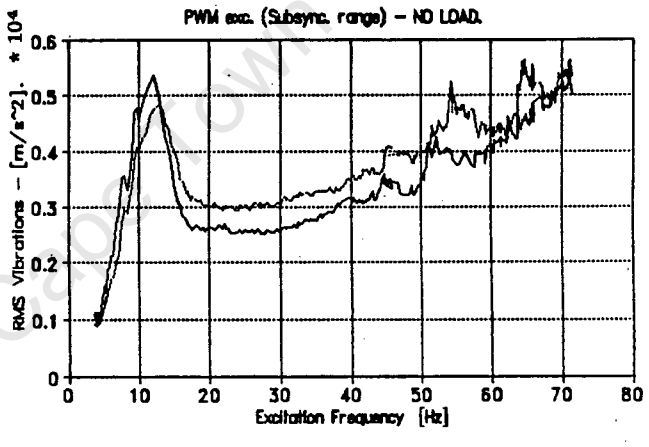


(c).

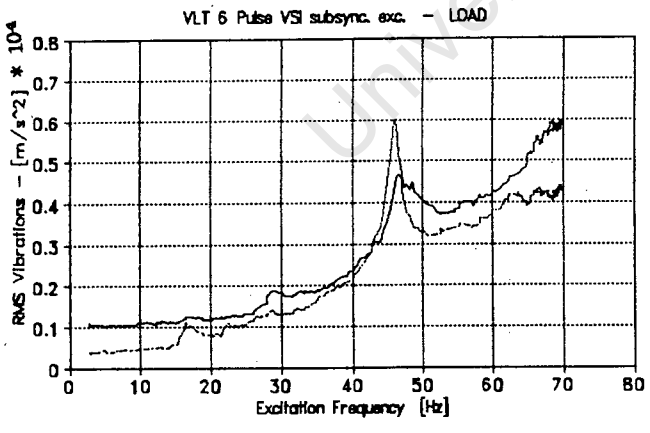


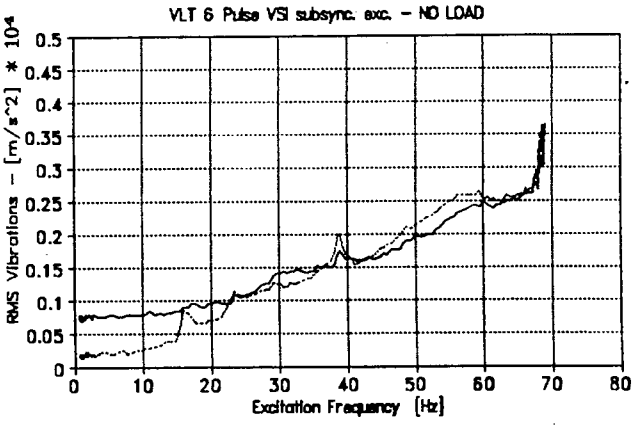


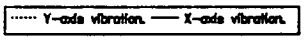


Fig. 7.5 R.M.S. Vibrations under $V_r/87$ configuration over the operating range. (a) Sinusoidal, (b) PWM, (c) Square wave excitation under Load (left), and No-load (right) condition respectively.

(i) **R.M.S. vibrations over the range up to 50 Hz:** Under **load** conditions, configured for (Vr/50), the r.m.s. vibration is higher across the whole range as compared to under **no load** conditions. Some resonance can be observed under load conditions at approximately 25 Hz and 40 Hz for Sinusoidal and Square Wave excitation. Some resonance at 10 Hz and 42 Hz under PWM excitation appears. For the no-load condition it appears that no resonance is evident under sinusoidal and PWM excitation, but for square wave excitation at 8 Hz and 34 Hz. The r.m.s. vibration under PWM excitation is considerably larger as compared to sinusoidal excitation and higher than under Square Wave excitation.

(ii) **R.M.S. vibrations over the range up to 70 Hz:** Under **load** conditions, configured for (Vr/87), the r.m.s. vibration is also higher across the whole range as compared to under **no load** conditions, especially for PWM excitation. Resonance can clearly be observed for PWM excitation at 13 Hz, 55 Hz and 65 Hz. The vibrations increase steadily as the rotor speed increases, due to mechanical effects such as eccentricity and unbalance. For Square wave excitation resonance occurs at 17 Hz and very dominantly at 45 Hz under load conditions. For sinusoidal excitation (no-load only) no resonance can be observed.

The r.m.s. vibration under PWM excitation is considerably larger as compared to sinusoidal excitation and is bigger than Square Wave excitation. The vibration severity $\Gamma$ (i.e. the magnitude of the r.m.s. vibration velocity) due to inverter supply on asynchronous motors can be deduced to be as:

$$\Gamma_{PWM} > \Gamma_{SQW} > \Gamma_{SINE} \qquad ...(7.7)$$

The vibration is of largest amplitude under PWM excitation because a large number of exciting forces, even though small, are present which may coincide with one or another natural system frequency.

## 7.7 Frequency Spectra at Rated Conditions.

The vibration frequency spectra in x-, y-, and z-axis direction for different excitation sources under no-load

and load condition, at rated supply conditions are given in Figs. 7.2, 7.6 and 7.7. In Fig. 7.2 the vibration acceleration frequency spectrum under **load and no-load conditions in axial z-directions** are shown. In Fig. 7.6 the vibration frequency spectrum under **no-load conditions are shown in x- and y-axis** direction. In Fig. 7.6 the vibrations under **load conditions in x- and y-axis** directions are displayed.

The acceleration frequency spectrum up to 12 kHz is displayed, the frequency spectrum indicates the acceleration components. The response of the accelerometer is also limited to that range as discussed in Chapter 2. The integrated signal for standard velocity measurements would not have had that many high frequency elements.

From the vibration nomogram attached in **Appendix 7.1.** the vibration r.m.s. velocity in [$m/s^1$] and the r.m.s. vibration displacement in [m] can be derived at specified harmonic frequency, given the vibration acceleration in [$m/s^2$]. The vibration quality grades of small sized and medium sized electrical machines as per ISO 2373 are attached.

(i). **Vibrations under load conditions:** The low frequency acceleration vibrations in the range up to 1500 Hz does not vary significantly between different excitation sources. However in the frequency range between 6 kHz to 8 kHz, an significant increase in vibration can be observed. Vibration amplitudes in this frequency range increases on average for x- and y-direction by 4.2 times for Square Wave excitation and 5.4 times for PWM excitation as compared to sinusoidal excitation.

(ii). **Vibrations under no-load conditions:** The dominant acceleration vibrations are in the frequency range between 5.5 kHz and 7.5 kHz. A substantial increase in frame vibrations under inverter excitation can be observed. Vibration amplitudes in this frequency range increase on average for x- and y-direction by 2.5 times for Square Wave excitation and 4.3 times for PWM excitation.

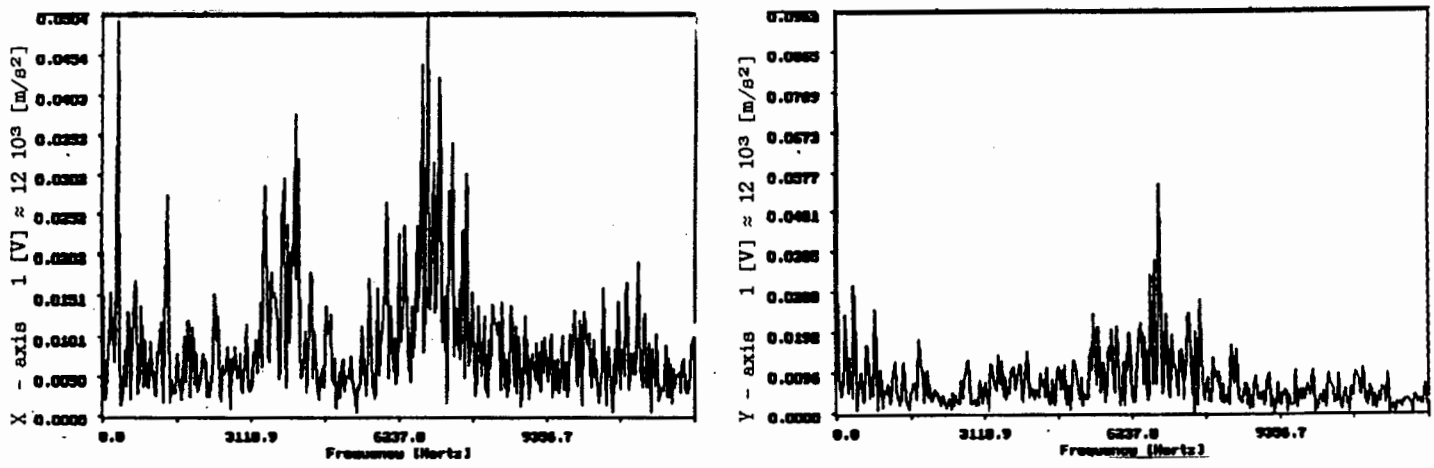


(a).

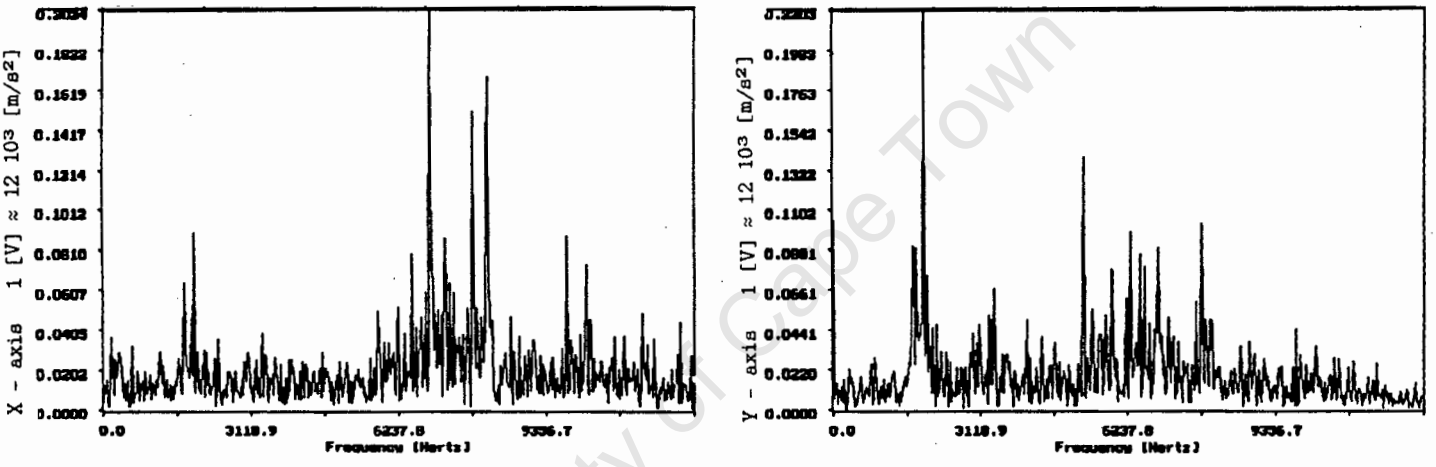


(b).

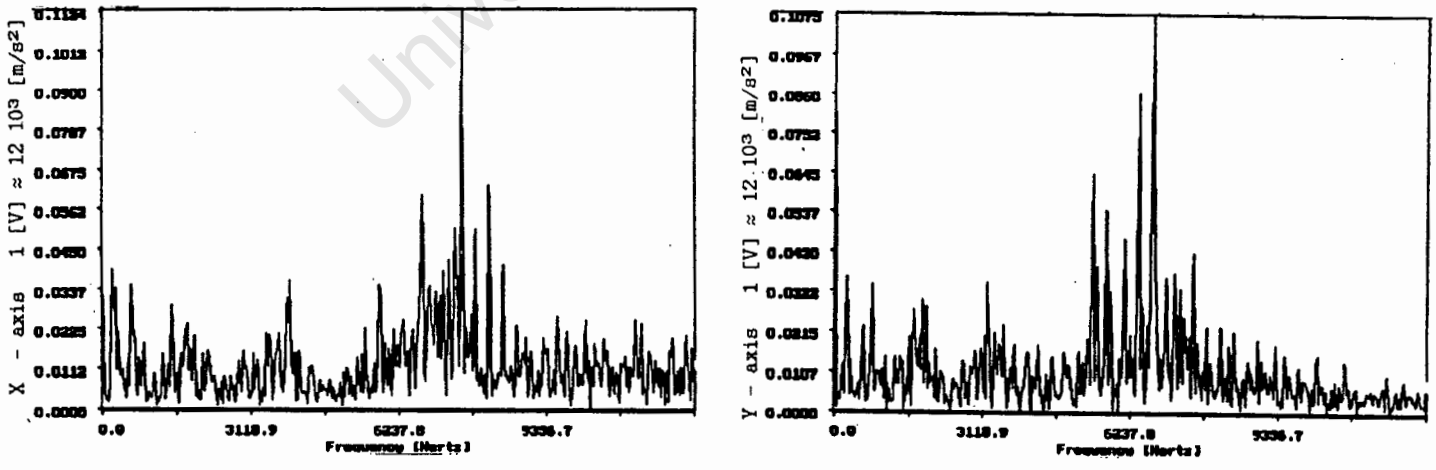


(c).

Fig. 7.6 Vibration frequency spectra in x- direction (left), and y-direction (right) respectively under no-load conditions. $380V_{LL}/50$ Hz. (a) Sinusoidal, (b) PWM, (c) Square wave excitation

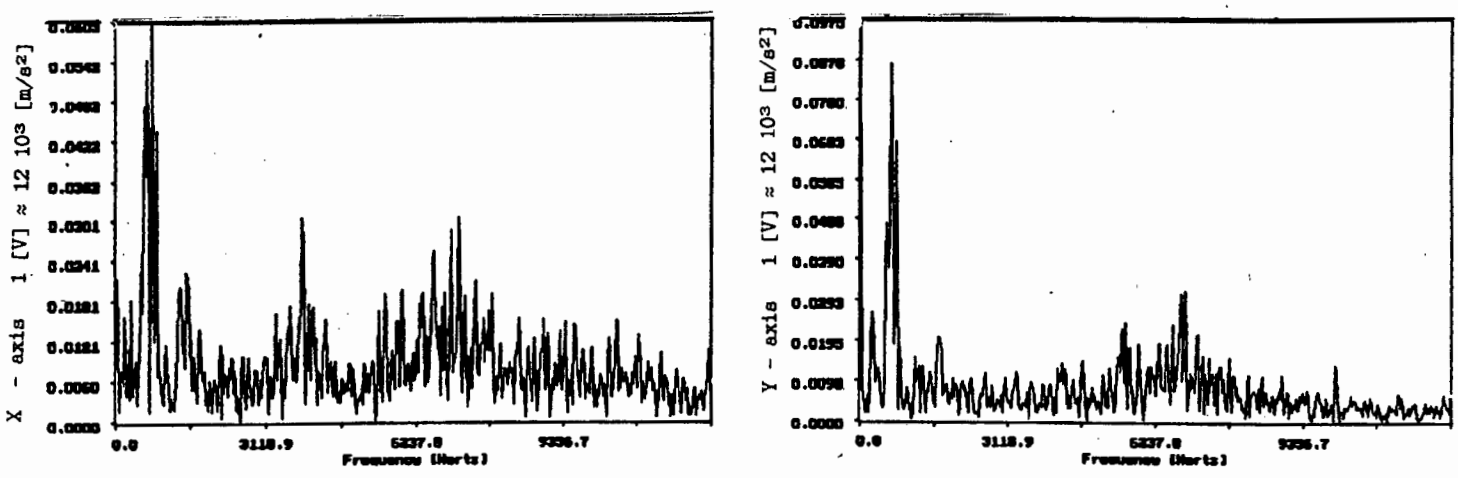


(a).

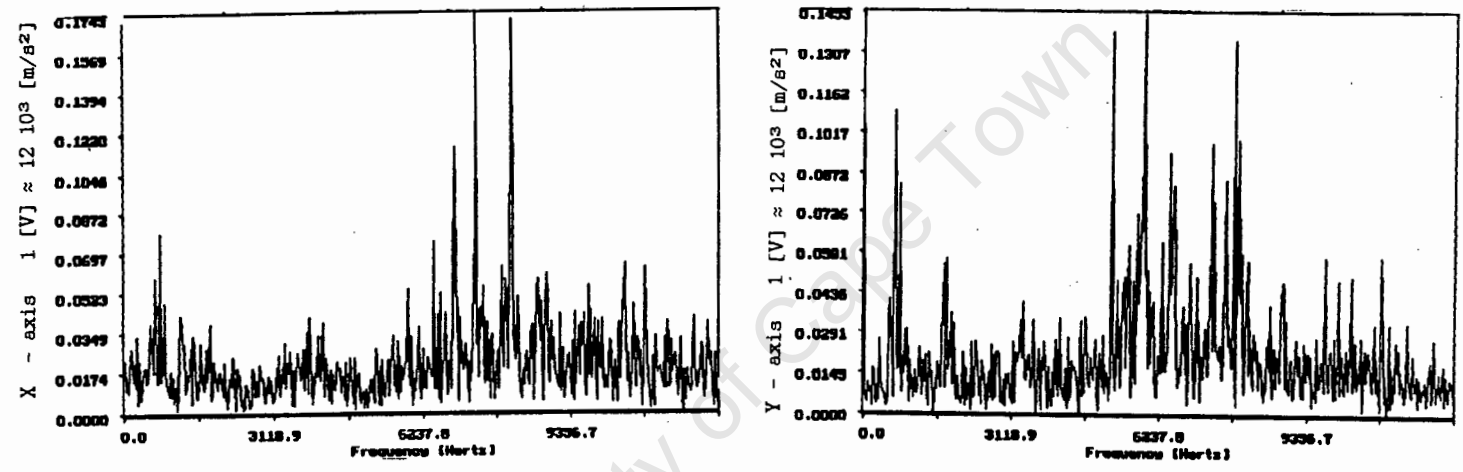


(b).

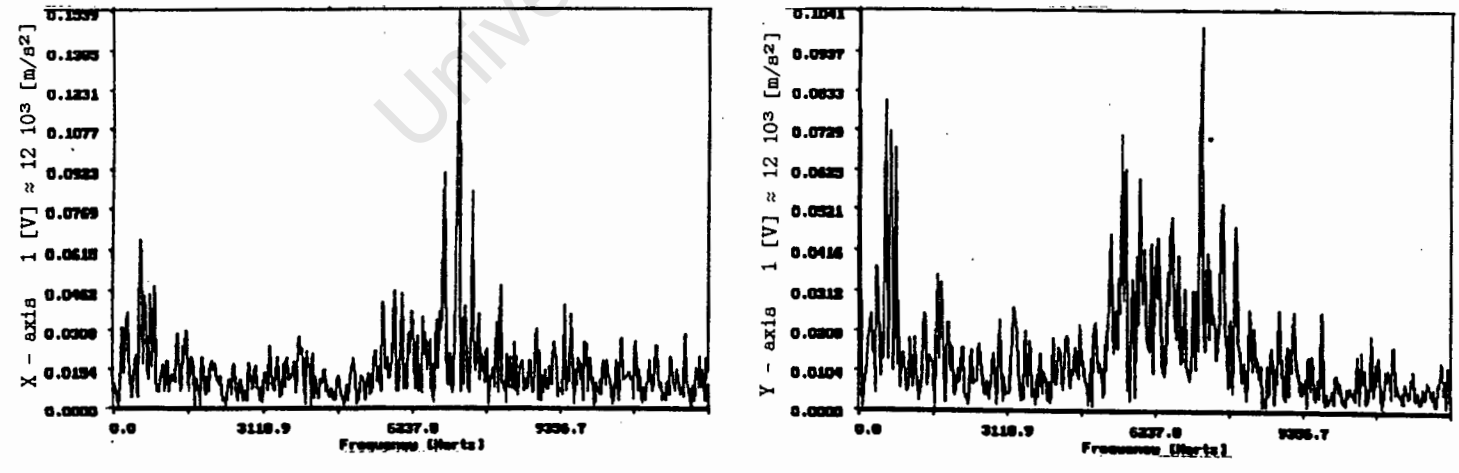


(c).

Fig. 7.7 Vibration frequency spectra in x-direction (left) and y-direction (right) respectively at load condition. $380V_{LL}/50$ Hz. (a) Sinusoidal, (b) PWM, (c) Square wave excitation

*It must be noted that all vibration amplitudes displayed are at different scales.*

Not all frequency components displayed can be isolated and interpreted as many are due to bearing vibration components, natural frequency and force frequency interactions.

## 7.8 Torque Pulsation - Vibration Correlation.

To analyze the correlation between r.m.s. vibration and the peak torque pulsations for different supply sources, the respective amplitudes of peak torque pulsations and r.m.s. acceleration versus frequency are compared over the whole exciting frequency range up to 50 Hz.

At high amplitude of torque oscillations, some torsional resonance will contribute to the actual torque pulsations. Clearly this would affect shaft vibrations and consequently frame vibrations.

If the frequency of a force wave is close to the natural frequency of a mechanical component, rotor shaft, frame, or bearing backlash, a loud noise is audible, even at low speeds and low excitation. This vibration coincides with the peak torque pulsation and vibration for the Square Wave VSI. Under load and no load conditions this is evident under Square Wave excitation at around 8 Hz.

From Fig. 7.8 a correlation between peak torque pulsations and vibration severity can be drawn. Under sinusoidal excitation the mentioned phenomena correlate at 26 Hz and 40 Hz. For PWM excitation at 12 Hz and 45 Hz, and for Square Wave excitation at 25 Hz and 38 Hz. Further analogies can be found comparing relevant figures in Chapters 6. and 7.

Vibrations are predictably enhanced if torsional natural shaft frequencies are close to natural mechanical motor or inverter supplied force frequencies.

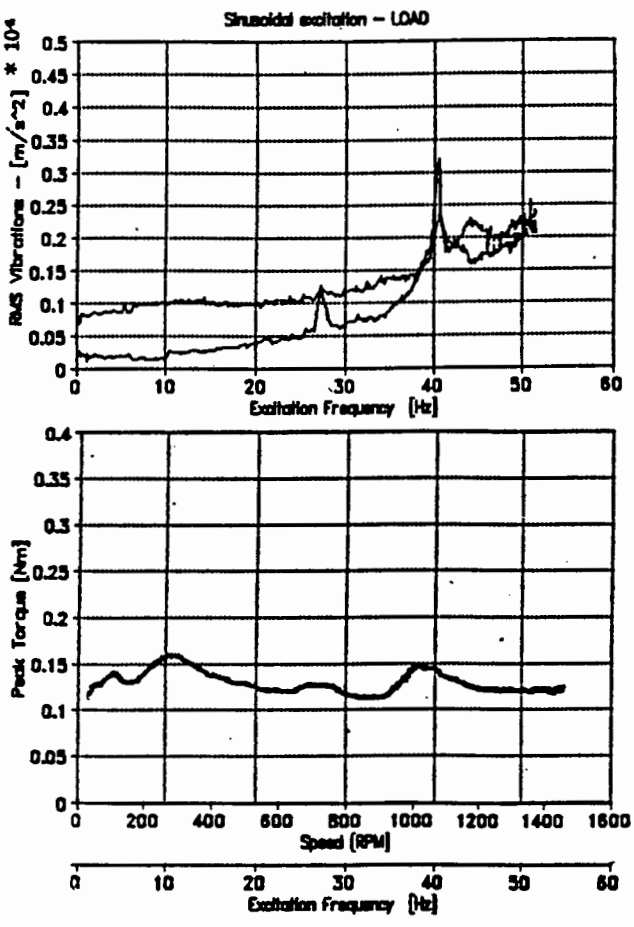


(a).

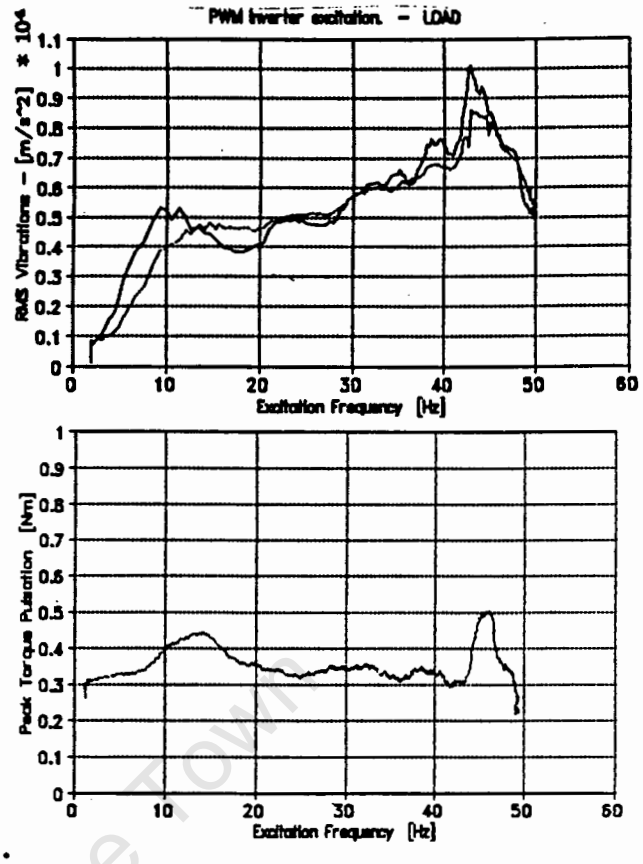


(b).

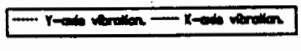


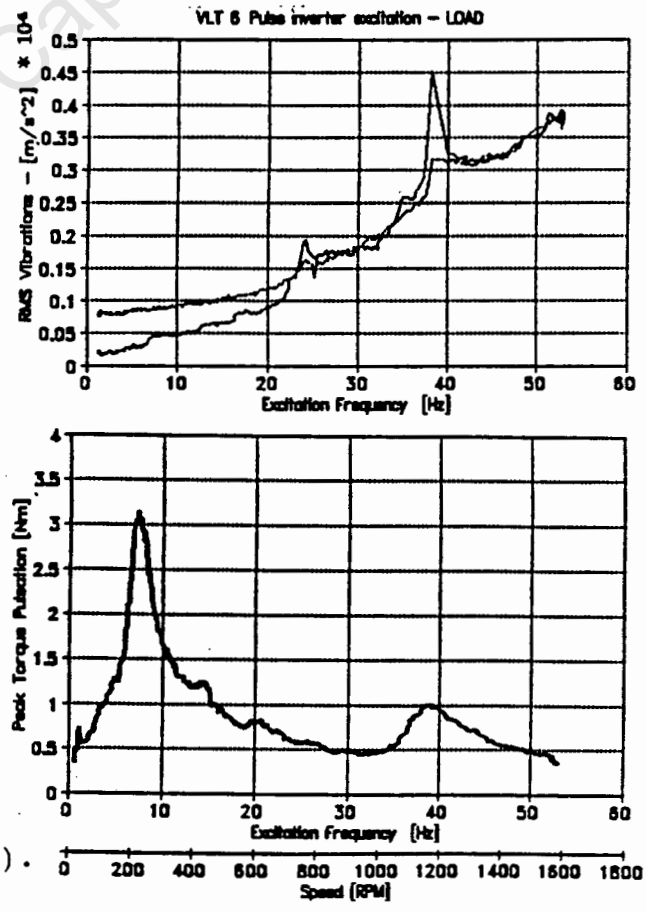


(c).

**Fig. 7.8** Vibrations and Torque pulsations ($V_r/50$). Correlation under load conditions for (a) Sinusoidal, (b) PWM, (c) Square wave excitation.

# CHAPTER 8. CONCLUSIONS.

The relevance of the effect on the electrical and mechanical performance of inverter-fed induction motors is emphasized. General trends and effects originating from higher time harmonics are indicated. Conclusions are based on a comparison under equivalent operating conditions with pure sinusoidal excitation. Measurements are performed under various load and operating conditions and with different excitation sources. A brief theoretical background is discussed in each chapter to substantiate the measurements accomplished.

The electrical and mechanical effects are outlined separately although electrical and electromagnetic effects cause diverse mechanical effects.

**Time harmonic effects on the electrical performance.**

The most important effects of non sinusoidal excitation manifest themselves in losses, efficiencies, power factor, temperatures and shaft voltages. All measurements agree with measurements and theory published so far. No information on actual aspects on shaft voltages were found in literature, but merely that shaft voltages are present in inverter-fed induction motors which was confirmed too.

From Chapter 3 the effect of higher time harmonics on losses, efficiencies and the power factor are evident. Losses increase due to time harmonics, thus the efficiencies decrease. Low order harmonics, as the $5^{th}$ and $7^{th}$ in Square Wave inverters affect the increase in losses to a larger extend than losses due to higher order voltage harmonics present in PWM inverters. The induction motor power factor is also reduced under inverter operation, particularly under PWM excitation. Increased voltage stress will cause long term deterioration of the insulation due to the dV/dt slope which will be largest in turns near the motor connection leads. Stresses resulting from PWM excitation are more severe as compared to Square Wave excitation due to higher frequencies and higher dV/dt value. Generally, modern standard induction motors are resistant against these voltage stresses.

A considerable increase in stator core temperature is measured in the presence of time harmonics in the supply as outlined in Chapter 4. The temperature increase arises due to increased losses under inverter-fed operation. At lower speeds the temperature will rise considerably at constant torque operation, due to reduced ventilation and cooling.

The influence of non-sinusoidal excitation sources on the shaft voltages induced has been determined in Chapter 5. The peak shaft voltage spikes are substantially higher due to commutation voltages and harmonic currents. The r.m.s. shaft voltages induced across the shaft do not show any obvious increase. The peak voltages increases proportional to the r.m.s. voltage, and at high phase voltages the shaft peaks are the largest.

**Time harmonic effects on the mechanical performance.**

The mechanical performance aspects influenced by higher time harmonics are mainly torque, torque pulsations and vibrations. Shaft voltages and currents will affect the working of the bearings and their lubricants. Temperature rise due to increased losses will affect the conductor insulations and lubricants in the bearings.

Harmonic steady state torques show a very small effect on the rated torques. Steady state torques depend to a large extend on the V/f constant. Pullout torques at low speeds without initial voltage boost are very low. A low frequency oscillating torque is present at rated operating conditions as shown in Chapter 6. Harmonic oscillating torques of are present under inverter excitation. The magnitude of the $6^{th}$ harmonic torque under Square Wave excitation is extremely high at low operating speeds and may be detrimental to the system if operated continuously at that speed. Harmonic torques are more prominent under Square Wave excitation due to $5^{th}$ and $7^{th}$ harmonic interacting components.

Time harmonic effects on machine frame vibrations under inverter supply are presented in Chapter 7. Vibrations increase under inverter excitation in axial, vertical and horizontal direction. The vibrations are most significant under PWM excitation followed by Square Wave excitation and then sinusoidal excitation. Critical speeds can clearly be observed in the operating region and are present under all different excitation sources. Vibration severity is larger under load condition and at higher speeds. Although these vibration amplitudes will be within the limit, they are substantially larger as compared to sinusoidal excited vibrations, thus exerting increased stresses and strains on the system. Critical speeds and higher torque pulsations coincide at certain fundamental operating frequencies, which should be avoided.

# CHAPTER 9. RECOMMENDATIONS FOR INDUSTRY.

The important part of a research project is to provide some additional, useful and relevant information to industry were it is applicable. The IEC standard [1.1] provides guidelines for the application of inverters with induction machines. Additional information with respect to the use of inverters with small sized induction machines and their performance is provided. It is assumed that inverters are efficient, have a relative high power factor, are equipped with good open and short circuit protection.

Recommendations are based on measurements performed with different inverter drives on a 3-kW squirrel cage induction motor. Only voltage source inverters were tested and are discussed, as they are more flexible in applications with standard machines. Standard small induction motors are generally designed with skewed slots to reduce asynchronous torques and crawling under mains on line starting conditions. This results in increased skew leakage, and current source inverters are not suitable as they require a low leakage reaction for commutation purposes. VSIs however require increased leakage reactance to reduce higher time harmonic currents. Moreover, the multi-motor capability of VSIs is another advantageous feature as compared to current source inverters were generally a good inverter and single motor match is required.

VSIs have a relative good dynamic response and can operate small size standard induction machines satisfactory under full load and light loading conditions.

## 9.1 Electrical Performance and Efficiency.

Economic considerations play a major role in actual decision making referring to the implementation of recommendations made. The crucial keywords of performance versus efficiency should be considered.

High efficiency motors and special purpose motors can be designed and build at a cost, but due to the economies of scale, standard induction motors are generally used as their cost price is relative low. Especially for small motors the cost ratio of special motors to standard motors will be very high and it is generally not justified to pay an extra premium for the specially designed motor. *(A gain of 16% reduction in losses [1.3] can be achieved, but the design improvement measures are relative expensive and standard design type induction machines (especially smaller types) are preferred).* The load factor and duty cycles of machines should be well established to determine the choice of the motor and inverter for a specific purpose and system.

It has been shown in [9.4] that larger machines have their maximum efficiency between 80% and 90% of their full load. For small machines the maximum efficiency is also slightly below rated current as determined Chapter 3. The fact that the maximum efficiency is below the rated current, it is justified to purchase larger motor of 1.15 to 1.25 times rated torque required.

The efficiency decreases as the load and load torque is decreased. For optimal performance the motor should be selected at a rating of approximately 1.2 times rated load required, were the rated load should be defined as the load under which the inverter-fed induction motor is operated for the longest time span. Energy savings on a single small machine are not too significant, but if many inverter-fed asynchronous motors are in use, the saving can be considerable. Oversizing or derating is furthermore required under inverter applications, as the motors predicted lifetime can only be maintained if excessive heating of the motor is prevented.

Temperature increases in small machines are affected more by harmonics than larger machines, as found in [4.5] and [3.10]. At low speeds for self ventilated motors the torque should be derated by an even larger extend as the cooling effect is very low. Generally, inverter application notes, the IEC standards [1.1] or guidelines provided in Chapter 4. should be used to derate motors to account for additional heating. Forced ventilation should be used to run the motor at rated torque for low speed

applications. Heavy load cycles for short periods can be tolerated even with inverter supply, if the thermal reserve of the motor is large enough and the decay time constant relative short. Insulation types used in the motor design must be considered as a variable to determine the derating factor. A motor with class F insulation should be used for constant torque applications with VSIs and be derated according to specifications [1.1] or equation (4.3), i.e. approximately 17% for small machines.

The magnitude of induced shaft voltages in small inverter-fed induction machines should be measured under operating conditions when the drive system is commissioned. The measured values must be compared to a reference table which should be developed from a database with maximum permissible peak voltage values such as given in Chapter 5. For planned maintenance systems, the measurement of shaft voltages (non destructive test) should be measured across the shaft and between shaft and frame. Good contact points are required to measure the peak voltages accurately with a peak detector instrument. As the peak voltages between shaft and frame decrease between measuring intervals, it can be concluded that the condition of the bearing deteriorating, as discussed in Chapter 5. The use of bearings with plastic cages [1.2] is recommended to insulate the shaft and reduce bearing currents due to increased reluctance in the flux path. A further advantage is reduced rolling noise of anti friction bearings. Experience shows positive results to reduced noise and bearing lifetime [1.2].



## 9.2 Mechanical Performance.

Due to the presence of harmonic torques the sensitivity of the load to torque oscillations must be determined. Natural torsional vibration frequencies of the shaft should be calculated for the motor to be used. Considering the performance capability of the motor as the supply voltage above rated 50 Hz remains constant, they must be derated to a operating torque proportional to $1/f^2$ and the pull out torque proportional to $1/f$. For constant torque operation at low speeds a required voltage boost on the inverter must be chosen as to maintain a constant air gap flux at low speeds.

Critical frequencies for an installed system must be determined during the commissioning period, and if vibrations are too severe at certain speeds, additional damping is required. The frame and structure must be reinforced or the natural frequencies of the system adjusted using different machine mountings. If the critical low operating frequencies fall outside operating region required, the VSD should be programmed to accelerate through the critical region and prevail operating outside that region. A reinforced shaft also reduces rotor vibrations, which is more important in larger 2 pole machines.

Harmonic and low frequency torque oscillations which are predominant at low speeds, vibrations transmitted via the shaft and axial rotor vibrations can be reduced by a proper flexible coupling such as the Fenner-type which has a damping factor in axial direction and also absorbs high frequency torque oscillations. Increased inertia would also reduce speed and torque pulsations.

From a subjective judgement it is clear that the noise level at especially low speeds under PWM inverter operation is substantially higher as compared to Square Wave and sinusoidal excitation. This is due to the high switching frequency of currents in the inverter and machine. At higher speeds the noise from the ventilation fan and possibly the load, are primary. It is also evident that the noise level of the motor under PWM excitation will be higher as the vibration too is of more intensive amplitude.

Inverter-fed asynchronous motors, excited by a PWM technique has superior properties which are of principal importance, including better efficiency and thus a marginal lower derating factor is required, lower torque pulsations over the whole operating range, especially at low speeds.

Asynchronous motor vibrations for the Square Wave inverter are smaller than those of the motor under PWM excitation which is the only advantage.

PWM VSIs and Square Wave VSIs can be used for multi-motor operations and no perfectly matched induction motor - inverter set is required.

## 9.3 Optimizing Induction Motor Parameters.

The performance for VSIs can be marginally improved by filtering the supply fed to the induction motor with an external inductance. This is crucial in the application of Square Wave inverters to limit the $5^{th}$ and $7^{th}$ harmonics. The pull out torque is inversely proportional to the total leakage inductance, and the p.u. value of the external inductance must be limited.

An optimal machine can be designed for VSIs as outlined in [9.1, 9.2] but the external leakage inductance can be increased by inserting a pre calculated optimal inductance in series with the supply to the induction motor. Motors with skewed slots have an increased leakage flux and should only be used with VSIs. To reduce motor heating, torque pulsations, winding stresses, vibrations and shaft voltages and increase efficiency of the motor an external leakage inductance of approximately 0.3 p.u. according to [9.1] should be used. Performance enhancements for a Square Wave inverter with external leakage are discussed in some detail in **Appendix 9.1.**

In paper [1.2, 3.14] it is demonstrated that induction motors can be operated under constant flux, even if the rated frequency is exceeded. The method is only applicable to machines designed for star operation under mains excitation. During inverter operation asynchronous motors can then be delta connected, resulting in a phase voltage increase of $\sqrt{3}$, thus the fundamental frequency will also be increased by $\sqrt{3}$ to keep the V/f ratio constant and thus air gap flux constant, as shown in Fig. 9.1. Machines must still be derated due to higher frequencies and thus increased iron losses, but the power output can be increased by 10% to 20% with respect to rated output under delta connection in the subsynchronous range.

In the paper [3.14] an increase in power output of $\sqrt{3}$ times rated output at 87 Hz is predicted for constant flux operation in the subsynchronous range, provided the pulsing pattern has a low harmonic content and no zero sequence components, which requires exact switching of the power modules.

Induction motors designed for star connection under mains excitation should be used to increase the torque output in the subsynchronous speed region by reconfiguring the motor to delta connection.

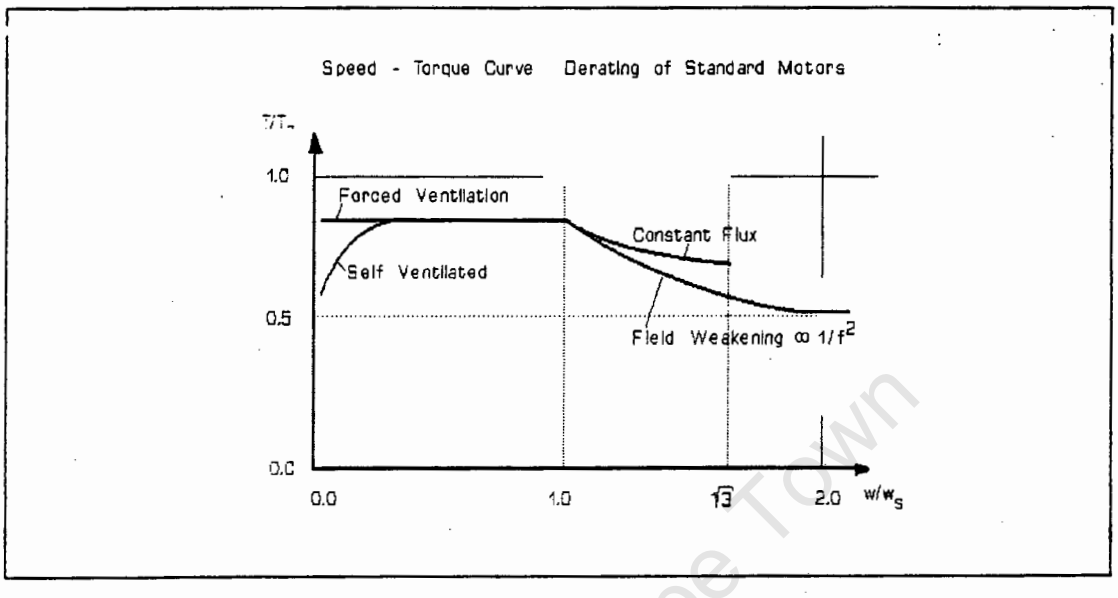


**Fig. 9.1** Approximate recommended operating Torque vs Speed characteristic for inverter-fed induction machines, from [1.1, 3.7, 3.14]

Slip compensation, a general design feature of VSIs should be adjusted to keep the speed constant under load conditions. The fundamental exciting frequency is increased slightly by a controller action to compensate for the speed reduction due to slip.

The inverter should be configured according to the load required, i.e. if the load torque is proportional to the speed or proportional to the speed squared (pumps, fans). The inverter V/f ratio can be configured for a pump load (e.g. fan load) where the V/f ratio increases proportional to the torque, which in turn in proportional to the square of the speed (frequency). This feature is generally available with standard inverters. An approximate V/f pump characteristic is shown in Fig. 9.2. Since the torque is proportional to the voltage squared, the pump configuration is ideal for certain loads and results in considerable energy savings.

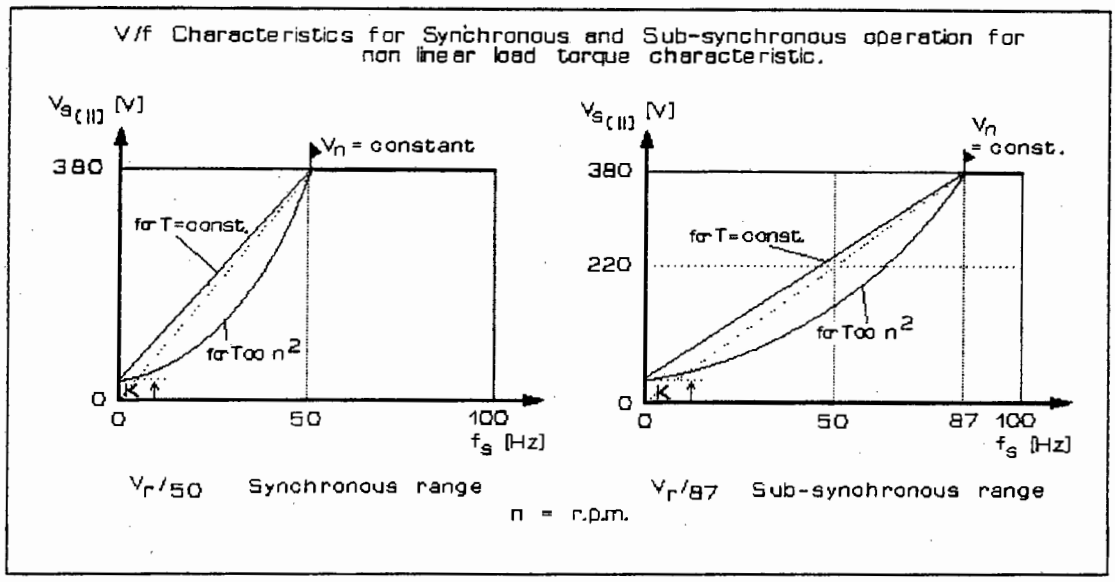


**Fig. 9.2** V/f characteristic under normal and pump torque configuration, for $V_r/50$ and $V_r/87$, [9.5].

If it would economically be justified to manufacture special purpose machines for voltage and current source inverters, design factors such as leakage flux, reduced rotor harmonic losses ($I_n^2R$) with low skin effect bar types, lower magnetic flux densities to reduce saturation, reduced stray load losses with zero skew motors should be considered. The rotor bars are made of copper. Using more phases than standard three phases on motors and in counterpart inverters would increase motor and inverter ratings.

# 2. Appendices - Chapter 2.

## 2.1 PC 30-D Data Acquisition Card.

### Overview

The PC-30B, C and D series of boards are full size, low cost, high accuracy analog and digital I/O boards for the IBM PC, PC/XT, PC/AT, PS/2 model 25, PS/2 model 30 and compatible series of computers. The series of boards is a development from the well known PC-30/PC-39 family, and is fully compatible with these earlier boards. Also members of the PC-30 family are the PC-30DS and PC-30DS/4. These are described in a separate manual.

- PC-30D. The PC-30D is a development of the PC-30C, with A/D throughput of 200 KHz. It is designed for use in PC/AT and AT compatible PC's. In addition to improved throughput, the PC-30D also contains FIFO buffers for A/D data, for improved operation in conjunction with multi-tasking operating system such as OS/2.



### A/D subsystem

The A/D subsystem's major component is a monolithic analog to digital converter, which accepts analog voltage inputs from sensors, such as pressure transducers and thermocouples, and converts them into 12 bit digital codes.

This code is transmitted to the host processor, which processes it according to the software in use at the time.

The A/D section allows for 16 single-ended inputs, and can be configured for unipolar (input range of 0 to 10V) or bipolar (input ranges of +/-5V or +/-10V) operation. Resolution is 12 bits. For unipolar inputs, the output code is straight binary, and for bipolar, offset binary.

The A/D may be operated in either single conversion or continuous conversion mode. In single conversion mode the board performs a single conversion on the selected input channel and stops on completion of this conversion. In continuous conversion mode conversions are performed at a set rate. This rate is set by programming the PC-30's internal timer or an external clock source.

The PC-30 contains logic which allows any sequence of channels, up to a sequence length of 31, to be selected and sampled under hardware control. This allows full throughput to be achieved even when converting multiple input channels.

A/D conversions may be monitored by either polled I/O, DMA or by interrupts. In polled I/O mode the software continuously polls the board's status register to check for completion of the current A/D conversion. DMA (Direct Memory Access) is used to transfer data direct from the A/D to memory. In interrupt mode, the board automatically generates a hardware interrupt on completion of each conversion.

### Key specifications

- A/D resolution: 12 Bits
- Nonlinearity: Less than +/-0.75 LSB
- A/D full scale input ranges: 0 to +10V, -5 to +5V and -10 to +10V (PC-30B/C only).
- Number of A/D inputs: 16 single ended.
- A/D throughput rate: 200 KHz (PC-30D), 100 KHz (PC-30C), 30KHz (PC-30B).

## 2.2 Software Simulation Package PWM_SIM.EXE .

PWM_SIM (written in C/C$^{++}$) is a package to simulate VSIs under different operating conditions and different leakage inductance parameters. Different modulation techniques as the six pulse Square Wave inverter, 12 pulse inverter and different PWM modulation techniques by selecting the carrier frequency and reference amplitude for sinusoidal modulation, are simulated. The voltage signal, current signal and their respective frequency spectra are displayed. Furthermore, inverter phase to phase voltage $V_{LL}$, Ripple current, carrier and modulation signals can be displayed. The total harmonic distortion, crest factor and specific frequency components amplitudes of the voltage and current signal can be viewed or written to a file. The package was used to simulate and analyze the voltage wave forms generated during different inverter operation conditions.

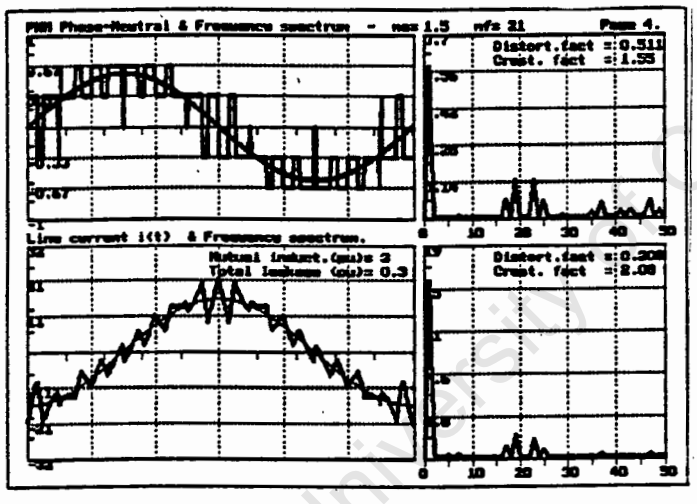

(a).

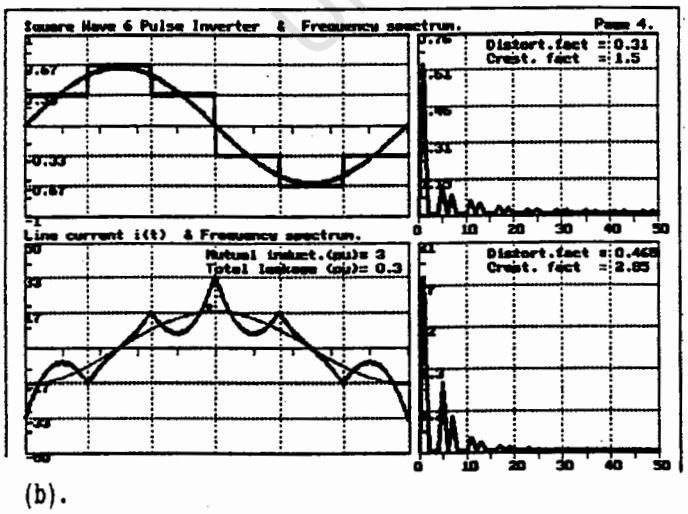

(b).

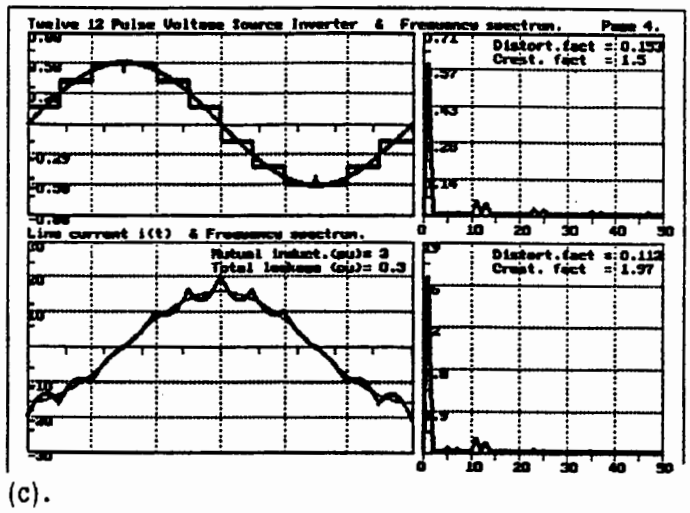

(c).

**Fig. A2.1** Typical simulation of a (a). PWM VSI and (b). Square Wave VSI and (c). 12-Pulse inverter. Voltage and current signal with respective frequency spectrum.

## 2.3 Equivalent Circuit Parameter Derivation.

The no load synchronous and locked rotor test at 25 Hz and 50 Hz had following measured results. (Stator core temperature at approximately 75°C ).

At 25 Hz (Per phase):

| No load test. | | | Locked rotor test. | | |
|---|---|---|---|---|---|
| S | = 368.08 | VA | S | = 231.51 | VA |
| P | = 150.49 | W | P | = 206.52 | W |
| $f_1$ | = 25 | Hz | $f_1$ | = 25 | Hz |
| $I_{rms}$ | = 3.312/√3 | A | $I_{rms}$ | = 6.745/√3 | A |
| $V_{rms}$ | = 111.12*√3 | V | $V_{rms}$ | = 34.32*√3 | V |

At 50 Hz (Per phase):

| No load test. | | | Locked rotor test. | | |
|---|---|---|---|---|---|
| S | = 730.85 | VA | S | = 261.25 | VA |
| P | = 215.35 | W | P | = 244.59 | W |
| $f_1$ | = 50 | Hz | $f_1$ | = 50 | Hz |
| $I_{rms}$ | = 3.32/√3 | A | $I_{rms}$ | = 7.35/√3 | A |
| $V_{rms}$ | = 220.03*√3 | V | $V_{rms}$ | = 35.53*√3 | V |

The parameters were calculated as outlined in more detail in paper [2.4], which takes the temperature and frequency dependance of the inductances and resistances into account by performing no-load and locked rotor tests at 25 Hz and 50 Hz sinusoidal excitation respectively. The parameters for the higher time harmonic equivalent circuits were determined separately, which are dependant on the harmonic order.

Secondary parameters are calculated taking the parallel circuit, $X_m$ and $R_m$ into account and using the equivalent circuit as given in [2.4] according to the Japanese Standards (JEC - 37, 1979).

Temperature dependance [2.6]:

$$R_1 = \frac{(234.5 + t_{ref})}{(234.5 + t)} R_{1ref} \qquad \ldots(A2.1)$$

were $R_1$ is the winding resistance at temperature t°C, and $R_{1ref}$ the winding resistance when measured at $t_{ref}$°C.

Core loss resistance is given as:

$$R_n = \frac{P_c}{3\ I_o^2}$$

were the core losses $P_C$ are frequency dependant.

Secondary circuit resistance and reactance, including the skin effect according to [2.4] can be approximated as:

$$R_{2n}' = a\ f_n + b \qquad \ldots(A2.2)$$

were $a = 2(R_{2(50)} - R_{2(25)}) / f_{(50)}$ and
$b = 2R_{2(25)} - R_{2(50)}$

$$L_{2n}' = k\ f_n^C \qquad \ldots(A2.3)$$

were $c = \ln(L_{2(50)}'/ L_{2(25)}')$ and $k = L_{2(50)}'/ f_n^C$.

The number in subscript brackets indicates the fundamental frequency of the test performed.

All other fundamental parameters were calculated by standard equivalent circuit theory.

## 2.4 True r.m.s. Wattmeter.

The true r.m.s. wattmeter build is shown in Fig. A2. 2. Accuracy compared to a digitized signal and measured value of the Fluke 8060 true r.m.s. multimeter is given. Selected captured signals are presented. The components used in the design are listed.

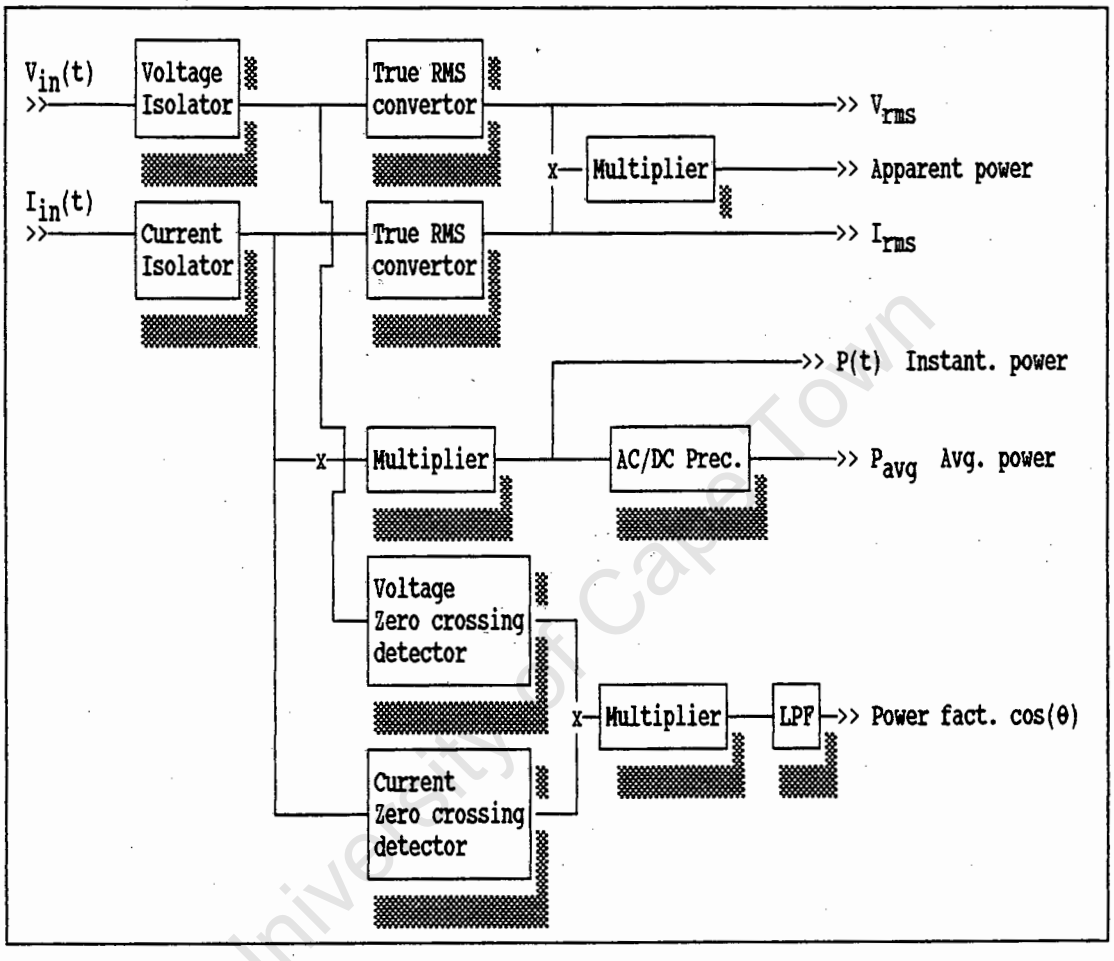




**Fig. A2.2** Block diagram of true r.m.s. power meter.

Precision components used in the design:

Precision isolation operational amplifier:
ISO 122P Burr Brown.

True r.m.s. to dc converter:
AD 534 Analog Devices.

Low offset, high frequency opamps:
LF 411 Analog Devices.

Precision multiplier:
AD 536A Analog Devices.

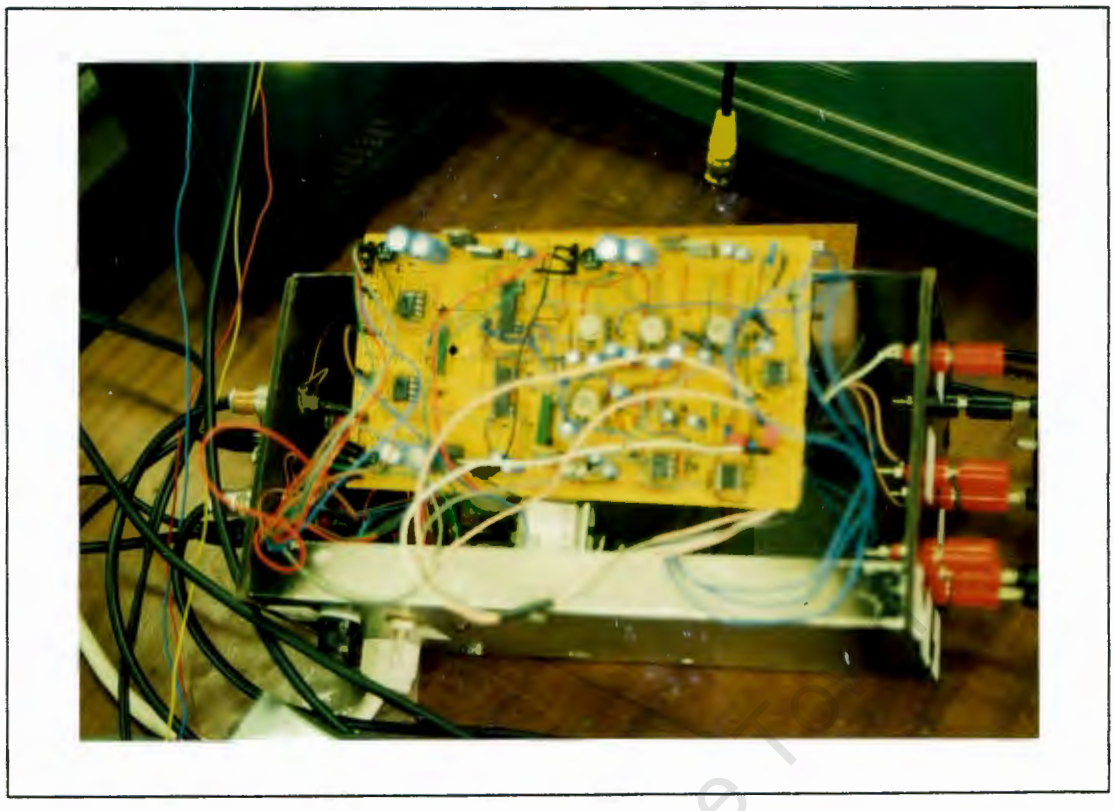

Fig. A2.3 True r.m.s. powermeter, exposed circuit.

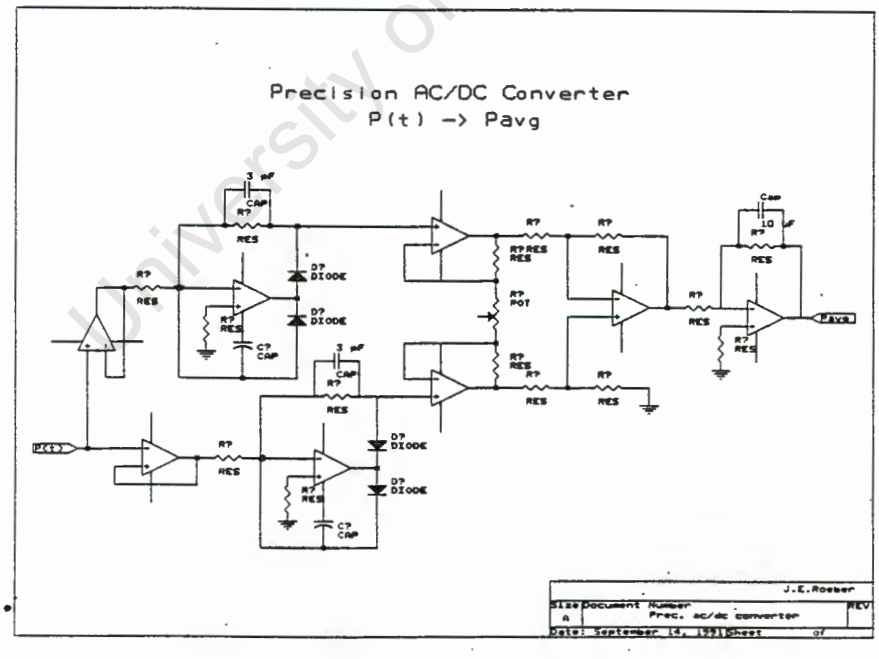


Fig. A2.4 Precision AC/DC converter - Averaging power circuit. (incorporated in cct. in Fig. A2.5).

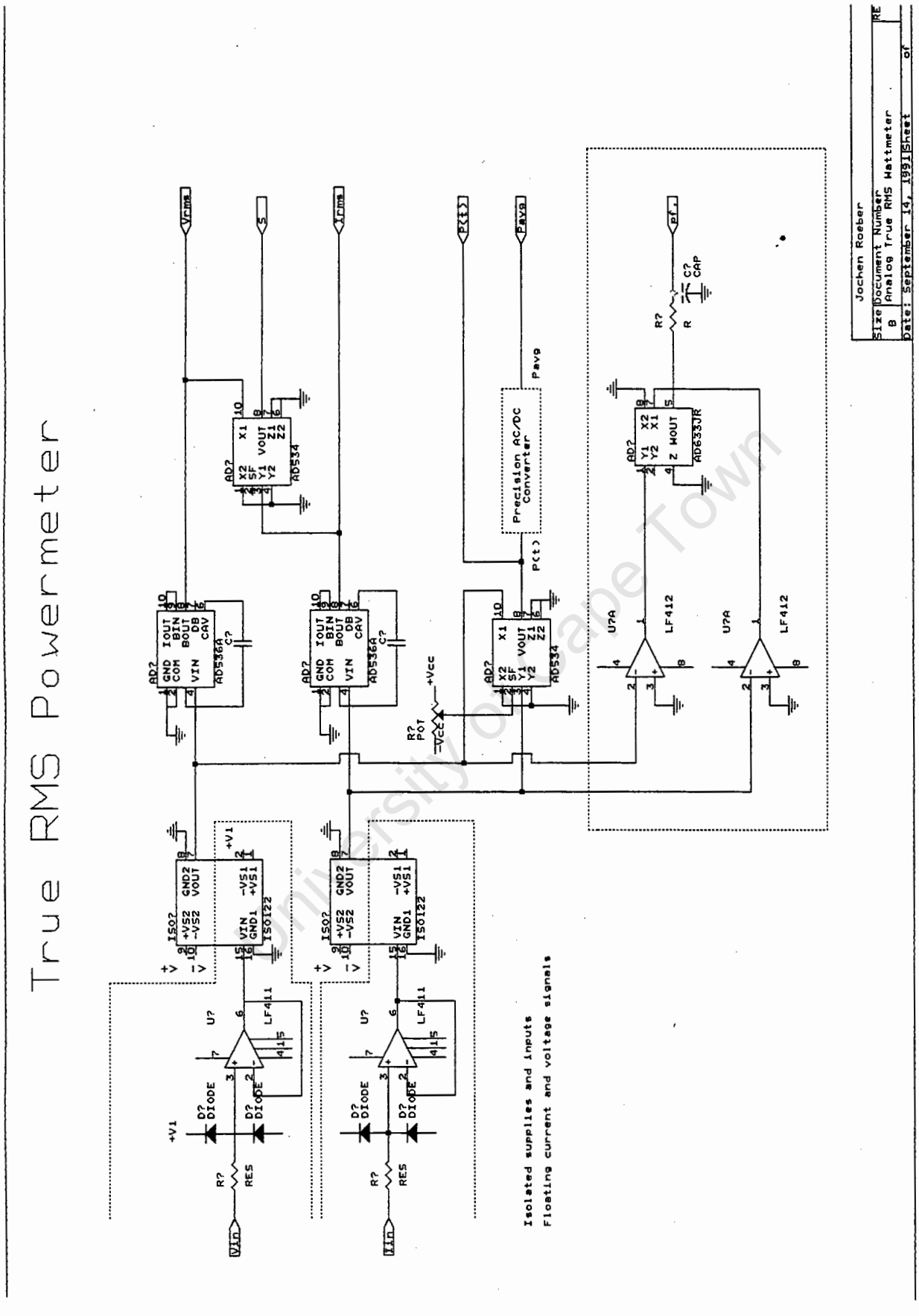


**Fig. A2.5 Circuit diagram of the true r.m.s. power meter.**

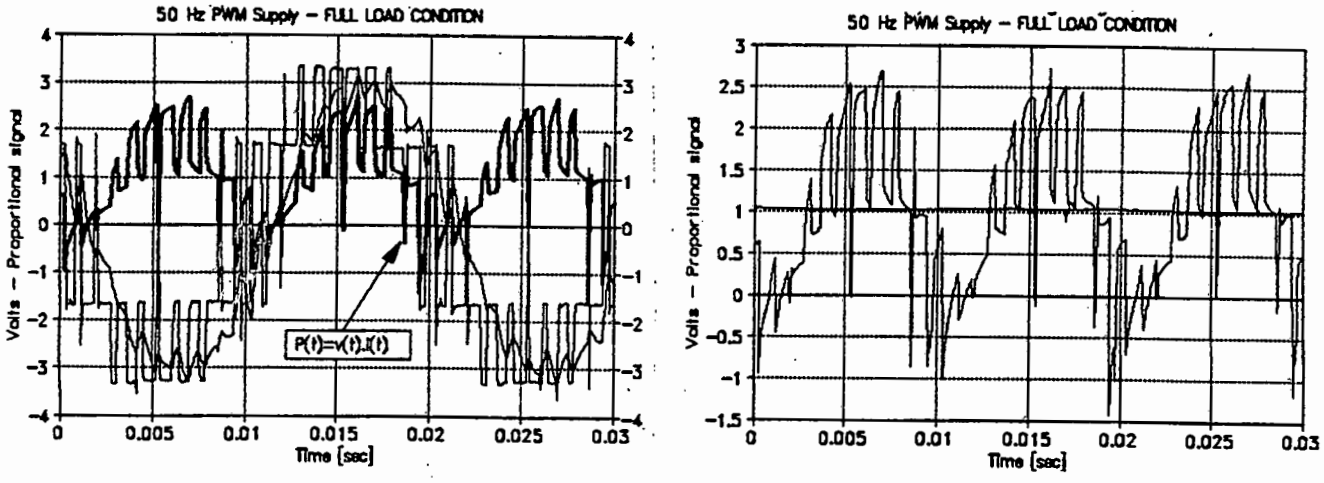


(a). (b).

**Fig. A2.6** (a). Voltage v(t) and current i(t) signals and instantaneous power P(t), (b). P(t) and the Average $P_{avg}$ signals. PWM excitation under load conditions.

**Table A2.1** Accuracy of wattmeter calculated from digitized signals and measured from $P_{avg}$ and r.m.s. convertors.

| Excitation (Under Load) | (%) Error $V_{rms}$ | (%) Error $I_{rms}$ | (%) Error $P_{avg}$ |
|---|---|---|---|
| PWM: | | | |
| Calculated | 0.2 | 0.7 | 1.0 |
| Measured | 0.6 | 0.5 | 1.0 |
| SQWave: | | | |
| Calculated | 0.6 | 0.9 | 0.6 |
| Measured | 0.1 | 0.3 | 0.6 |

The accuracy of the wattmeter under load and no load conditions can be approximated to the region of 1% , as calibrations were repeated with consistent results. This device proves to be a viable alternative to the Yokogawa powermeters. A dedicated transputer based digital power meter will be superior for inverter application power measurements and should be implemented to obtain even better precision for efficiency measurements.

## 2.5 HBM Slip ring Torque Transducer.

Torque measurements were performed with a HBM (German company) strain gauge slip ring torque transducer with good dynamic frequency response to measure torque pulsations.

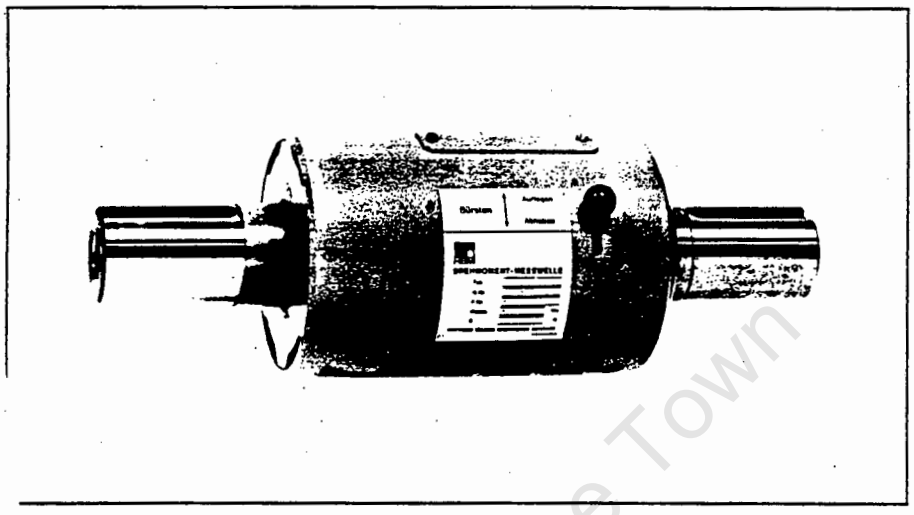

Torque Transducers T 1 and T 2



**Technical Data**

| Type | | T 1/... | T 2/... |
|---|---|---|---|
| Nominal torque ($M_{nom}$) | Nm | 50; 100; 200; 500 | 10; 20; 50<br>100; 200; 500 |
| | kNm | 1; 2; 5; 10 | 1; 2; 5; 10; 20; 50 |
| Nominal sensitivity (nominal output signal at nominal torque) | mV/V | 1.5 | 1.5 |
| Sensitivity* tolerance | % | ± 0.1 | ± 0.2 |
| Temperature effect per 10 K at nominal temperature range<br>on the sensitivity (related to the actual value)<br>on zero signal (related to the nominal sensitivity) | %<br>% | ± 0.1<br>± 0.05 | ± 0.1<br>± 0.1 |
| Linearity error including hysteresis related to the nominal sensitivity | % | < ± 0.1 | < ± 0.2 |
| Relative standard deviation of repeatability according to DIN 1319 | % | < ± 0.05 | < ± 0.05 |
| Input resistance at reference temperature between connections 2 and 3 | Ω | 350 ± 2 | 350 ± 2 |
| Output resistance at reference temperature between connections 1 and 4 | Ω | 350 ± 1.5 | 350 ± 1.5 |
| Nominal range of energising voltage | V | 0.5 ... 12 | 0.5 ... 12 |
| Maximum permissible energising voltage | V | 18 | 18 |
| Reference temperature | °C | + 23 | + 23 |
| Nominal temperature range** | °C | + 10 ... + 60 | + 10 ... + 60 |
| Service temperature range** | °C | − 10 ... + 60 | − 10 ... + 60 |
| Storage temperature range | °C | − 50 ... + 70 | − 50 ... + 70 |
| Range of nominal speed for<br>Types with nominal torque ≤ 2 kNm<br>Types with nominal torque 5 kNm and 10 kNm<br>Types with nominal torque 20 kNm and 50 kNm | <br>min⁻¹<br>min⁻¹<br>min⁻¹ | <br>0 ... 6000<br>0 ... 4000<br>- | <br>0 ... 6000<br>0 ... 4000<br>0 ... 2500 |
| Mechanical values, related to $M_{nom}$ (see also table "Mechanical limit values")<br>Limit load, static<br>Breaking load, static<br>Permissible dynamic load<br>(vibration amplitude peak-to-peak not to exceed $M_{nom}$) | <br>%<br>%<br>% | <br>150<br>300<br>70 | <br>150<br>300<br>70 |

* The sensitivity is the actual output signal at nominal torque.
** Please note temperature of bearings at higher speeds.

**Schematic Diagram**

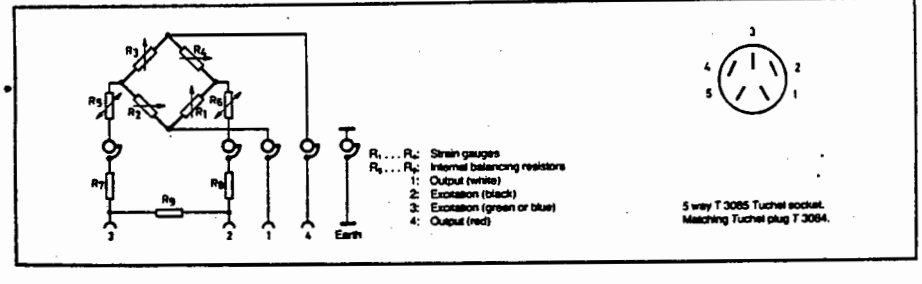


**Fig. A2.7** Torque transducer (HBM), picture, Technical Data and schematic diagram.

The signal from the strain gauge bridge is conditioned in a instrument amplifier and then logged to the data acquisition system. The torque transducer sensitivity is 1.5 mV / 1 V, which is 0.15%. The torque signal is high pass filtered to investigate torque variations. A low pass filter gives the average torque.

## 2.6 Shaft Voltage Sensors, External Trigger Circuit Diagram.

The shaft voltage was measured form the shaft by carbon brushes, the signal fed to a differential amplifier via screened cables.

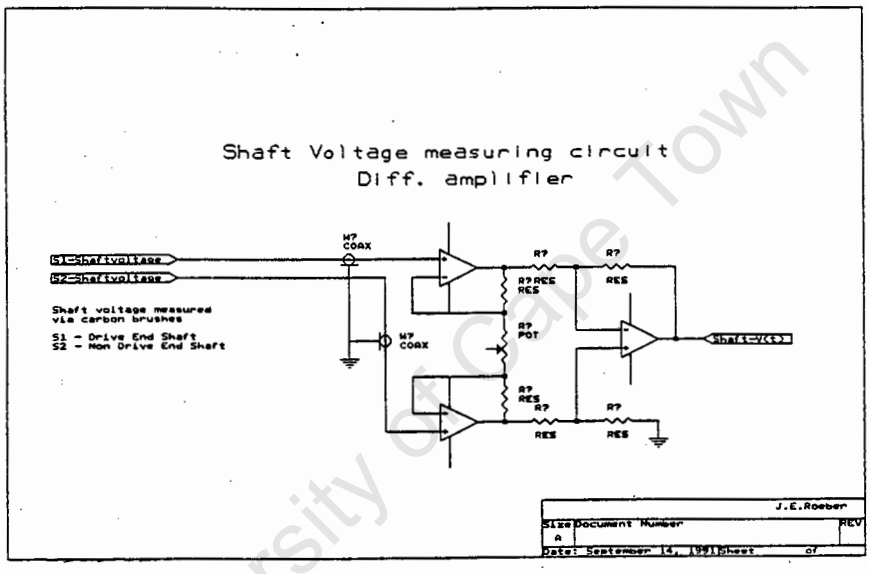


**Fig. A2.8** Shaft voltage signal differential amplifier circuit diagram.

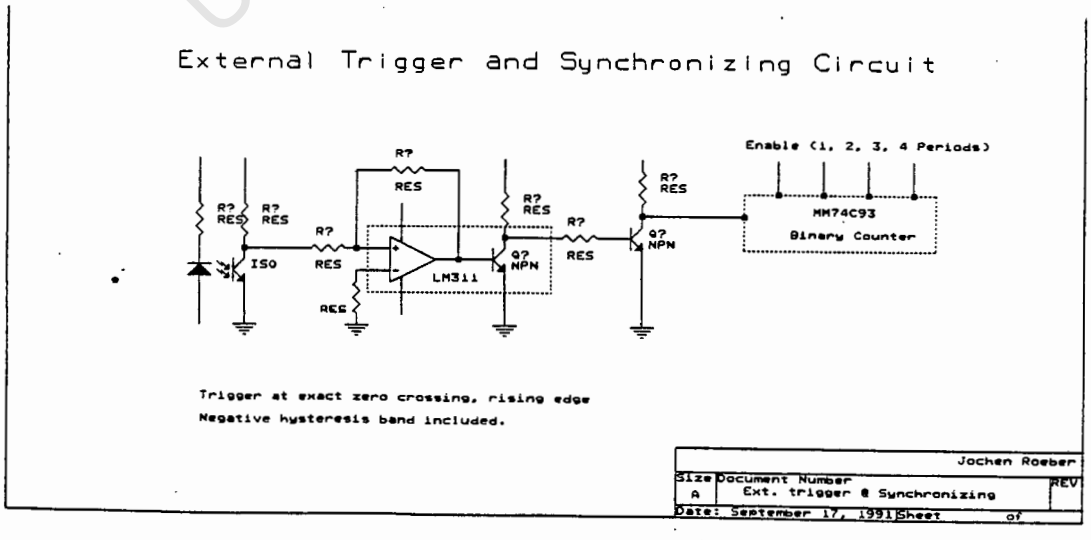


**Fig. A2.9** External triggering circuit.

## 2.7 Temperature Measurement.

Temperature was measured with LM35-D temperature transducer placed in the machine laminations. To reduce noise and interference the signal was filtered to give a average steady state constant. The time constant is not crucial as temperatures change very slowly.

Precision Centigrade Temperature sensor: LM35-D National Semiconductor Corporation.

## 2.8 Accelerometer Application Information.

The accelerometer application notes are given below. The frequency response is given in Fig. A2.10.

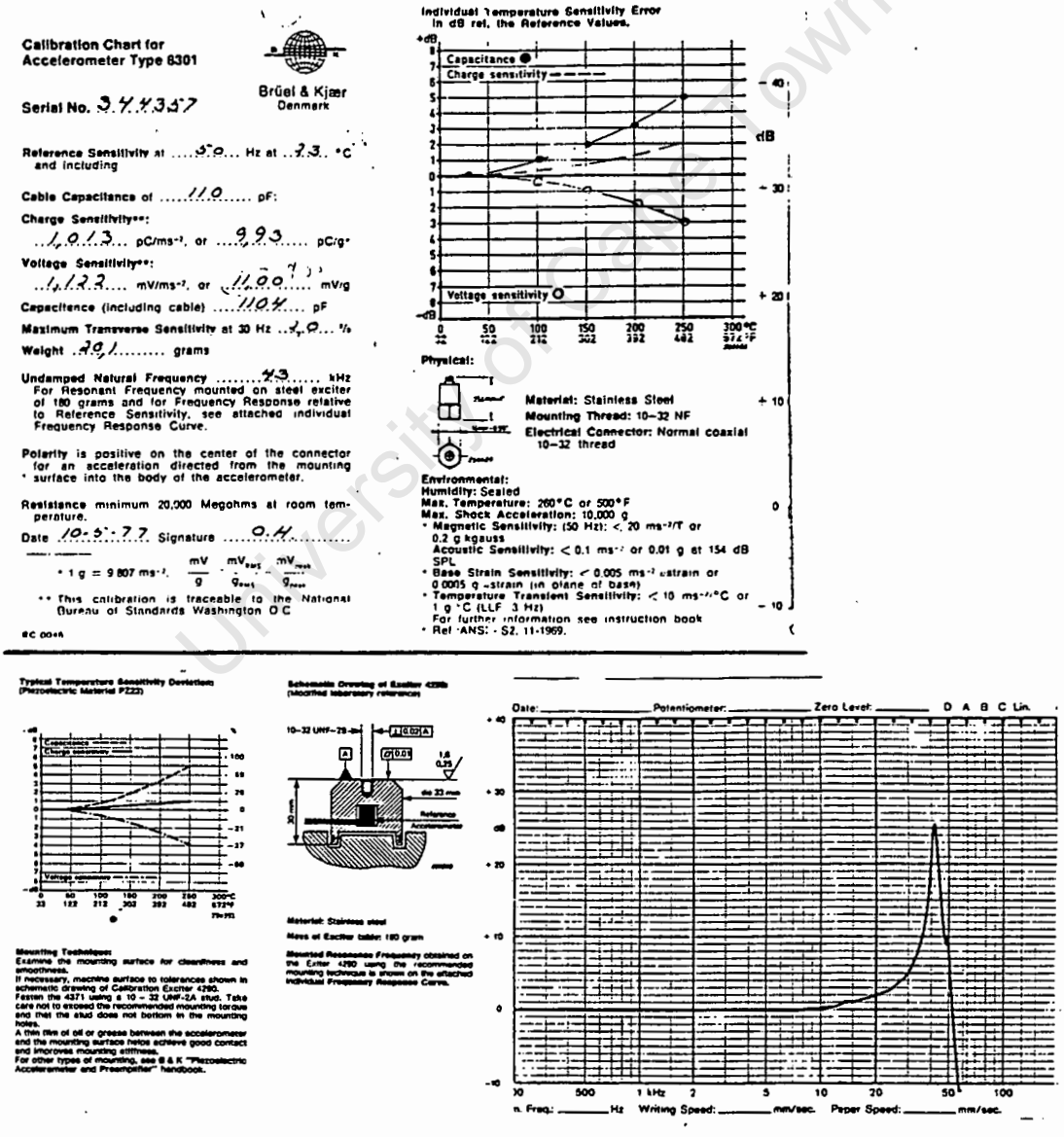


**Fig. A2.10** Frequency response of the B&K accelerometer.

## 2.9 Calibration Data and Measurement Equipment.

### 2.9.1 Measurement Equipment.

All calibration statistical calculations were performed with standard Quattro Pro spreadsheet functions.

Equipment used is outlined in Chapter 2.

### 2.9.2 Calibration.

**Current:**

Constant: ..... 0.013
Std. Err. of Y Est: ..... 0.003321
R squared: ..... 0.999952
No. of Observations: ..... 13
Degrees of Freedom: ..... 11

X-Coefficient: ..... 0.188251
Srd.Err. of Coefficient: .. 0.00093

1 [A] = 0.1908 [V]
1 [V] = 5.24 [A]

**Voltage:**

Phase A: 1 [V] = 100.15 [V]
Phase B: 1 [V] = 100.36 [V]
Phase C: 1 [V] = 99.45 [V]

**Torque: (HBM Strain gauge slip ring configuration).**

Constant: ..... -0.68449
Std. Err. of Y Est: ..... 0.137988
R squared: ..... 0.999807
No. of Observations: ..... 27
Degrees of Freedom: ..... 25

X-Coefficient: ..... 12.279
Srd.Err. of Coefficient: .. 0.034131

1 [Nm] = 12.27 [V]
1 [V] = 0.081 [Nm]

**Speed: (DC Tacho generator).**

Constant: ..... 36.92
Std. Err. of Y Est: ..... 1.61688
R squared: ..... 0.99992
No. of Observations: ..... 17
Degrees of Freedom: ..... 15

X-Coefficient: ..... 673.02
Srd.Err. of Coefficient: .. 0.4983

R.p.m.
1 [r.p.m.] = 0.001484 [V]
1 [V] = 673.02 [r.p.m.]
Offset: 36.92 [r.p.m.]

Radians/sec.
1 [rad./sec.] = 0.0141 [V]
1 [V] = 70.47 [rad./sec.]
Offset: 0.615 [rad./sec.]

Frequency.
1 [Hz] = 0.089 [V]
1 [V] = 11.21 [Hz]
Offset: 0.615 [Hz]

## 3. *Appendices - Chapter 3.*

### 3.1 Frequency Spectra of Voltage and Currents.

No-load voltage and current signals with current frequency spectra are given in Fig. A3.1.

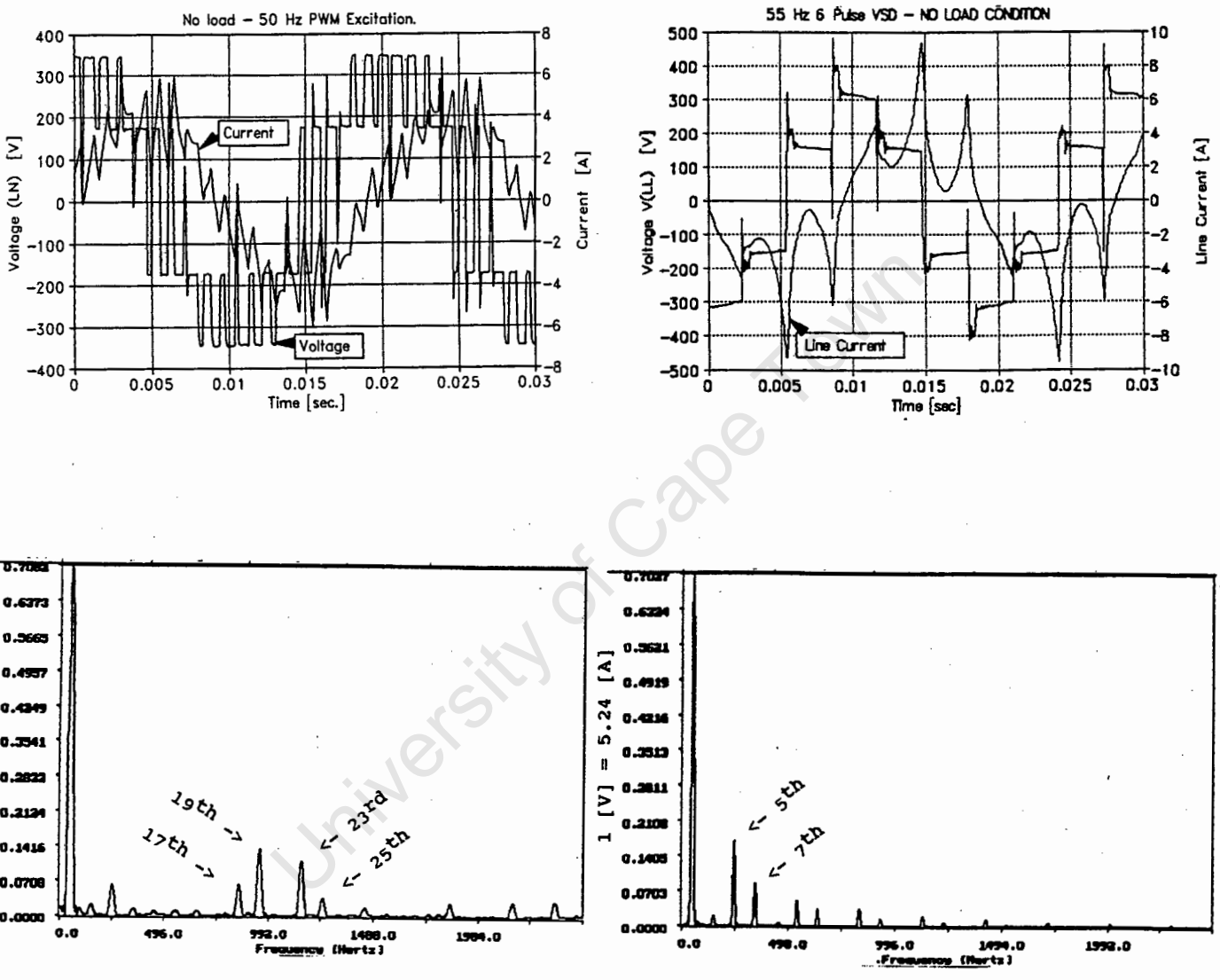


(a). (b).

**Fig. A3.1** No load Voltage and current signals with current frequency spectrum for (a). PWM and (b). Square Wave excitation.

From the no load current frequency spectrum it can be observed that the higher time harmonic components are only marginally smaller than under load condition. The power factor is much worse, as deduced from the phase shift between voltage and current signal.

## 3.2 PWM Modulation over the Operating Range.

Fig. A3.2 shows a sample of analysis of PWM waveforms using the software written by the author.

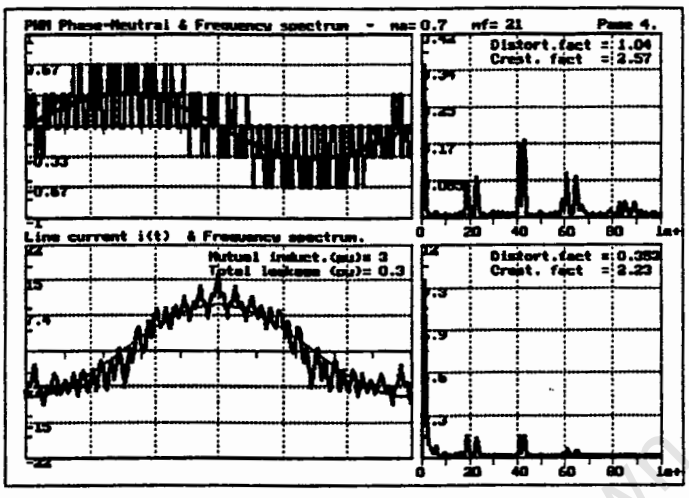


(a).

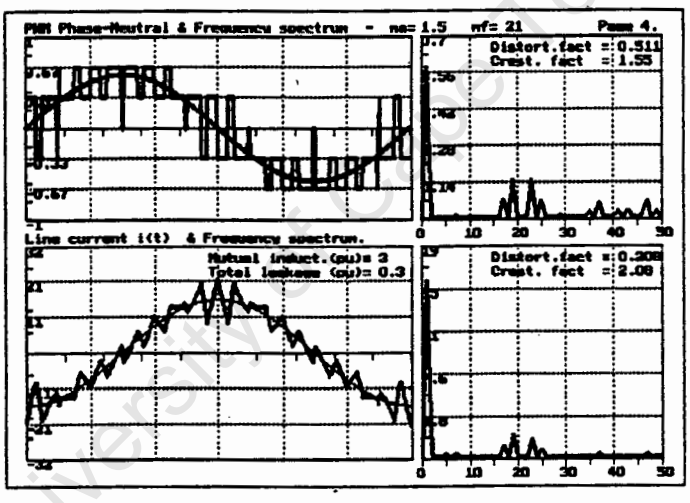


(b).

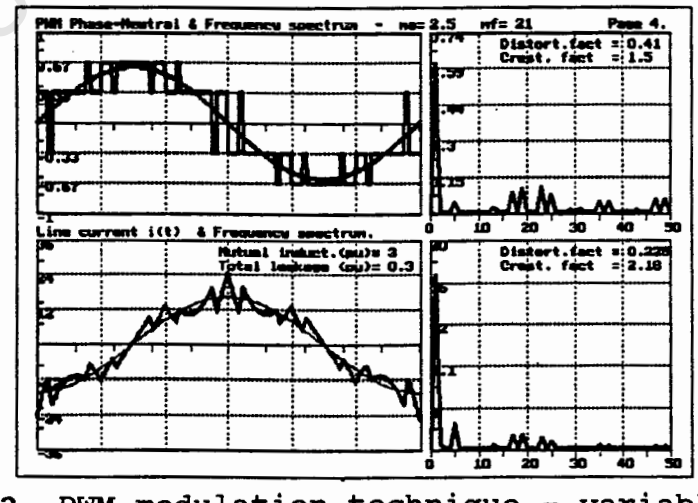


(c).

**Fig. A3.2** PWM modulation technique - variable voltage, variable frequency. (a). $f_1 \approx 30$ Hz, (b). $f_1 \approx 50$ Hz (c). $f_1 \approx 60$ Hz.

## *6. Appendices - Chapter 6.*

### 6.1 No Load Pulsating Torques.

No load pulsating torques under subsynchronous characteristic operating configuration, and running conditions, as shown in Fig. A6.1.

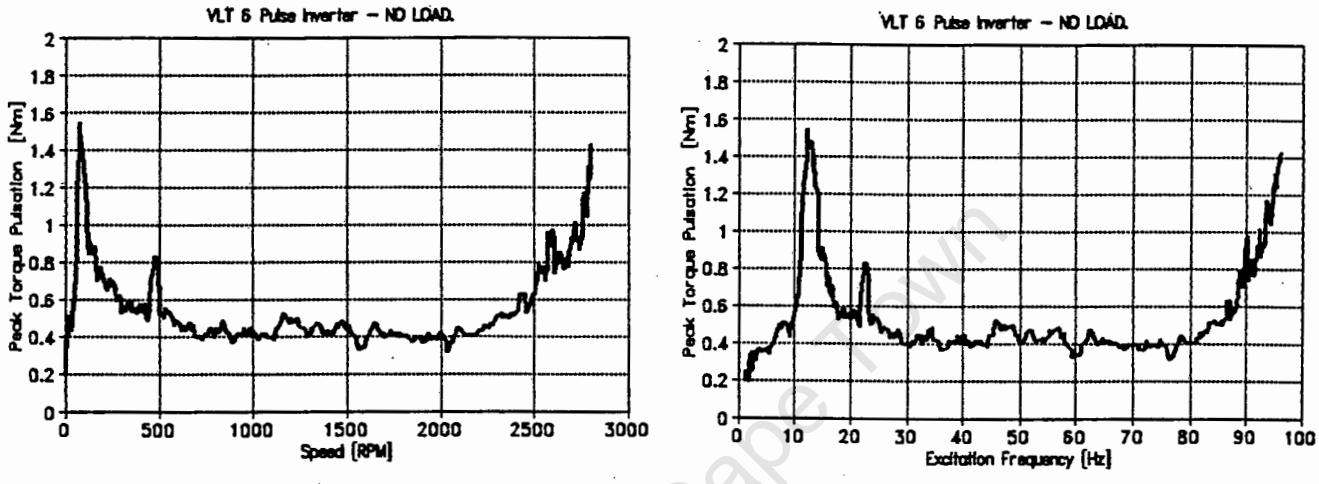


(a). (b).

**Fig. A6.1** Square Wave excitation, Peak Torque pulsations under subsynchronous configuration ($V_r$/87). (a). Torque pulsations vs excitation frequency, (b). Torque pulsations vs speed.

# 7. *Appendices - Chapter 7.*

## 7.1 Vibration Nomogram and Vibration Quality Grades.

The nomogram of vibrations is shown in Fig. A7.1. Vibration quality grades are presented in Table A7.1.

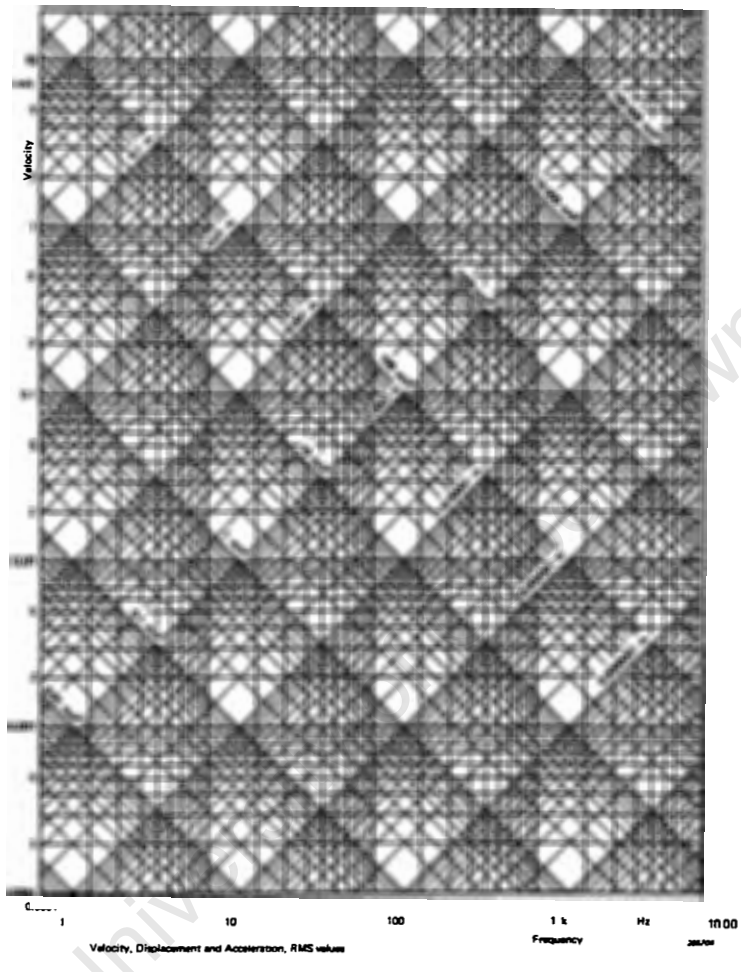


**Fig. A7. 1** Frequency Nomogram. Source [2.3].

**Table A7.1** Vibration quality grades of small- and medium sized rotating electrical machines (as per ISO 2373 [2.3]).

| Vibration quality grade | Nominal speed $n$, $s^{-1}$ | | Axial height, mm | | |
|---|---|---|---|---|---|
| | | | $56 \leq h \leq 132$ | $132 < h \leq 225$ | $225 < h \leq 400$ |
| | over | up to | $h$, the permissible vibration severity in mm $s^{-1}$ | | |
| *N*, Normal | 10 | 60 | 1.8 | 2.8 | 4.5 |
| *R*, Reduced vibration | 10 | 30 | 0.71 | 1.12 | 1.8 |
| | 30 | 60 | 1.12 | 1.8 | 2.8 |
| *S*, Special | 10 | 30 | 0.45 | 0.71 | 1.12 |
| | 30 | 60 | 0.71 | 1.12 | 1.8 |

## *9. Appendices - Chapter 9.*

### 9.1 Induction Motor Performance with External Leakage Reactance.

Based on the paper [9.1] motor performance with increased external leakage inductance was investigated, Figs. A9.1, A9.2 and A9.3. In [9.2] the discussion focuses mainly on the reduction in temperature rise in the rotor bars. In this section the voltage and current waveforms, powerfactor, torque pulsations and shaft voltages are measured.

**Voltage and current signal.**

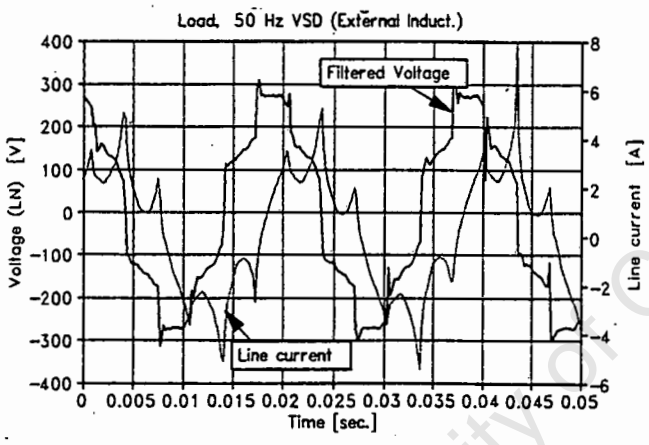


(a).

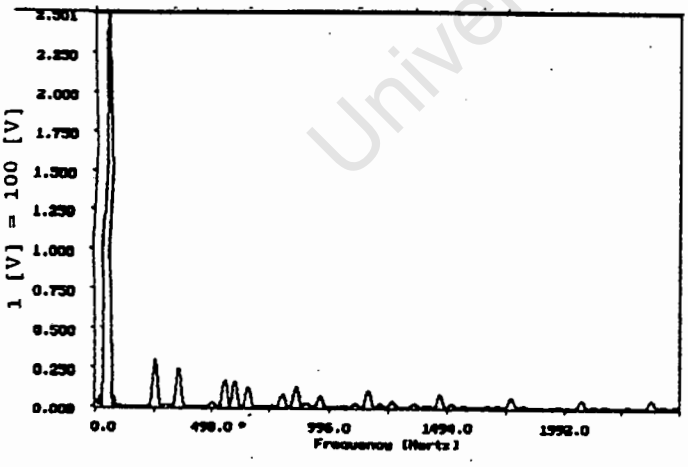


(b).

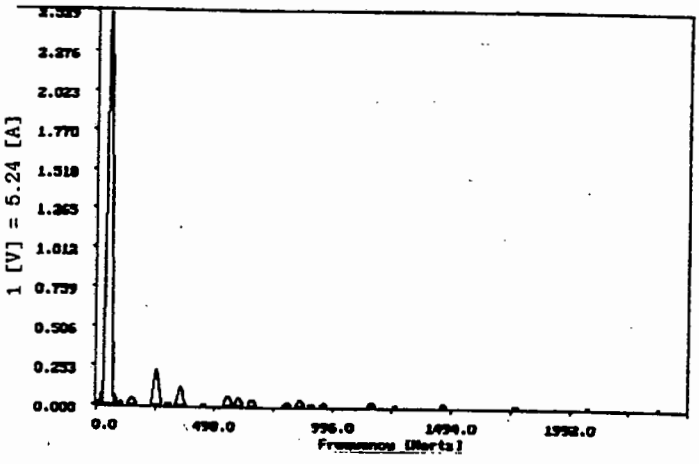


(c).

**Fig. A9.1** Characteristics of induction motor with external inductance fed from a square wave inverter under load condition: (a) Voltage and current waveform, (b) Voltage spectrum, (c) Current spectrum.

Three series inductances of approximately 9.8 [mH] are connected in series with the three phase supply to the induction motor, increasing the total leakage reactance by nearly 60% . Especially high frequency components are filtered out and will thus reduce harmonic effects on the induction machine. The pull-out torque is then however reduced.

**Peak torque pulsations.**

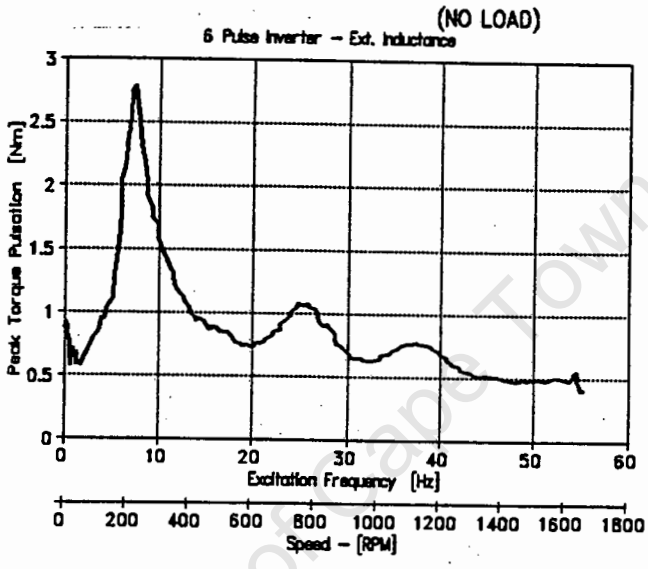


(a).

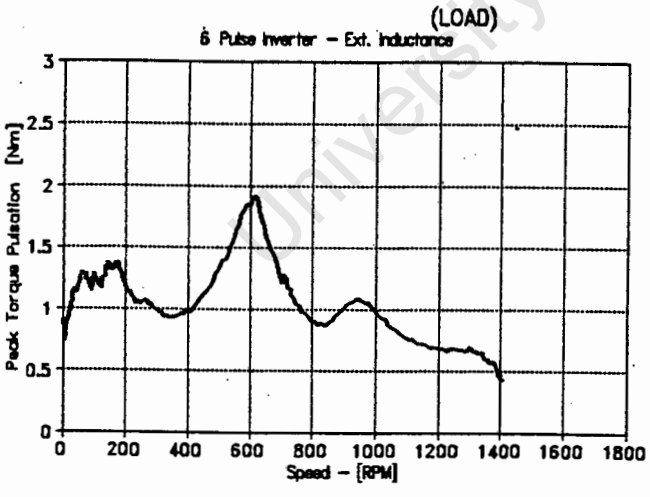


(b).

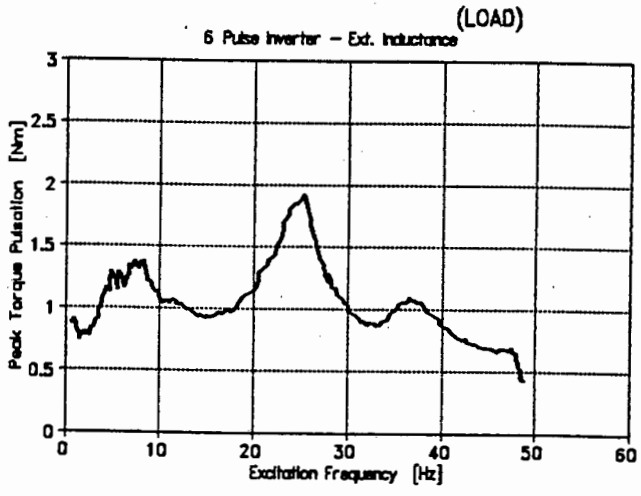


(c).

**Fig. A9.2** Characteristics of induction motor with external inductance fed from square wave inverter: (a) Peak torque pulsations at no-load condition, (b) Peak torque pulsations load condition vs speed and (c) Peak torque pulsations vs excitation frequency.

**Induced shaft voltages.**

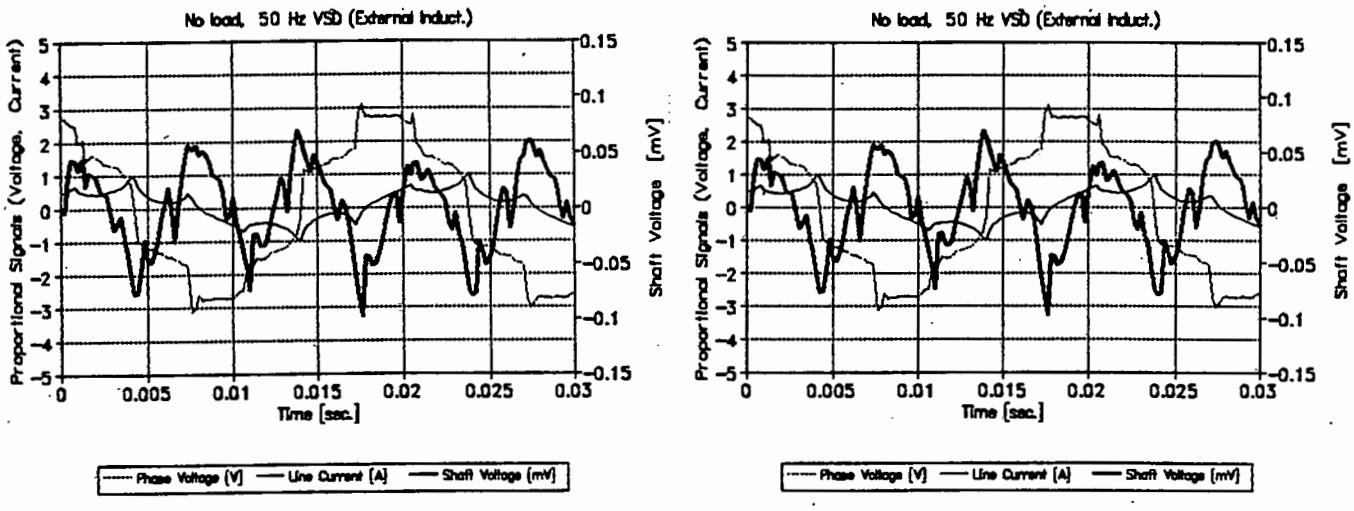


(a). (b).

**Fig. A9.3** Characteristic of induction motor with external inductance fed from square wave inverter: (a) Induced shaft voltages at no-Load condition (b). Induced shaft voltage under load condition.

**Simulation of increased leakage reactance.**

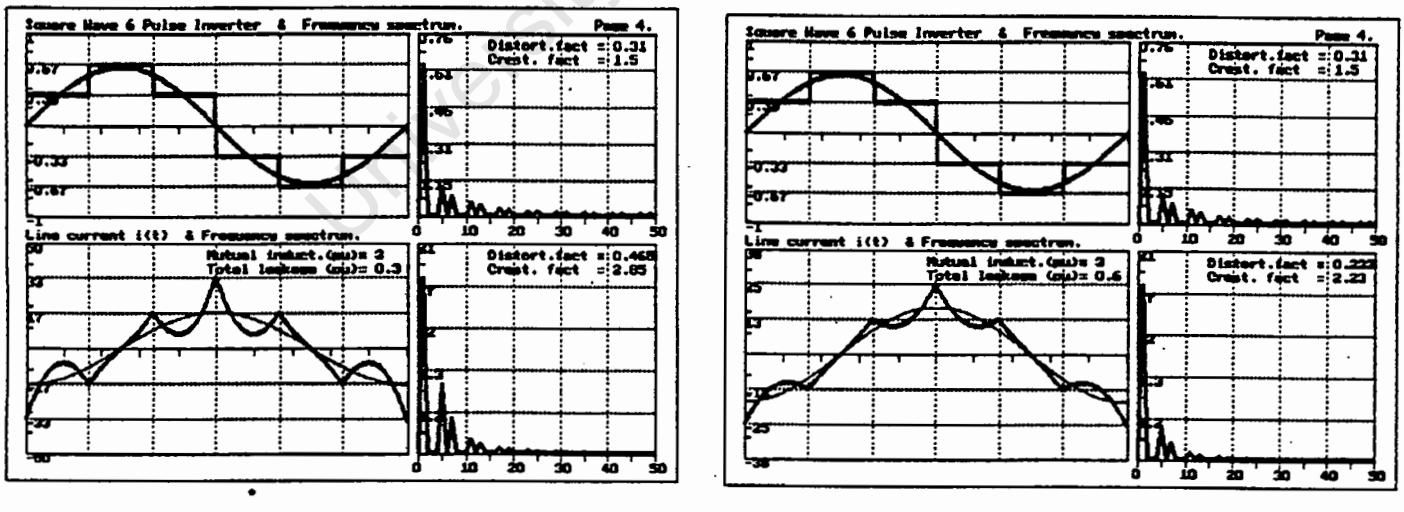

(a). (b).

**Fig. A9.4** Computer simulation results of induction motor fed from square wave inverter: (a) without external leakage reactance and (b) with external leakage reactance.

# REFERENCES


**Chapter 1.**

[1.1] Guide for the application of induction machines when fed from inverters; IEC Draft international standard, Project No. 2/032/2, 1990.

[1.2] *Schoener, J. and Seifert, D.;* "Electrical and mechanical features of inverter-fed asynchronous motors", International Conference on Electrical Machines ICEM '86, Munich, 1986, pp.785 - 790.

[1.3] *Kleinrath, H.;* "Inverter-fed AC Machines", Bulletin ASE/UCS 1983 No.12, pp. 1386-1989.

[1.4] *Bose, B.K.;* Power electronics and ac drives, Prentice Hall, USA, 1987.

[1.5] *Mohan, N.;* Power Electronics: Converters - Applications and Design, John Wiley & Sons, 1989.

[1.6] *Kloss A;* "Harmonics in power systems with converters", ABB Review, 1991, No. 4, pp 29 - 34.

**Chapter 2.**

[2.1] *Enslin, J; Van Wyk, J;* "Measurement and compensation of fictitious power under non-sinusoidal voltage and current conditions", IEEE Transactions on Instrumentation and measurement, Vol 37, No. 3, pp. 403 - 408.

[2.2] *Lindsay, J;* "Measurement problems in determining the efficiency of thyristor-supplied motor drives", IEE Transactions on IAS Vol IA-15, No. , 1979, pp. 8 - 13.

[2.3] *Timar, P. L. (Editor).* Noise and Vibration of Electrical Machines, Elsevier 1989.

[2.4] *Miki, I; Matsuse, K;* "A method of determining equivalent circuit parameters of an induction motor fed from various inverters", Electric Energy Conference 1987, Adelaide, pp. 423 - 417.

[2.5] *Kataoka, T; Kandatsu, Y; Akasaka, T;* "Measurement of equivalent parameters of inverter fed induction motors", IEE Transactions on Magnetics, Vol. Mag -23, pp. 3014 - 3016.

[2.6] *Stevens, R;* Electrical Machines and Power Electronics, Van Nostrand Reinhold Co., 1984.

[2.7] *Pönnighaus, R;* Loss modelling of an inverter-fed induction motor, M. Eng. Thesis, University of Stellenbosch, 1989, pp. 33 - 35.

[2.8] *Case, M;* Verbal discussion and consultation, University of Cape Town, March 1991.

[2.9] *Alger, P;* Induction Machines; Gordon and Breach Science Publishers, 1970.

[2.10] *Brüel & Kjaer Co.* Piezoelectric Accelerometers and Vibration Preamplifiers, Theory and Application Handbook. 1986.

**Chapter 3.**

[3.1] *Jordan, H.; Klingshirn, E.;* " Polyphase Induction motor Performance and Losses on Nonsinusoidal Voltage Sources". Transactions IEEE Vol. PAS-87, No. 8, March 1968.

[3.2] *Chalmers, B.J.;* "Induction motor losses due to non-sinusoidal supply waveforms". Proc. IEE. Vol 115, No. 12, 1968, pp. 1777 - 1782.

[3.3] *Kliman, B.;* "Harmonic effects in PWM inverter induction motor drives". Transactions IEEE IAS 1972 Annual Meeting, pp. 783 - 790.

[3.4] *De Buck, G.;* "Losses and Parasitic torques in Electric Motors Subjected to PWM waveforms". Transactions IEEE IAS Vol IA-15, No 1, 1979, pp. 47-53.

[3.5] *Green, B; Boys, B;* "Inverter AC-drive efficiency". IEE Proc. Vol 129, Pt. B, No. 2, 1982. pp. 75 - 81.

[3.6] *Venkatessen, K.; Lindsay, L.;* "Comparative Study of the losses in Voltage and current source inverter fed induction motors". Transactions IEEE IAS Vol 1A-18 No 3, 1982, pp. 240 - 246.

[3.7] *Scholey, D.;* "Induction motors for variable frequency power supplies". Transactions IEEE IAS Vol. IA-18 No.4, 1982, pp. 368 - 372.

[3.8] *De Buck, G.; Gistelinck, P; De Backer, D.* "A simple but Reliable Loss model for Inverter-Supplied Induction Motors". Transactions IEEE IAS Vol. IA-20.1, 1984, pp. 190 - 202.

[3.9] *Andersen, C.; Bieniek, K.;* "On the Torques and Losses of Voltage and Current Source Inverter Drives". Transactions IEEE Vol IA-20, No2, 1984. pp. 321 - 327.

[3.10] *Hentschel, F.; Shehata, M.;* "Comparative Study of the Losses in Inverter-fed standard Squirrel-cage induction machines." Int. Conference on Electrical Machines, ICEM '86, Munich, pp. 320 - 323.

[3.11] *Grantham, C.;* "Inverter supplied induction motor performance calculations and measurements.", Electric Energy Conference 1987, Adelaide, 1987.

[3.12] *Reisinger, E.;* "Measurement of Iron Losses Due to Alternating and Rotating Magnetization". Electric Energy Conference 1987, Adelaide, 1987.

[3.13] *Klug, L.; Ibrahim, S.;* "Computation of power and efficiency of induction motors at frequency speed control". Modelling, Simulation & Control, A, AMSE Press, Vol 13, No. 1, 1987, pp. 1-8.

[3.14] *Brandes, J.;* "Zusatzliche Verluste bei Induktionsmaschienen mit Kafiglaufern", ETZ, Bd. 108 (1987) Heft 8. pp. 316 - 321.

[3.15] *Wahsh,S.;* "Additional losses in three phase cage induction machines with PWM inverters", Int. Conference on Electrical Machines, ICEM '88, Pisa, Vol 1. pp. 621 -626.

[3.16] *Gieras, J.;* "Computation of losses in an inverter-fed double cage induction motor". Mediterranian Electrotechnical Conference MELECON '91, Ljubiliana, pp.1298 - 1301.

[3.17] *Gieras, J. F.; Banii-Issa, M.;* "Opertaion and Performance of a Double-squirrel cage induction motor subjected to non-sinusoidal Voltage Waveform", Int. Conference Power High Tech '89, Valencia, 1989.

[3.18] *Baush, H.; Lange, B.; Sahm, D.;* "Experimental investigation of losses in a PWM inverter / induction machine drive system", Int. Conference on Electrical Machines, ICEM '90, Boston, 1990.

[3.19] *Novonty, D.; Nasar, S; Maley, D.; Jeftenic, B.;* "Frequency Dependance of Time Harmonic Losses in Induction Machines", ICEM, Boston, MIT, 1990, pp. 233 - 238.

[3.20] *Heller, B.; Hamata, V.;* Harmonic Field Effects in Induction Machines, Elsevier Scientific Publishing Company, New York, 1977.

[3.21] *Lazim, T; Shepherd, W;* "Analysis of Induction Motors Subjected to Nonsinusoidal Voltages containing Subharmonics", Transactions IEEE , Vol. IA-21, No. 4, 1985.

**Chapter 4.**

[4.1] *Say, M. G.;* "The performance and design of alternating current induction machines", Pitman Press, London, 1958.

[4.2] *Sen,P.;* "Derating of Induction Motors due to Waveform Distortion", IEEE Transactions on Industry Applications, Vol. IA-26, No.6. 1990, pp.1102 - 1107.

[4.3] *Fitzgerald, A; Kingsley, C; Umans, S;* Electric Machinery, Mc Graw-Hill Book Company, 1985.

[4.4] *Daugherty, R; Franzini, J;* Fluid Mechanics with Engineering Applications, Mc Graw Hill Book Company, 1977.

[4.5] *Kreith, F; Black, W;* "Basic Heat transfer", Harper & Row Publishers, New York, 1980.

[4.6] *Nates, R;* Verbal discussion and consultation, Department of Mechanical Engineering, UCT, August 1991.

**Chapter 5.**

[5.1] *Haus, O.;* "Shaft voltages and bearing currents, their cause, effects and remedial measure", - (in German), ETZ A, Vol.85, 21 Feb. 1964, pp. 106 - 112.

[5.2] *Alger, P.; Samson, H.;* "Shaft currents in Electrical Machines", Transaction AIEE, 1924, pp. 235 - 245.

[5.3] *Freise, W; Jordan, H;* "Ascertaining the shaft voltages and bearing currents in electrical machines considering magnetic potentials in the iron " (in German), Elekrotechnik und Maschienenbau (E.u.M.), Vol. 80, Part 4., 1963, pp. 80 - 84.

[5.4] *Jordan, H.; Teagen, F.;* "Shaft fluxes resulting from variations in air gap permeances." - (in German), ETZ A, Vol 85, 25 Dec. 1964. pp. 865 - 867.

[5.5] *Ames, R. L.;* "A.C. Generators: Design and Application", Chapter 2., John Wiley & Sons Inc.

[5.6] *Roeber, J; Gieras, J;* " Experimental investigation of shaft voltage induced in an inverter-fed motor ", Int. Conference on Electrical Machines ICEM '92, Manchester, 1992, submitted for publication.

[5.7] *Amman, C; Reichert, K; Posedel, Z;* "Shaft voltages in turbogenerators: operating experience with RC-grounding device and new possibilities for monitoring the condition of turbogenerators", Int. Conference on the Evolution and Modern Aspects of Synchronous Machines, Zürich, 1991, pp. 703 - 708.

**Chapter 6.**

[6.1] *Lipo, A.; Krause, C.; Jordan, E.;* "Harmonic Torque and Speed pulsations in a Rectifier-Inverter Induction Motor Drive". Transactions IEEE, Vol. PAS-88, No. 5, 1969, pp. 579 - 587.

[6.2] *Sattler, P.; Strötgen, E.;* "Auswirkung der Versorgung einer Stromrichtergespeisten Asynchron-maschiene aus dem $16^2/_3$ Hz Netz auf die Pendelmomententwicklung". ETZ Arch., Vol 6, No. 1, 1984, pp. 25 - 32.

## Chapter 7.

[7.1] *Subrahmanyam, V.;* "Axial forces in induction motors with skewed slots", Proc. IEE, Vol.118, No. 12, 1971, pp. 1759 - 1760.

[7.2] *Ellison, A.; Yang, S.;* "Natural frequencies of stators of small electric machines", Proc. IEE, Vol. 118, No. 1, 1971, pp. 185 - 190.

[7.3] *Labrush, E.;* " Controlling Two-Pole Induction Motor System Vibration". IEEE , Vol. IA-16, No. 6, 1980. pp. 837 - 840.

[7.4] *Girgis, R.; Verma, S.;* "Method for accurate determination of resonant frequencies and vibration behaviour of stators of electrical machines", Proc. IEE, Vol. 128, Pt. B, No. 1, 1981, pp. 1 - 11.

[7.5] *Girgis, R.; Verma, S.;* "Experimental verification of resonant frequencies and vibration behaviour of stators of electrical machines. - Part 1. Models, experimental procedure and apparatus". IEE Proc. Vol. 128, Pt. B, No. 1, 1981. pp. 12 - 21.

[7.6] *Girgis, R.; Verma, S.;* "Experimental verification of resonant frequencies and vibration behaviour of stators of electrical machines. - Part 2., Experimental investigations and results". IEE Proc. Vol. 128, Pt. B, No. 1, 1981. pp. 23 - 31.

[7.7] *Holmes, D.G.;* "A real-Time Spectral Analyzer to measure Electrical Harmonics and Motor Vibrations", Electric Energy Conference, Adelaide, 1987, pp. 427 - 432.

## Recommendations.

[9.1] *De Buck, F;* "Design adaption of inverter-supplied induction motors", IEEE PAS, Vol. 1, No. 2, 1987, pp. 55 - 61.

[9.2] *De Buck, F;* "Optimal leakage for induction motors supplied by a voltage source inverter", ICEM, 1987, Brussels.

[9.3] *Hassan, D;* "Specifying adjustable-speed ac drive systems and currently available industry standards", IEEE , Vol. IA-23, No. 4, 1987, pp. 581 - 585.

[9.4] *Huget, W;* "Squirrel cage induction motors - Performance versus efficiency", IEEE, Vol. IA-19, No. 5, 1983, pp. 819 -823.